

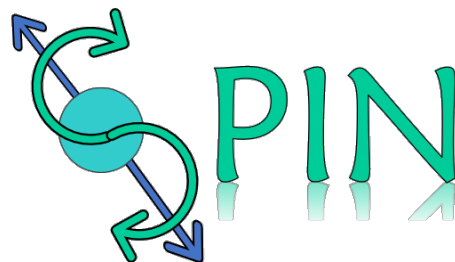


UNIVERSIDAD DE MEDELLIN

Facultad de ciencias básicas

Master thesis

Thesis to qualify for the title of Master in Modeling and Computational Science



**SPIN: [S]imple [P]ython [I]pywidgets [N]otebook
Interface to obtain the optoelectronic properties
of materials employing DFT**

José Manuel Vergara Álvarez

Advisor: Julian David Correa Abad, Ph.D.

Advisor: Elizabeth Florez Yepes, Ph.D.

Medellín, Colombia.
November 27th , 2022

Master Thesis

Master in Modeling and Computational Science

SPIN: [S]imple [P]ython [I]pywidgets
[N]otebook Interface to obtain the
optoelectronic properties of materials employing
DFT

Author: José Manuel Vergara Álvarez

Advisor: Julian David Correa Abad, Ph.D.

Advisor: Elizabeth Florez Yepes, Ph.D.

Medellín, Colombia.
November 27th , 2022

Abstract

The objective of this study was development of a graphical user interface to make an accessible, user-friendly, fast learning, and easily portable work environment for atomic simulations. The Simple Python Ipywidgets Interface to obtain the optoelectronic properties of Nanostructures (SPIN) is an open source graphical user interface that allows users to work with standard SIESTA files and perform end-to-end atomic level simulation processes, that is, it contains the complete flow, from the construction and visualization of structures or systems until the pre-processing, execution, and post-processing of calculations such as structure optimization, electronic properties like band structure and density of states (DOS) and optical properties. SPIN is an easy-to-use and fast-learning solution written in Python and built from Ipywidgets, however, the end-user can use all available features without the need for Python language knowledge. In this sense, to verify the use of the interface, different approaches have been studied:

First, we present the effect of different structural defects on electronic and optical properties of blue phosphorene nanotubes of both armchair and zigzag chirality. In addition, we have considered the influence of an applied electric field on the electronic states of either pristine and defect-laden structures. The main defective features considered are double vacancies and Stone-Wales defects, although results with these imperfections are, as well, compared with those arising when single vacancies of two types are regarded. The possible transition from semiconducting to metal-like behavior induced by the applied field for large enough zigzag nanotubes is predicted. Deviations of the optical response of defective systems compared to the pristine case are mainly revealed for the visible range and above, with an evident quantitative anisotropy related to the specific polarization of the incident light: parallel or perpendicular to the nanotube growth direction. This characterization of structural defects and their effects on the optoelectronic properties of blue phosphorene nanotubes is required to define how the surface of the nanotubes could be utilized to develop new optoelectronic devices.

In second place, the efficiency of (14, 14) armchair and (14, 0) zigzag based blue phosphorene nanotube (BPNT) to identify and remove three popular toxic antibiotics – Sulfanilamide (SAM), Sulfadimethoxine (SMX), and Sulfadiazine (SDZ) – from the water bodies were studied using density functional theory calculations. Analyzed molecules are weakly adsorbed on the pristine BPNTs with adsorption energy of about $-0,312$, $-0,285$ and $-0,377$ eV. Further, the electronic properties of the fundamental and antibiotics-adsorbed BPNT are investigated. The effect of single-vacancy BPNTs on the adsorption affinity of antibiotic molecules was studied. Compared with pristine systems, despite the increase in the reactivity of the zigzag BPNTs to the sulfonamides, armchair configurations show a transition from bipolar-magnetic semiconductor to not magnetic metallic system, suggesting that defective armchair BPNTs also can be employed as a sensor for antibiotic molecules, besides single-vacancies increases the E_{ads} values of all evaluated systems by up to 89% indicating an improvement in the capacity of BPNTs to adsorbed biologically active sulfonamide-based compounds like SAM, SDZ, and SMX.

Finally, the adsorption of single H atom and H_2 on blue-phosphorene monolayer with and without Pt atom adsorbed on the surface has been investigated using density functional theory with the Perdew-Burke-Ernzerhof exchange correlation functional. Using H adsorption energy as a descriptor, catalytic activity of evaluated systems for hydrogen evolution reaction was estimated. Obtained results evidence the impact of Pt atom on fundamental properties of the Blue-phosphorene monolayer, consequently, affecting its catalytic activity toward hydrogen evolution reaction. These data, potentially, can be a useful basis for designing and developing novel functional materials with predetermined catalytic properties.

Keywords: Blue-phosphorene, GUI, DFT, optoelectronic properties, Adsorption affinity

Contents

1	Preliminary aspects	1
1.1	Introduction	1
1.1.1	Graphical user interfaces and computational tools focused on atomic level simulations	1
1.1.2	Two-dimensional materials	2
1.1.3	General aspects, properties and applications of phosphorene	2
1.1.4	Nanotubes, a morphology of great interest	3
1.1.5	Modulate the properties of nanosystems: Structural defects and electric field	5
1.1.6	Nanotubes with potential application in the removal of antibiotics from aqueous media	6
1.1.7	Catalytic activity of blue phosphorene for hydrogen evolution reaction	6
1.2	Problem Description	7
1.3	Justification	9
1.4	Hypothesis	9
1.5	Objectives	10
1.5.1	General objective	10
1.5.2	Specific objectives	10
2	Computational details and model construction	11
2.1	SPIN: [S]imple [P]ython [I]pywidgets [N]otebook Interface to obtain the optoelectronic properties of materials employing DFT	11
2.2	Impact of different structural defects on fundamental properties of blue phosphorene nanotubes	12
2.3	Adsorption affinity of Sulfonamides onto Blue-phosphorene nanotubes	13

2.4	Impact of single Pt atom adsorption on fundamental properties of blue phosphorene and its activity toward hydrogen evolution reaction	16
3	SPIN: [S]imple [P]ython [I]pywidgets [N]otebook Interface to obtain the optoelectronic properties of materials employing DFT	18
4	Impact of different structural defects on fundamental properties of blue phosphorene nanotubes	35
5	Adsorption affinity of Sulfonamides onto Blue-phosphorene nanotubes	46
6	Impact of single Pt atom adsorption on fundamental properties of blue phosphorene and its activity toward hydrogen evolution reaction	61
7	Conclusions	83
7.1	SPIN: [S]imple [P]ython [I]pywidgets [N]otebook Interface to obtain the optoelectronic properties of materials employing DFT	83
7.2	Impact of different structural defects on fundamental properties of blue phosphorene nanotubes	83
7.3	Adsorption affinity of sulfonamides onto Blue-phosphorene nanotubes	84
7.4	Modulation of Blue-Phosphorene for <i>Pt</i> atom adsorption by hydrogen evolution reaction	85
	References	99

1. Preliminary aspects

1.1. Introduction

1.1.1. Graphical user interfaces and computational tools focused on atomic level simulations

The vast majority of studies and research carried out over the last few years at the atomic level have been possible thanks to the growing computing power. That has allowed an important advance in theoretical and computational methods to describe materials at the electronic level, which has constituted and allowed the creation of valuable tools to obtain reliable information at the atomic level [1]. One of the most popular approaches is the density functional theory (DFT), which is implemented differently in many free and licensed computational codes. Among which we can find SIESTA [2], GPAW [3], Quantum ESPRESSO [4], VASP [5], among others, which provide the ability to perform efficient calculations of electronic structures and ab initio molecular dynamics simulations, both of molecules and solids. It should be noted that power tools have been developed that work in console or terminal (by command line) such as sisl [6] and VASPkit [7] that facilitate pre- and post-processing in SIESTA and VASP respectively. There are also programming languages such as Python, with computational environments such as Jupyter notebook [8] and some packages responsible for performing simulations and calculations at the atomic level such as ASE [9], Pyprocar [9], sisl [6] and pymatgen [10] whose purpose is to facilitate the handling of workflows. We can also find some software that provides a graphical user interface focused on density functional theory calculations, such as sisl-gui [6], UI4dft [11] and gpaw-tools [12] that provides an interesting advance in terms of the implementation of graphical user interfaces that simplify the process of simulating materials at the atomic level, giving the user the possibility to calculate, visualize and save density of states (DOS), band structure, charge densities and optical properties of the investigated structures for SIESTA and GPAW, respectively. Another powerful tool is the commercially available ASAP (Atomistic Simulation Advanced Platform) program [13], which gives the possibility of several analysis tools and features such as electronic properties, thermodynamics properties, geometry evolution, chemical reactions and more, employing the

SIESTA code.

1.1.2. Two-dimensional materials

In 1947, PR. Wallace [14] first studied graphene from a theoretical point of view, where it was proposed as a limiting case of 3D graphite, but it was not until 2004 that graphene was successfully isolated by Andre Geim and Konstantin Novoselov [15]. This fact opened a wide field of research on two-dimensional (2D) materials, so much so that based on their work both won the Nobel Prize in Physics in 2010, an event that caused a "graphene gold rush" [16] and a great interest in the synthesis of new two-dimensional materials so that today there is a large set of isolated and theoretically proposed 2D materials [17–19], these materials have fascinating properties that give them great potential to be used in numerous industrial applications such as small molecule sensors, flexible and low power electronics and spintronic devices, optoelectronic applications in photonics, photovoltaics, and plasmonics, as well as batteries, supercapacitors, and applications in thermoelectric energy [20]; among them, we find phosphorene, which has unleashed a wave of scientific research activities in the field of materials since its successful isolation in 2014 [21, 22].

1.1.3. General aspects, properties and applications of phosphorene

Phosphorene is a two-dimensional material composed of a monolayer sheet structure of black phosphorus, this being a thermodynamically stable allotrope of phosphorus [21], which was synthesized in the year 1914 [23]. Phosphorene is a semiconductor material that has a honeycomb structure with a fold or puckered hexagon [24]. It can be obtained by mechanical exfoliation, with a sticky tape [25], by liquid exfoliation [26]. This material has interesting properties that are basically caused by its unique structure that has a strong in-plane covalent bond network and weak van der Waals interactions between surface layers [27]; For this reason, this material is predicted to be an excellent alternative to graphene.

One of the most remarkable characteristics of this material is its anisotropic behavior in the plane between the armchair (AM) and zigzag (ZZ) directions [28]. Phosphorene has a direct band gap ranging from 0.3 eV to 2 eV , which is modulated by changing the number of stacked layers, due to quantum confinement.

These characteristics allow phosphorene to have great potential in photodevice applications in the ultraviolet (UV) and near-infrared (NIR) regions. The possibility of modulating the phosphorene bandgap is also an advantage over graphene, which lacks a gap. It allows phosphorene to have a moderate on/off coefficient ($10^4 - 10^5$), while retaining high carrier mobility, making it suitable for many applications such as digital transistors. Furthermore, phosphorene exhibits greater flexibility due to its smaller Young's Modulus compared to graphene [21, 24, 27, 29–32]. It can be shown that phosphorene contains desirable qualities and parameters for device applications such as digital transistors because the candidate materials must have high carrier mobility for fast operation, a high on/off coefficient (a larger bandgap at 0.4 eV), high conductivity and low off-state conduc-

tance for low power consumption; Phosphorene meets these characteristics, which make this material play a important role in this type of application, and, in addition, makes it a more favorable option in general terms than graphene, since this material shows superior properties in some aspects but lacks necessary characteristics in others, e.g. compared to phosphorene, graphene has extremely high carrier mobility, but due to its lack of a band gap the material is impractical in field effect transistor applications (FET), since its on/off coefficient is small ($\sim 5.5 - 44$). [27, 29]. It should also be noted that in phosphorene, its pleated or "puckered" structure provides a suitable surface for interaction with drugs, bioactive molecules, fluorescent molecules, and metal atoms allows a series of biological applications such as targeted drug delivery, detection of biomolecules, cell imaging, and cancer therapy [33].

Having the phosphorene as start point, other 2D phosphorus allotropes have been proposed. These have been classified according to their absorption spectrum as red phosphorene, blue phosphorene and green phosphorene. Of these, blue phosphorene (BP) has stood out because, like black phosphorene, it is predicted to be stable and was recently proposed (2014) [34] and synthesized (2018) [35, 36]. Its primary cell is hexagonal, unlike black phosphorene, it has an isotropic structure. BP is a semiconductor material, and due to its characteristics, studies have been carried out to use it in applications such as optoelectronic and nanoscale devices, due to tunable electronic and dielectric properties that occur since the material has a specific band gap for the width and the edge of the [37] structure. Various first-principles calculations exploring the geometric, electronic, and magnetic properties of blue phosphorene monolayers, doped with light non-metal atoms such as *C* and *O*, have been performed. These calculations show that these systems feature spin-polarized band gap. However, the main source of magnetism in these two systems is quite different. This phenomenon may provide a route to functionalities of optical and spintronic devices [38]. We can also find applications in transistors, negative differential resistive devices, and lithium ion batteries [31, 39, 40].

1.1.4. Nanotubes, a morphology of great interest

The physico-chemical properties of two-dimensional materials can be modulated by changing the material morphology to form quantum dots [41], nanoribbons [42], nanowires [43], nanorods [44], microrods/microscale platelets, nanotubes, nanoparticles, nanoscales, and microscale scales [21, 22], each of these systems have different degrees of quantum confinement.

Nanotubes (NTs) have been considered one of the most outstanding morphologies due to the great interest that has been given to them in recent decades. This is due to the fact that there is currently an urgent demand for tubular electronics to satisfy the wide range of needs in optoelectronic devices, which emphasizes the importance of nanotube research, in particular, for its electronic and optical properties [45]. Nanotubes are a class of one-dimensional (1D) materials, whose thickness varies depending on the 2D material from

which they come, and they have unique properties, such as high hardness, mechanical resistance and flexibility. Similarly, they have optoelectronic properties modulable through their diameter. In addition, they can conduct electric current effectively and have high thermal conductivity. Due to that, they are potential materials in microelectronics, photovoltaic energy, gas detection, infrared photodetection, photocatalyst, and biomedicine applications [46–56].

The "wrinkled" structure of phosphorene nanotubes gives them anisotropic behavior in the plane between the armchair (AM) and zigzag (ZZ) [28] directions. For nanotubes, the winding direction is a determining factor of its electrical properties. Furthermore, the band gap and its optical properties can be modulated by its diameter [45]. We can mention the research carried out by Yu et al [57], where they found that armchair-type phosphorene nanotubes have semiconducting properties along the axial direction, and that compressive stress can significantly improve the carrier mobility; Additionally, they showed that both strain effects and size effects are significant. Thus, armchair-type phosphorene nanotubes have promising applications in nanoscale field-effect transistors, infrared photodetectors, and strain sensors.

Regarding blue phosphorene nanotubes (BPNTs), Aierken et al [58] showed that blue phosphorene is more suitable for producing small nanotubes. On the other hand, Montes et al [48] showed that BPNTs are indirect bandgap semiconductors. This bandgap turns out to be very sensitive to tube diameter, giving BPNTs great potential as a one-dimensional platform for electronic devices. Moreover, Xiao et al [59] perform first principles calculations of the electronic structure and carrier mobility in BPNT, where it is evident that the value of carrier mobility in the armchair direction ($\sim 3.3 \times 10^2$) is less than the values obtained for the zigzag direction ($\sim 1.5 \times 10^5$), and the latter presents values comparable to those of Carbon nanotubes ($\sim 10^6$) and higher than those of phosphorene nanotubes ($\sim 4.2 \times 10^2$). Ju et al [50] investigated the electronic structure and related properties of BPNTs using first-principles calculations to explore their photocatalytic activity, showing that the value of the formation energy of BPNTs with diameters greater than 8 \AA is very close to that of carbon nanotubes, indicating that these structures could be stable. It is also pertinent to rescue the DFT study of the structural, electronic, dielectric, and elastic properties of blue phosphorene nanotubes reported by Hao et al [61], where it is observed that the properties of AM and ZZ type BPNTs are almost the same, and isotropy is evident for a radius of up to 13 \AA . In fact, in both directions, the structure has Young's Modulus of approximately 136 GPa this being smaller than that of graphene, which indicates that the structure exhibits greater flexibility; also, band gaps are sensitive to the effects of axial deformation. Additionally, Montes and Schwingenschlöggl [62] studied the adsorption of some molecules such as CO , CO_2 , NH_3 , NO and NO_2 in zigzag and chair-type BPNT, finding that these nanotubes outperform the gas sensing performance of other one-dimensional materials, in particular, *Si* nanowires and carbon nanotubes, and two-dimensional materials, in particular graphene, phosphorene, and MoS_2 , furthermore, they demonstrated that BPNTs are highly promising candidates for sensors functional gas.

1.1.5. Modulate the properties of nanosystems: Structural defects and electric field

Nanotubes often suffer from various types of topological defects during their growth. Experiments and theory have shown that the existence of defects, such as vacancies or Stone-Wales defects in nanostructures, can produce a significant influence on mechanical and electronic properties, proving to be useful in achieving new properties and broadening the range of applications [63]. Expanding on some examples, Zhou et al [64], investigated the effects of monovacancies, divacancies, Stone-Wales defects, and octagon-pentagon pair defects in carbon nanotubes with ZZ chirality and found that the existence of vacancies and the defect of the octagon-pentagon pair reduces the band gap, while the SW defect induces an opening of the band gap in the CNTs. More interesting still, the bandgaps of the (8, 0) and (14, 0) CNTs configurations with two octagon-pentagon pair defect show 0.517 eV and 0.163 eV, which are slightly smaller than the perfect CNTs. Also, with increasing defect concentration, there is a decrease in the bandgap, causing the two types of CNTs to change from a semiconductor to metallic conductor. Sorkin and Zhang studied the effect of monovacancies and divacancies on the mechanical properties of black phosphorene nanotubes (PNTs) [65]. According to their findings, divacancies in armchair PNTs (AM) and monovacancies in zigzag PNTs (ZZ) have the lowest vacancy formation energy, which decreases with tube diameter in AMPNTs and increases in ZZ PNTs. In the case of phosphorene, Sorkin and Zhang studied the effect of monovacancies and divacancies on the mechanical properties of PNTs [65]. According to their findings, vacancies in AM-type PNTs and single vacancies in PNTs with ZZ chirality have the lowest vacancy energy, which decreases with tube diameter in AMPNTs and increases in ZZPNTs. However, research on phosphorene nanotubes is limited compared to carbon nanotubes.

Another possibility to modulate the properties of nanosystems is the application of an external electric field on the structures. For example, Ospina et al [66] investigates the effect of external electric fields on optical and electronic properties of blue phosphorene nanoribbons, and found that the energy gap decreases as the electric field intensity increases, and the nanoribbons shows a transition from semiconductor to metal. This phenomenon could be used to develop new tunable optoelectronic devices. Besides, their theoretical results for the imaginary part of the dielectric function show that the inter-band linear optical response of blue phosphorene nanoribbons is also affected by changes in electronic properties due to the influence of the applied electric field. For CNTs, Tien et al [67] show that band gap modulation of monovacance defect semiconductor carbon nanotubes can be easily achieved by applying a transverse electric field and found that the band structures of defective CNTs vary quite differently from that of the pristine nanotube, and are highly dependent on the applied direction of the transverse electric field.

1.1.6. Nanotubes with potential application in the removal of antibiotics from aqueous media

Sulfonamide molecules constitute an important class of drugs, comprising several types of pharmacological agents that possess antibacterial, antiviral, anticarbonic anhydrase (CA), diuretic, protease inhibitor, cyclooxygenase 2 (COX2) inhibitor, and anticancer activities, among others [68]. Sulfonamide antibiotics are produced in large quantities and are widely used in human therapy and livestock production. As a result, more and more pharmaceutical residues from sewage effluents, hospital effluents, and other untreated wastewater will seep into surface and groundwater, then migrate and transform into the aquatic environment. Concerns arising from exposure to sulfonamide antibiotics in aquatic environments include acute and chronic toxic effects and antibiotic resistance to microorganisms. However, the removal of antibiotics by existing water treatment technologies is incomplete [69, 70]. An alternative is to take advantage of the potential of some structures and nanosystems as adsorbents of organic pollutants, such as emerging pollutants, present in bodies of water. For example, Liu et al [71], investigated how sulfonamide adsorption behaves on multiwalled carbon nanotubes. Among the sulfonamides evaluated are Sulfanilamide (SAM), Sulfamerazine (SMR), Sulfadimethoxine (SMX), Sulfadiazine (SDZ), Sulfadimidine (SMT), and Sulfamethoxydiazine (SMD). Their results indicate that CNTs have potential application in the removal of sulfonamides from aqueous solutions by adsorption process, which can reach a high efficiency (in a pH adsorption range of 3 to 9). Recently, Bhuvanewari et al [72], studied the molecular interaction of armchair-type blue phosphorene nanotubes (10, 10) with Sulfapyridine (SP) which is an antibacterial drug Sulfanilamide (SAM), and found that the interaction properties of the BPNTs that interact with the antibiotic, such as the remarkable Bader charge transfer, the significant adsorption energy and the prominent average band gap variation, indicate high efficiency of the BPNT to eliminate the toxic antibiotics from water bodies.

1.1.7. Catalytic activity of blue phosphorene for hydrogen evolution reaction

With the growing demand and use of fossil fuels as an energy source, important problems have developed in the world called "energy crises", because of the finite nature of fossil fuels. Likewise, their combustion results in a "greenhouse" effect. Thus an alternative means of energy production and storage are required. For this reason, the scientific community has developed a great interest in researching and designing sustainable alternatives for energy resources, among which hydrogen energy presents a viable option because is one of the cleanest fuels and represents one of the energy sources most promising to replace traditional fossil fuels. However, its potential only has a good prospect if hydrogen production can be carried out in a "green" and low-cost way. These requirements are fulfilled by the electrocatalytic hydrogen evolution reaction (HER), which is the cathodic reaction in the electrochemical splitting of water and offers the potential to produce H_2 [73-76]. Currently, the main commercial electrocatalysts for HER are composed of noble metals such as platinum (Pt) and materials based on it, because they are the most

efficient catalysts. However, Pt has a low abundance and a high cost, which limits its application in industry [77–80]. For this reason, the exploration and development of new catalysts with low cost and high efficiency is highly desirable for practical of HER.

Due to the fascinating properties already mentioned, 2D materials, including phosphorene, have great potential in numerous applications in electrocatalytic HER [20–22, 73, 81–86]. Nonetheless, recent studies have shown that the HER activity of pristine phosphorene is much lower than other common electrocatalysts such *Pt* or *MoS₂* [87] and the activity of systems like bulk or nanosized phosphorene is not satisfactory for practical applications [88]. In that sense, several strategies have been implemented in order to optimize hydrogen adsorption to improve the HER activity such as the introduction of extrinsic active sites by metal doping. For example, *Co* [85], *Au* [89], *Pd* [90], *Pt* [91–93], hetero-atoms doping, and adsorption of functional groups like like *NH₂* and *OH* [94]. Another alternative to modulate the catalytic HER on phosphorene is the creation of optimal active sites with system defects [87, 95, 96], system strain modulation [97], and functionalization [98]. On the other hand, a recent study [99] analyzed the behavior of Metal-doped Phosphorene in the HER reaction. Their results indicated that owing to the enhanced electro-conductivity, abundant metal-P active sites, and optimized adsorption energy by doping, the Phosphorene-Metal exhibits enhanced hydrogen evolution reaction activities and stability in comparison to the bare phosphorene.

Blue-phosphorene has also motivated the scientific community to investigate its catalytic properties, for example, Ju et al [100] found that blue-phosphorene nanotubes are promising candidates as photocatalytic materials for oxygen evolution reaction (OER). On the other hand, some studies have shown that doped BP has excellent photocatalytic potential for *NH₃* production, electrocatalytic oxygen reduction reaction (ORR) and HER, which indicates BP can be used to design applications experimentally for water molecule splitting [101–103]. Moreover, various studies of hetero-structures and engineering band gap of BP by functionalization have been performed [104–106] given an interesting possibility for designing efficient photocatalysts.

1.2. Problem Description

The fascinating opto-electronic properties of derivatived of 2D materials give them the potential to be used for countless purposes and applications, and it is of great interest to the scientific community to be able to modulate this range of properties and applications. Two of the strategies used to modulate the properties of nanostructures are to generate artificial defects in the structures by irradiation of ions or electrons [63] or by the application of an external electric field. For this reason, the effect of including various defects and applying an external electric field in nanotubes from different materials, mainly carbon, are studied [64, 65, 67, 107–120]. It has been shown that despite the great amount of theoretical efforts in the analysis of materials such as BPNTs, the vast majority of studies to date are not systematic and do not allow a complete analysis of the capabilities of the

material. For this reason, there is still certain untreated aspects with respect to BPNTs, among which we find the effect of neutral structural defects on opto-electronic characteristics, such as single atom vacancies or single vacancies, double vacancies or divacancies and structural defects of the type Stone-Wales and the influence of the application of an external electric field on the electrical and optical properties of these nanosystems.

Additionally, it has also been shown that another untreated theoretical is the potential of BPTNs to adsorb or sense antibiotics from aqueous media and the effect that the inclusion of defects in the structure could have in this type of applications. It should be noted that this type of residual substance present in aqueous environments generates great concern due to its potential risk to the environment and biological survival. Because it represents a high risk to human health and can affect the evolutionary structure of the bacterial community, strengthening bacterial resistance to these products [121]. Some materials, such as Carbon, are used in efficient techniques for the removal of antibiotics from wastewater due to their properties, and it has been shown that the nanotubes of this material have potential application removing of antibiotics from aqueous solutions [71], the reason for which, it would be interesting to analyze and contrast the capacity of BPTNs to retain this type of contaminants.

Since the opto-electronic properties of 2D and derivatived materials open the doors to an innumerable set of applications. The use of user-friendly interfaces and graphical environments that allow multiple calculations to be carried out in a simple way, is required. These interface must integrate fundamental elements in the process such as the construction and visualization of structures or systems, the pre-processing, execution, and post-processing of calculations. In this sense, there are tools whose purpose is to simplify this type of procedure, among which we can find powerful implementations for pre- and post-processing such as VASPkit that work through the console or command line, which is not always the case. more convenient. There are also excellent alternatives like ASE, Pyprocar, sisl and pymatgen that provide elements to extract, visualize, and analyze information, but require users to have proficiency in the Python programming language. Most of the mentioned tools involve investing a lot of time in understanding how the tool works, and usually, it also involves learning the programming language in which it is written in case you are not familiar with it. Therefore, the development of simple, usable, friendly and intuitive open source user interfaces are of great help. The GUI4dft and Gpaw-tools softwares provides an interesting advance in terms of the implementation of graphical user interfaces that simplify the process of simulating materials at the atomic level, however, these softwares are focused solely on the SIESTA and GPAW packages, respectively. For this reason, in this work, we propose the development of a graphical user interface using Ipywidgets (interactive HTML widgets for Jupyter notebooks and the IPython kernel) to develop an accessible, user-friendly, fast learning, and easily portable work environment for atomic simulations. The interface will integrate the construction process of the atomic structures and the performance of electronic structure calculations, having different packages or calculators at the user's choice as the core. As an initial version that allows us to validate the use of the tool, we will use the SIESTA [2] pack-

age as the core. In this sense, to verify the use of the interface, the optical and electrical properties of blue phosphorene nanotubes and their potential in optical applications will be studied, as well as their potential and capacity to adsorb or sense sulfonamide antibiotics in bodies of water.

On the other hand, the great interest in researching and designing low cost and high efficiency sustainable alternatives for energy resources such as hydrogen energy has provided the opportunity to explore the catalytic activity of various two-dimensional materials including blue-phosphorene, however, the behavior of integrating a blue-phosphorene with other active material like platinum has not been studied yet and it could be another strategy to enhance Hydrogen adsorption. In that sense, the catalytic activity of BP, modified with a single *Pt* atom (BP-*Pt*), toward HER is investigated using density functional theory (DFT). The effects of *Pt* on fundamental properties of the BP are investigated in detail and their consequent impact on catalytic properties of the complex BP-*Pt* system is discussed.

1.3. Justification

The use of simulation environments at the atomic level is a great strategy for the systematic study of nanomaterials, however, it is necessary to have platforms and interfaces that are easy and intuitive to use, in which the minimum effort and time should be invested for its use and implementation. For this reason, in this work, a graphical user interface based on Ipywidgets of jupyter notebook is developed, which allows us an integration in the processes of construction of atomic structures, the realization of electronic structure calculations and the preliminary analysis of the results obtained. As an application example, the properties electrical and optical properties of single-walled blue phosphorene nanotubes with and without structural defects, in addition to the influence of the application of an external electric field on the opto-electronic properties of these nanosystems is analyzed in order to identify their potential in optical applications. In addition, the potential of these structures in applications whose purpose is to adsorb toxic antibiotics (sulfonamides) from bodies of water is analyzed. On the other hand, the catalytic activity of a BP modified with a single *Pt* atom and the effect of *Pt* on fundamental properties of the BP is investigated.

1.4. Hypothesis

- The use of graphical environments for the development of simulations at the atomic level can favor the research processes of the physical-chemical properties of different nanomaterials by reducing the time invested in learning how to use the tools and their execution in high performance computing environments.
- The structural defects allow to modulate the optical and electrical properties of the phosphorene nanotubes and in turn modify their interaction with sulfonamide molecules.

-
- The inclusion of a single platinum atom on a blue-phosphorene monolayer modulate the electronic properties improvement the Hydrogen evolution reaction.

1.5. Objectives

1.5.1. General objective

Develop a graphical interface for simulations at the atomic level, which allows the simple study of the physical-chemical properties of nanomaterials.

1.5.2. Specific objectives

- Develop a graphical interface that simply integrates different stages in the simulation process at the atomic level.
- Determine the opto-electronic properties of blue phosphorene nanotubes and the effect of both structural defects in the structures and the application of an external electric field.
- Determine the sensor potential of blue phosphorene nanotubes against organic molecules.
- Determine the effect of platinum atom on the hydrogen adsorption behavior of blue-phosphorene monolayer.

2. Computational details and model construction

2.1. SPIN: [S]imple [P]ython [I]pywidgets [N]otebook Interface to obtain the optoelectronic properties of materials employing DFT

SPIN, our simulation environment, is an open-source graphical user interface that seeks to integrate tools and packages to provide an intuitive, easy-to-use, and fast-learning solution for the atomic-level simulation of materials. In SPIN, the construction, visualization of structures, the pre-processing, execution, and post-processing of calculations are integrated. In the developing proposed simulation environment, the Jupyter Notebook tool has been used, which is an open source project that has support for multiple languages, including Python, the programming language in which this work is developed. The graphic elements of the simulation environment have been built using the widgets provided by the Ipywidgets library, which are objects that allow building interactive graphical user interfaces(GUI) in jupyter notebook. The Py3Dmol [122] and NGLview [123] libraries have also been integrated, which allows us to visualize 3D molecules created in the interface in an interactive way. The architecture of the interface is divided into four main components: The first one provides us with a view of the structure, which can be created manually, updated from a file (all Openbabel [124] formats are supported), load some predefined molecules or build systems like bulks, nanotubes or nanoribbons. The second component provides us with the elements to introduce the calculation parameters and build the initial files (inputs) according to the core of the selected calculation (for the initial version, the SIESTA package was implemented). In the third component, we can select and execute different calculations, for example, the structure's relaxation, the band structure's calculation, the density of states, or optical properties. Finally, the fourth component gives us the tools to customize plots of results fully obtained.

2.2. Impact of different structural defects on fundamental properties of blue phosphorene nanotubes

The structure and electronic properties have been studied employing first-principles calculations within the framework of the density functional theory. The package *ab initio* SIESTA [2] was used. Where localized double- ζ , single-polarized atomic orbitals are employed as a basis set, together with norm-conserving pseudopotentials. The exchange-correlation functional used corresponds to the generalized gradient approximation (GGA). All calculations have been performed using a $1 \times 1 \times 5$ supercell. The structures are relaxed through the FIRE minimization algorithm until the force on the atoms are smaller than $0.04 \text{ eV}/\text{\AA}$ [125]. The Brillouin zone sampling is carried out via a Monkroost-Pack grid of $1 \times 1 \times 2$. A Mesh cutoff value of 350 Ry was used. The study was carried out with the inclusion of collinear spin-polarization for single-vacancies systems and without for all other systems (pristine nanotubes, double-vacancies or divacancies (DV), and nanotubes with Stone-Wales (SW) defects).

The optical properties have been determined within the framework of the independent particle approximation, through the imaginary part of the dielectric function, which is given by [126]:

$$\varepsilon_{2,\sigma}(\omega) = \left(\frac{2\pi e}{m\omega}\right)^2 \sum_{c,v} |M_{(c,\sigma),(v,\sigma)}|^2 \delta(E_{c,\sigma} - E_{v,\sigma} - \hbar\omega), \quad (2.1)$$

where, the indices c and v represent the respective sets of quantum numbers associated with the energy state of the conduction and valence band, respectively, including $\sigma = \uparrow, \downarrow$ for the z component of the Spin. $M_{(c,\sigma),(v,\sigma)}$ describes the corresponding element of the electric dipole moment matrix. In practice, the conservation energy is guaranteed with a Gaussian function with HWHM equal to 0.06 eV . Two polarizations of the incident light have been considered: the directions x and z (perpendicular and parallel to the growth direction of the nanotube, respectively). To ensure convergence of the optical absorption spectrum, a grid of $1 \times 1 \times 101$ was used. The total of the imaginary part of the dielectric function is finally given by:

$$\varepsilon_2 = \varepsilon_{2,\uparrow} + \varepsilon_{2,\downarrow} \quad (2.2)$$

Having obtained ε_2 , using the Kramers-Krönig relations, its real part, $\varepsilon_1(\omega)$, is evaluated. With knowledge of the full dielectric function, it is possible to derive other optical properties as a function of frequency. A relevant quantity in this sense, given the viability of its experimental measurement, is the refractive index. It can be evaluated from:

$$n(\omega) = \frac{1}{\sqrt{2}} \left[\varepsilon_1(\omega) + \sqrt{\varepsilon_1^2(\omega) + \varepsilon_2^2(\omega)} \right]^{1/2}. \quad (2.3)$$

BPNT structures can be seen as a coiled blue phosphorene monolayer (BPML) and, similarly to carbon nanotubes [127], they can be intertwined in different directions. In the present investigation, we consider the so-called achiral nanotubes, in which the rolling

line runs along the zigzag and armchair direction of the monolayer. Furthermore, the unit cell of BPNTs is determined by the chiral and translational vectors, which are given by $\vec{C}_h = n\vec{a}_1 + m\vec{a}_2$, $\gamma \vec{T} = u\vec{a}_1 + v\vec{a}_2$ respectively; where \vec{a}_1 y \vec{a}_2 are the BPML unit cell vectors. The geometric and electronic structure of BPNTs is characterized by a pair of indices (n, m) . So, for achiral zigzag-type blue phosphorene nanotubes (ZZ-BPNT) $m = 0$, while for armchair-type blue phosphorene nanotubes (AM-BPNT) $n = m$ (see panel (a) on the figure 2.1). As n and m increase, the diameter of the BPNTs increases. Unlike carbon nanotubes, BPNTs have two radii, determined by the buckling of phosphorus atoms in the original BPML.

As mentioned, we investigated the effects of structural defects in nanostructures. In particular, we will study the simple vacancies or monovacancies (SV) of two types (A and B), which are obtained by eliminating an atom from the original structure, the divacancies (DV), which can be constructed by eliminating a pair of adjacent atoms, the Stone-Wales (SW) defects, which are formed by rotating a $P - P$ bond in the hexagonal lattice by 90 degrees. A graphical view of these imperfections can be seen in the panels (b), (c), (d) and (e) from the figure 2.1. In order to contrast and identify the influence that these defects have on the electronic properties of the material. Eight different nanotube sizes are considered for armchair and zigzag configurations, ranging from $n = 7$ to $n = 14$, for all studied systems.

2.3. Adsorption affinity of Sulfonamides onto Blue-phosphorene nanotubes

Generally, to activate the surface of nanotubes, whether carbon or other material, it is necessary to induce defects, dope, decorate, or functionalize the nanotube wall to achieve an increase in its adsorption capacity [128–132].

Therefore, in this work, we analyze the adsorption of a sulfanilamide molecule (SAM) on pristine and defective single vacancy (SV) blue phosphorene nanotubes. So that it is possible to contrast and identify the incidence of SV in the adsorption capacity of the BPNT. Our analyses consider BPNTs of type AM and ZZ, characterized by the chiral numbers (14, 14) and (14, 0), respectively. A supercell of $1 \times 1 \times 5$ guarantees that the SAM molecule do not interact with their images. The analyzed adsorption sites for SAM can be seen in figure 2.2.

The calculation of structural and electronic properties is performed within the framework of DFT, as it is implemented in the ab initio SIESTA package [2] where localized double- ζ polarized atomic orbitals are employed as basis set, together with conserved norm pseudopotentials. For the exchange and correlation functional used, the one proposed by Dion et al [133] and whose exchange was modified by Klimes et al [134]. This functional include van der Waals interactions and is labeled as (KBM). All structures are relaxed through the FIRE minimization algorithm, until the force on the atoms is smaller

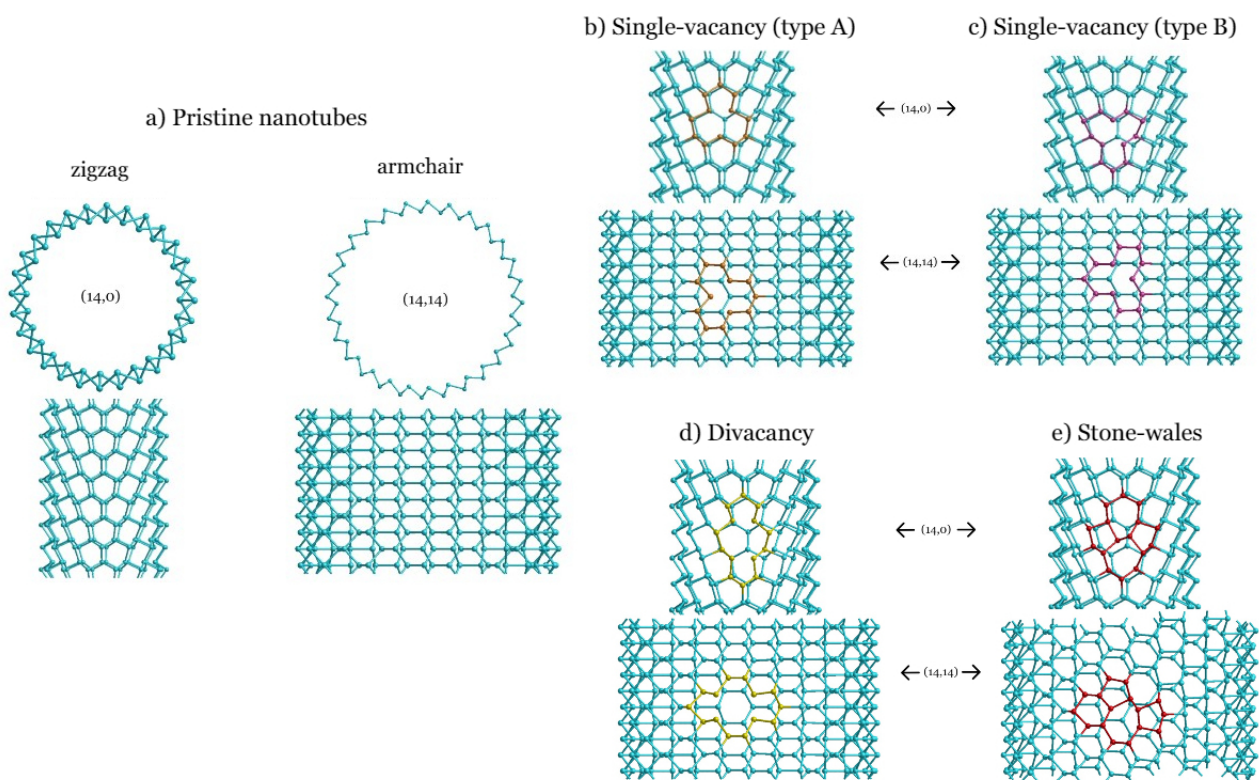


Figure 2.1: Panel a) contains a cross-sectional (top) and longitudinal (bottom) view of a pristine nanotube of the zigzag type (14, 0) and the armchair type (14, 14). Panels b), c), d) and e) show a schematic view of the simple vacancies (A and B), divacancies and Stone-Wales type defects of BNNTs of size (14,0) and (14,14), respectively.

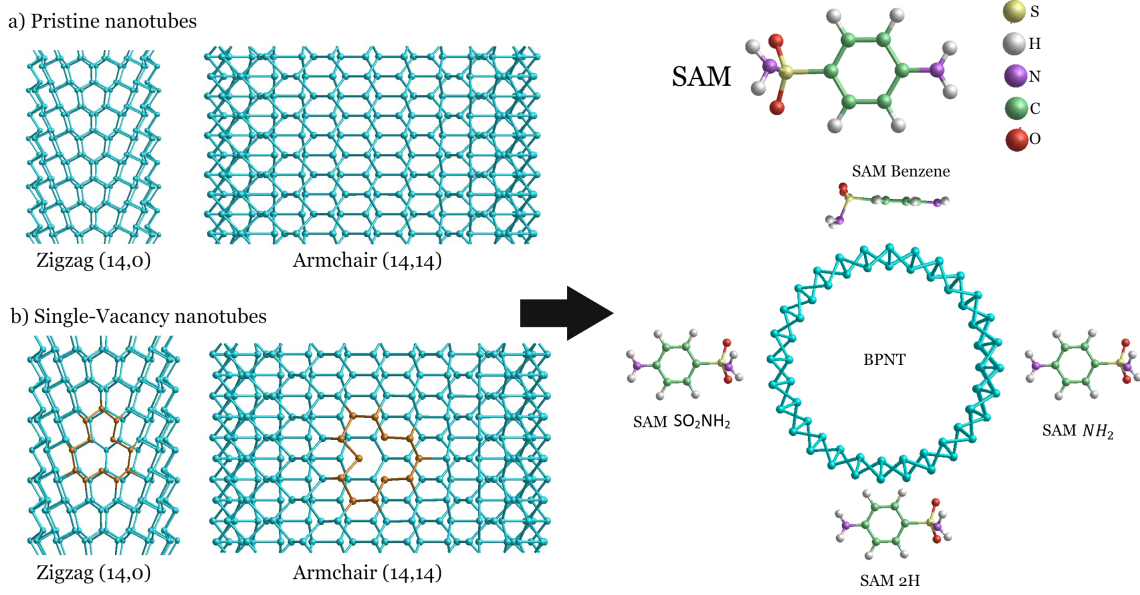


Figure 2.2: Schematic view of all evaluated SAM adsorption sites for both, pristine and single-vacancy nanotubes.

than $0.04 \text{ eV}/\text{\AA}$ [125]. The Brillouin zone sampling is carried out via Monkhorst-Pack-grid of $1 \times 1 \times 2$. A Mesh cutoff value of $350 R_y$ was used. The study was carried out with the inclusion of collinear spin-polarization for SV systems and without spin-polarization for pristine BPNT structures.

The adsorption energy between the molecule and the BPNT is characterized by evaluating the adsorption Energy (E_{ads}), which is defined as:

$$E_{ads} = E_{Total} - E_{BPNT} - E_{Adsorbate}, \quad (2.4)$$

where $E_{Adsorbate}$ is the total energy of SAM, E_{Total} is the total energy of the system composed of the BPNT and the adsorbate and E_{BPNT} is the BPNT total energy.

Further, conventional transition state theory is adopted to determine the recovery time of BPNTs from the interaction of the toxic antibiotics [135, 136]. The following equation, which encompasses the attempt frequency θ_0 , adsorption energy from eq. 2.4, Boltzmann's constant (k_B), and the temperature (T), is employed to reckon the recovery time of the blue-phosphorene nanotube. Recovery time captures the time cost for the desorption of a target molecule from the sensing material's surface [137] and could be obtained according to the transition state theory and Van't Hoff-Arrhenius explanation:

$$\tau = \theta_0^{-1} \exp\left(\frac{-E_{ads}}{k_B T}\right), \quad (2.5)$$

where the frequency factor θ_0 is assume to be 10^{12} Hz and 10^{16} Hz , under visible and UV light conditions, respectively [137-139], k_B is approximately $8,617 \times 10^{-5} \text{ eV/K}$ [137] and T is evaluated in 300 (ambient temperature), 310, 320 and, 330 K.

2.4. Impact of single Pt atom adsorption on fundamental properties of blue phosphorene and its activity toward hydrogen evolution reaction

Periodic density functional calculations were performed using the Vienna ab initio simulation package (VASP) [5] within the generalized gradient approximation (GGA), utilizing Perdew, Burke and Ernzerhof for the exchange-correlation energy functional [140]. The kinetic energy cut-off of 500 eV for the plane wave basis set was selected. Integration of the reciprocal space for all surfaces was carried out using $5 \times 5 \times 1$ grids of special k-points within Monkhorst-Pack scheme for the geometry optimization procedures [141]; while $17 \times 17 \times 1$ grid was used for the Density of States calculations. Blue-phosphorene monolayer was represented by a 4×4 supercell in all performed calculations. All complex are fully relaxed employing the conjugate gradient algorithm until the force in each atom is less than $0.001 \text{ eV}/\text{\AA}$. The criterion for the convergence of the total energy is set as 10^{-4} eV per atom. A vacuum of 18 Å along the z direction was included to avoid possible interactions between cell images repeating in z direction.

Adsorption of a single Hydrogen (H) and Platinum (Pt) atoms on various top, bridge, fcc, and hcp sites were studied first to define the preferable adsorption locations on the BP monolayer. Additionally, we evaluated the adsorption energies of a single H atom, two H atoms, and H_2 molecule on BP and BP-Pt surfaces. For the H_2 molecule, three orientations were considered, parallel, perpendicular, and tilted to the plane of the surface, as can be seen in Fig. 2.3.

The adsorption energy values were calculated from the following expression:

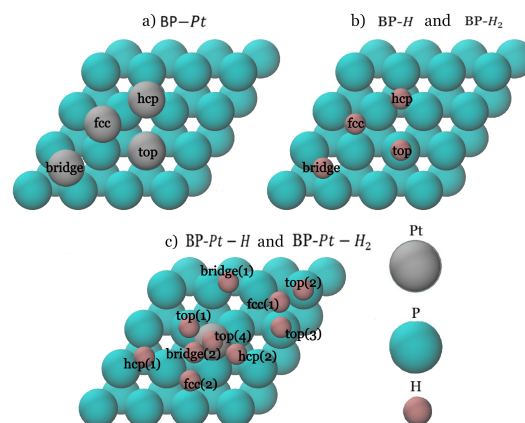


Figure 2.3: Adsorption sites available on BP surface (panels a and b) and on BP surface decorated with platinum atom (panel c).

$$E_{ads} = E_{Surf+Adsorbate} - (E_{Surf} + E_{Adsorbate}), \quad (2.6)$$

where E_{Surf} correspond to the energy of the pure BP or BP–Pt and $E_{Adsorbate}$ the energy of the adsorbate (atomic H , H_2 or Pt) in a vacuum, respectively. For H , atomic H energy was used as reference.

The effect of van der Waals corrections, as implemented by Grimme et al., [142] on adsorption energies was tested and because of the closeness of the results with and without dispersion corrections, most calculations have been carried out without the corrections, unless specifically stated otherwise.

To construct a volcano curve, hydrogen adsorption energies have been obtained for the 12 metals used in work of Nørskov et al. [143], employing 4×4 supercells with 4 atomic layers and 18 Å of vacuum. In electrocatalysis instead of using energy of a single H atom as in eq. 2.6, it is common to employ half of the energy of H_2 in the gas phase as the reference. Thus, HBE values for the volcano curve were obtained using the following expression:

$$E_{Ads,H} = E_{Surf+H} - (E_{Surf} + \frac{1}{2}E_{H_2,g}) \quad (2.7)$$

The numeric difference between the $E_{H,g}$ and $\frac{1}{2}E_{H_2,g}$ is 2.25 eV, thus, if HBEs were calculated using eq. 2.6, the whole curve would have shifted to the left for a value of 2.25 eV, without affecting the trends of activity. Experimental values for HER exchange current were taken from the works of Nørskov et al. [143] and Trasatti [144] and were plotted versus the corresponding HBEs.

3. SPIN: [S]imple [P]ython [I]pywidgets [N]otebook Interface to obtain the optoelectronic properties of materials employing DFT

SPIN: [S]imple [P]ython [I]pywidgets [N]otebook
Interface to obtain the optoelectronic properties of
materials employing DFT

J. M. Vergara^a, M. E. Mora-Ramos^b, E. Flórez^{a,*}, J. D. Correa^{a,*}

^a*Facultad de Ciencias Básicas, Universidad de Medellín, Medellín-Colombia*

^b*Centro de Investigación en Ciencias-IICBA. Universidad Autónoma del Estado de
Morelos. Av. Universidad 1001, C.P. 62209, Cuernavaca, Morelos, Mexico*

Abstract

The Simple Python Ipywidgets Notebook interface to obtain the optoelectronic properties of materials (SPIN) is an open source graphical user interface that allows users to work with standard SIESTA files and perform end-to-end atomic level simulation processes. It contains the complete flow, from the construction and visualization of structures or systems until the pre-processing, execution, and post-processing of calculations such as structure optimization, electronic properties like band structure, density of states (DOS), and optical properties. SPIN is an easy-to-use and fast-learning solution written in Python and built from Ipywidgets. However, the end-user can use all available features without the need for Python language knowledge.

Keywords: Python, Electronic properties, Optical properties, DFT, GUI, SIESTA

PROGRAM SUMMARY

Program Title: SPIN

Developer's repository link: <https://github.com/JoseMVergara/SPIN>

Licensing provisions: MIT

Programming language: Python

Nature of problem: The program can be used in complete workflow in which fundamental elements in the atomic level simulation of materials are integrated.

*Corresponding author

Email addresses: elflorez@udemedellin.edu.co (E. Flórez),
jcorrea@udemedellin.edu.co (J. D. Correa)

Preprint submitted to Computer Physics Communications

November 20, 2022

Solution method: SPIN, is an open source graphical user interface that seeks to integrate a set of tools and packages to provide an intuitive, easy-to-use and fast-learning solution, given the possibility to make different processes such as the construction and visualization of structures or systems and the pre-processing, execution, and post-processing of calculations. SPIN is an Ipywidgets based Interface that allow users to work easily in any operating system (Windows, Linux and Mac), because it works on Jupyter Notebooks.

1. Introduction

The vast majority of atomic level studies and research carried out over the last years have been possible thanks to the increasingly growing computing power. It has allowed an important advance in theoretical and computational methods to describe materials at the electronic level. As a result, valuable tools to obtain reliable information at the atomic level have come to practical realization [1]. One of the most popular approaches is the density-functional theory (DFT), which is implemented in different formats, with a large number of either free or under-license computational codes and environments. Among them we find SIESTA [2], GPAW [3], Quantum ESPRESSO [4], VASP [5], and others. These powerful tools give users the possibility to performing electronic structure efficient calculations and *ab initio* molecular dynamic simulations of both molecules and solids. This would allow to understand the observed behavior of such structures, including structural, mechanical, electronic, magnetic and optical properties; as well as to predict those features of compounds that have not yet been determined experimentally [6]. Softwares whose purpose is to integrate and facilitate tasks of the different stages in the realization of this type of calculations are already available; that is, to perform pre-processing, execution and post-processing. In that sense, potent command line tools have been developed such as some sisl utilities [7], and VASPkit [6], which facilitate pre- and post- processing in SIESTA and VASP respectively. Also, it is important to highlight that the end users of the aforementioned software do not need to know their base programming language (like Fortran, C or Python) in order to make use of them. However, basic knowledge of the BASH command language is required, which can present challenges for clients and it is not always the most convenient option.

There are also programming languages such as Python, where it is pos-

sible to find computational environments such as Jupyter notebook [8], and some packages responsible for performing simulations and calculations at the atomic level which are excellent alternatives: ASE [1], sisl [7], Pyprocar [9], and pymatgen [10]. Their purpose is to ease the management of atomic simulation workflows while providing elements for extracting, visualizing, and analyzing information; but, at the same time, require users to have proficiency in Python programming language.

Most of the mentioned tools involve investing a lot of time in understanding how they actually work. Usually, it also involves learning the underlying programming language in which they were prepared. This becomes a drawback for those who are not familiar with it. To overcome this issue, the development of simple, usable, friendly and intuitive open source user interfaces are necessary and can be of great help. Software like sisl-gui [7], Gui4dft [11], gpaw-tools [12], and ASAP (Atomistic Simulation Advanced Platform) program [13], provide advances in terms of the implementation of graphical user interfaces. That simplifies the process of simulating materials at the atomic level. They allow the user to calculate, visualize and save the density of states (DOS), band structure, charge densities, and optical properties of the investigated structures. However, it may be inconvenient that they are focused on specific software or only available with commercial licenses. For example, the ASAP program provides several tools for the analysis of features such as electronic and thermodynamical properties, geometry evolution, chemical reactions, and more, employing the SIESTA code. For this reason, in this work, we propose the development of an Open-source graphical user interface using Ipywidgets with the purpose of obtaining an easy, user-friendly work environment for atomic simulations, fast learning and easily portable to the cloud. These are interactive HTML widgets for Jupyter notebooks and IPython kernel. The interface will integrate the construction process of the atomic structures and the performance of electronic structure calculations, having different packages or calculators at the user's choice as the core. As an initial version, that allows us to validate the usefulness of the tool, we will use SIESTA software as the core.

2. Implementation

2.1. Software architecture

SPIN, our simulation environment, is an open source graphical user interface that seeks to integrate a set of tools and packages to provide an

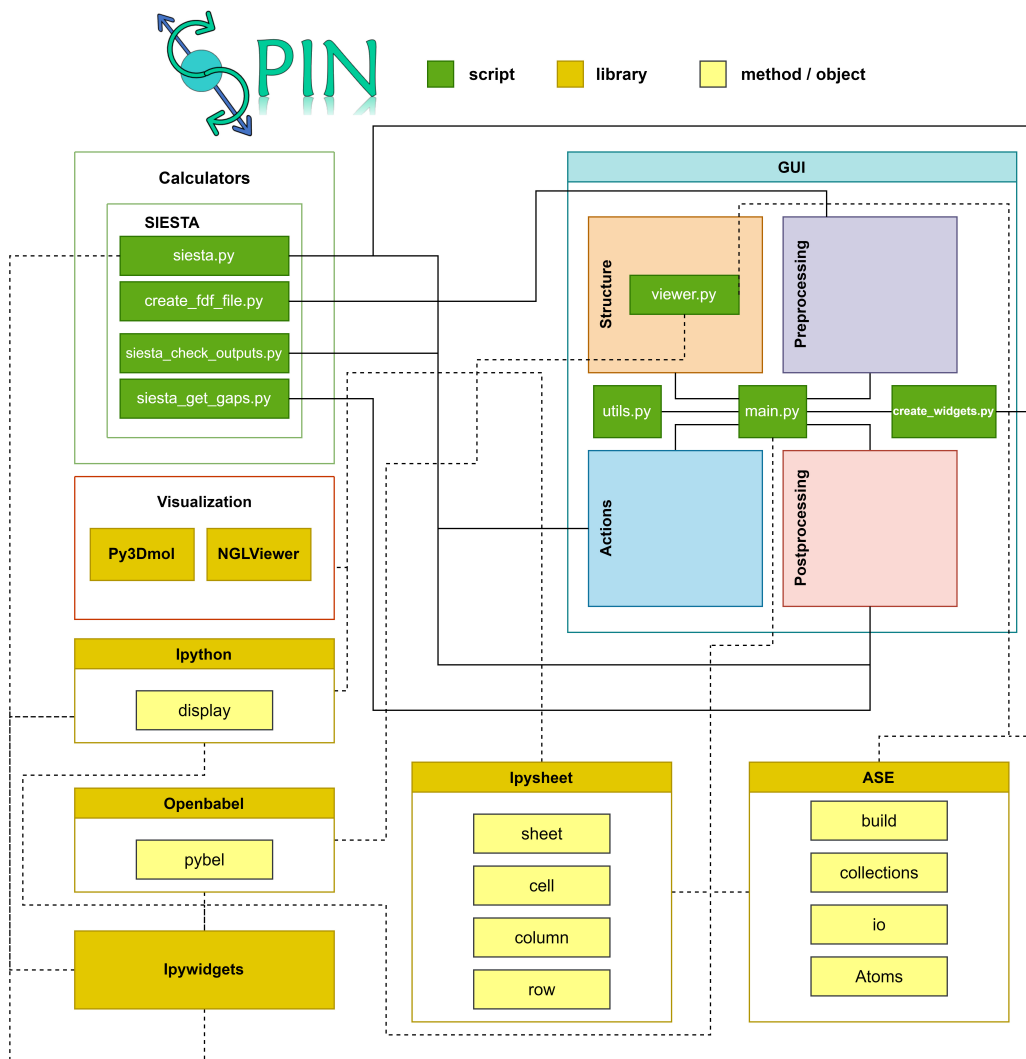


Figure 1: The interaction between SPIN and the main required packages.

intuitive, easy-to-use and fast-learning solution. In SPIN, fundamental elements in the atomic level simulation of materials, such as the construction and visualization of structures or systems and the pre-processing, execution, and post-processing of calculations are integrated. In its development, the Jupyter Notebook tool has been used. It is an open source project that can support multiple programming languages, including Python, the one in which this work is developed. As for the graphic elements of the simulation environment, they have been built using the widgets provided by the Ipywidgets library. These are objects that allow the building of interactive graphical user interfaces (GUI) in Jupyter notebooks. The Py3Dmol [14] and NGLview [15] libraries have also been integrated, which allows us to visualize, in an interactive way, the 3D molecules created in the interface. Relationships between SPIN scripts and the main packages are shown in Figure 1. The interface architecture is divided into four main components. The first one provides with a view of the structure, which can be created manually or updated from a file (all Openbabel [16] formats are supported). Also, it is possible to load some predefined molecules or build systems like bulks, nanotubes or nanoribbons. The second component provides with elements to introduce the calculation parameters and build the initial files (inputs), according to the core of the selected calculation (as commented, SIESTA package is used to implement the initial version). In the third component, the possibility of selecting and executing different types of calculations is implemented. For instance, structural relaxation, calculation of the band structure, density of states or optical properties. Finally, the fourth component allows to make fully customized plots of results obtained. All requirements for SPIN are given in Tab. 1.

2.2. Software functionalities

DFT calculations require some insight from the user on how the algorithm should treat the problem, e.g, which operators or parameters are appropriate or when is convergence achieved. In the following we shall discuss the different components in calculations with SPIN (also shown in the flow chart Figure 2). This beta version includes the three basic parts of SPIN for DFT calculations employing SIESTA code; i.e, *Geometric structure*, *Configure* (DFT parameters), and *Calculation* (control workflow).

2.2.1. Description of a geometric structure

The Geometric description has two tabs: Structure options and Viewer.

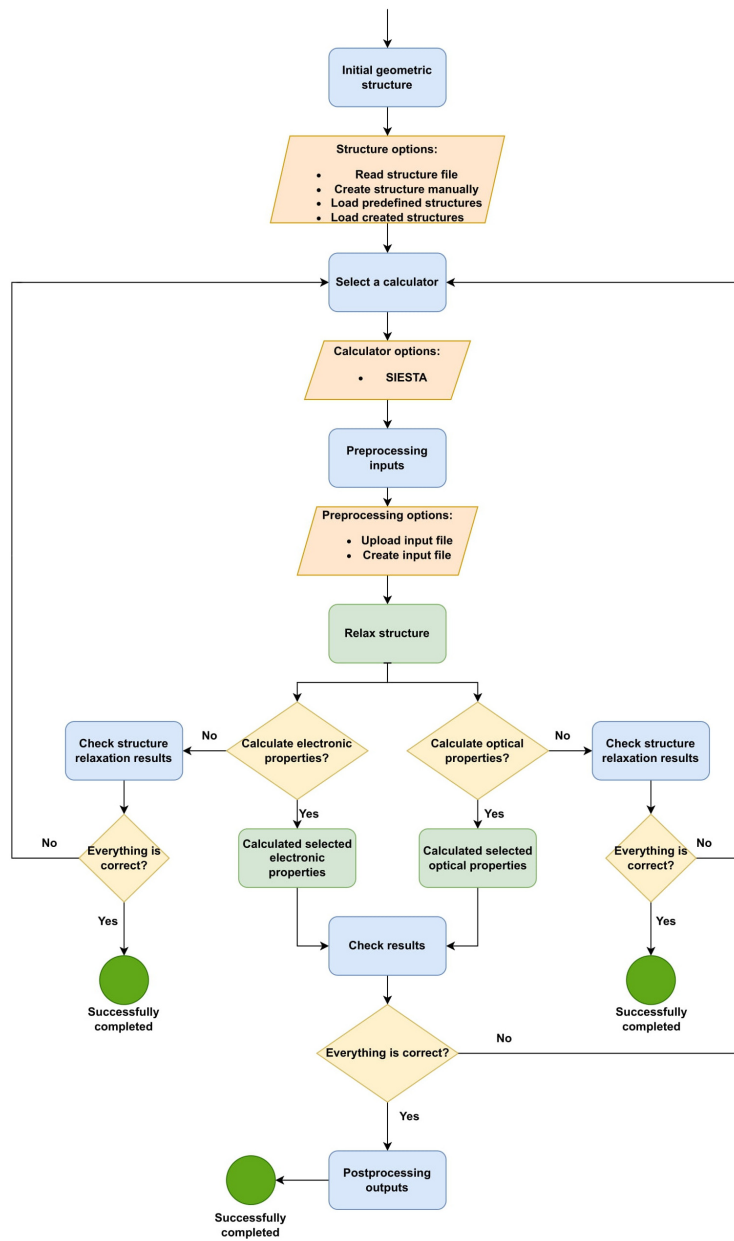


Figure 2: SPIN flow chart
6

Python library	Version
siesta	4.1.5
matplotlib	3.4.3
numpy	1.21.2
pandas	1.3.2
ase	3.22.0
openbabel	3.1.1
ipysheet	0.5.0
ipywidgets	7.5.1
py3dmol	1.7.0
nglview	3.0.3
ipyfilechooser	0.6.0
openpyxl	

Table 1: SPIN requirements

Structure options. Is the tab used to generate a first set of atomic coordinates. This tab includes four options:

- **Upload file:** Allows to load external structure files in the formats supported by Openbabel. The program supports SIESTA file formats *.fdf also.
- **Create structure manually:** This is the default option for entering atomic coordinates and unit cell vectors. Coordinates need to be included in Angstrom units.
- **Structures predefined:** Allows access to ase build options.
- **Load created structures:** This option gives the possibility of loading previously built structures.

Viewer. The viewer is only a preview of the made structure in this beta version.

2.2.2. Description of SIESTA parameters

In this section, the user can configure the DFT parameters for SIESTA calculations. There are two options:

- **Upload input file :** In this option, parameters from a previous *fdf* file can be reloaded. Only the parameters in fdf are read.

- **Create input file:** Setup of all basis DFT parameters. Also one may define the type of calculation. For this, four options are predefined:
 - **Relax structure:** This option is mandatory to run any other procedure, since it creates the file "label-relaxed.cif" that contains the equilibrium structure required for bands, DOS and optical calculations.
 - **Calculate Bands structure:** Defined the option to get the band structure for periodic systems.
 - **Calculate Total and Partial Density of states:** Giving the DOS and PDOS in the system. For PDOS, current beta version does not include a plotting facility.
 - **Calculate Optical properties:** Defined the option to get the optical properties for periodic systems.

2.2.3. Description of Control workflow and calculations

This section allows user to select and perform single or multiple calculations.

3. Illustrative example

3.1. Graphene

A complete review of graphene's electronic properties is written in [17]. The simple ways to obtain graphene in the laboratory together with its remarkable electronic, thermal, mechanical, and optical properties turn it into the most studied two-dimensional (2D) material [18]. This explosion of interest in graphene and the release of 2D materials matches an incredible growth of computational tools aimed at analyzing and characterizing their properties, and to predict new ones (even new 2D systems) [19]. The all computational tool density functional theory (DFT) stands out by its power for quantitatively predicting several properties of complex materials. Currently, there is access to many commercial and academic DFT implementations.

Graphene is a triangular lattice with two carbon atoms in the unit cell. The vector of the unit cell and the atomic positions of carbon atoms for graphene are given in the Table 2.

The geometric parameters of the unit cell can be included in SPIN-GUI. The first step is to activate the configuration and instantiate the App in a Jupyter Notebook, employing the following instructions:

Parameter	\hat{i}	\hat{j}	\hat{k}
\vec{a}	$\frac{3}{2}a_{cc}$	$\frac{\sqrt{3}}{2}a_{cc}$	0
\vec{b}	$\frac{3}{2}a_{cc}$	$-\frac{\sqrt{3}}{2}a_{cc}$	0
\vec{c}	0	0	15.
Atom _A	0	0	0
Atom _B	a_{cc}	0	0

Table 2: Geometric parameters of graphene unit cell. $a_{cc} = 1.44\text{\AA}$ represents the distance between two carbon atoms in the structure.

```

1 from spin import *
2 App = Spin()

```

Then, one may use module structure of the SPIN-GUI to build the desired one and define the unit cell. When running the `App.Structure()` command, four different options are available for structure building. These are: upload input file, create the structure manually, use any of SPIN predefined structures, or load already created SPIN structures (see figure 3 panel a). So, for the case of graphene, we are going to select the second option (create structure manually). The first step is to introduce how many atoms will be involved; that is, two in this example (figure 3 panel a). Once it is made, SPIN-GUI asks for the coordinates of each atom and the values of unit cell, as can be seen in figure 3 panel b. These values can be found in table 2. After the structure creation, the *Viewer* tab gives the possibility to visualize and edit the created graphene structure (see figure 4).

The next step is the creation of SIESTA input files, for which the only python command required is `App.preprocessing()`. When `App.preprocessing()` is called, SPIN-GUI shows some of the most used SIESTA parameters as inputs in *Create input file* tab. Besides, the end-user can select the kind of task to perform: obtaining structural optimization, determining the electronic band structure, calculating the density of states (DOS) and/or evaluating the optical properties. Any SIESTA parameter not found in the *Create input file* tab can be quickly and easily introduced in the *Additional parameters* tab. For graphene example, the structural and electronic properties have been studied by means of first principles calculations, within the framework of DFT, where localized single- ζ , single-polarized atomic orbitals are employed as basis set, together with norm-conserving pseudopotentials. The included exchange-correlation functional corresponds to the so-called generalized gradient approximation (GGA), using Perdew, Burke and Ernzerhof

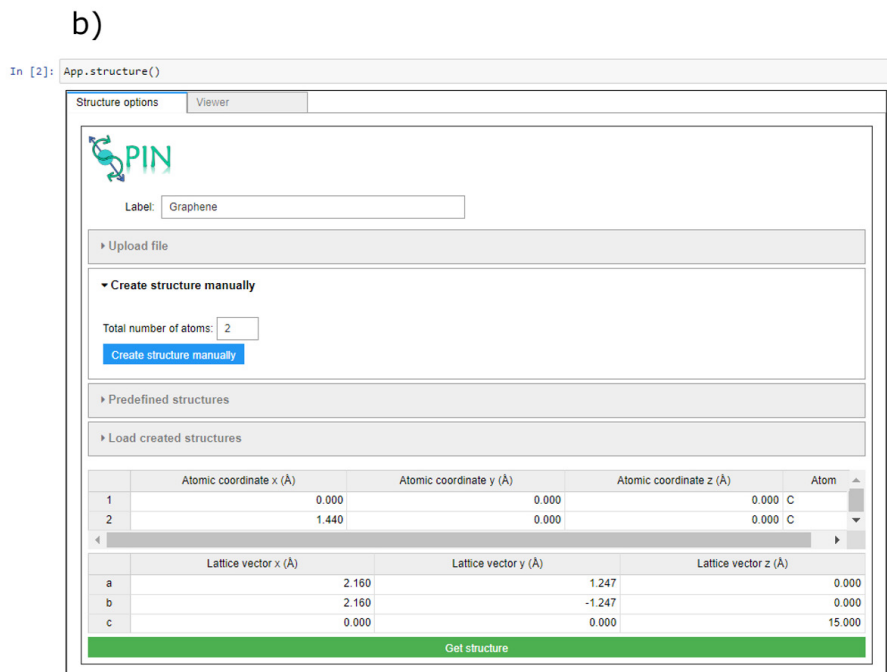
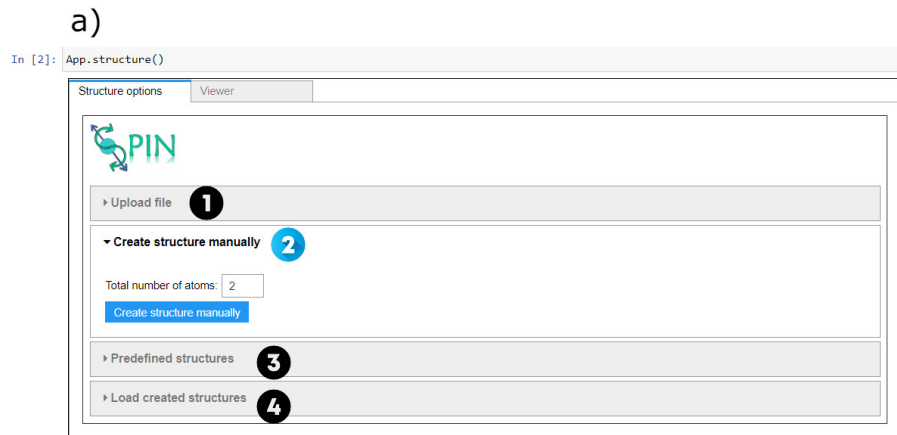


Figure 3: Structure tab of the GUI. It contains the Graphene creation example step by step.

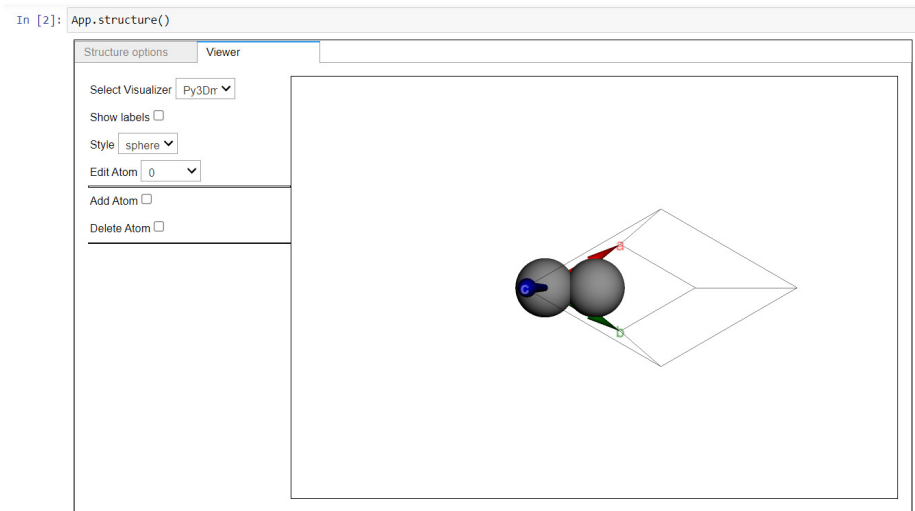



Figure 4: Viewer tab of the GUI.

description [20]. All structures are relaxed through the FIRE minimization algorithm. The criterion of convergence for the total energy is set as 10^{-4} eV per atom [21]. Integration over the reciprocal space for all surfaces was carried out using $81 \times 81 \times 1$ grids of special k-points within Monkhorst-Pack scheme for the geometry optimization procedures [22]. The value of Mesh cutoff used is 250 Ry. Calculation was carried out without the inclusion of spin-polarization. Additionally, "Relax structure" and "Calculate Band Structure" options were selected. The input files configuration can be seen in detail in figure 5. Once the inputs were completed, and "Make fdf" button was clicked, the folder containing graphene example job must have been created, and all the flow and outputs will be stored there.

When the input files and jobs are created, the user is able to perform selected calculations. To do this, the invocation of Calculations() is mandatory. As it can be seen in figure 6 panel a), end-user can choose one or multiple created jobs and, accordingly, one or multiple actions. In the latter case, execution is sequentially made. Pressing the "Run" button will start the selected calculations. As each of the processes ends, an initial basic report will be generated that allows the user to know in a general way some characteristics of the results, according to each type of calculation. For example, in figure 6 panel b), the result for Total Energy of the system after structural optimization can be found. In the case of band structure calcu-

App.preprocessing()



▼ SIESTA

siesta [Open SIESTA manual](#)

Upload input file (.fdf)

▼ Create input file

▼ DFT calcule control

Basis set: SZP

Mesh cutoff: 250 Ry

XC Functional and Author: GGA PBE

Energy shift: 0.02 Ry

Max. SCF iterations: 150

Mixing weight: 0.1

Number pulay: 5

Spin polarization: non-polarized

kgrid_Monkhorst_Pack: Gamma Enter kgrid_Monkhorst_Pack

81	0	0
0	81	0
0	0	1

Relax structure

Num CG steps: 200

Variable cell: True

Type of Run: FIRE

Max force tol [eV/Ang]: 0.04

Calculate Band structure

bandLineScale: ReciprocalLatticeVec

Do you want enter bandLines or bandPoints? bandLines bandPoints

```
%block BandLines
1 0.5000000000 0.000000000 0.0000  M
300 0.0000000000 0.000000000 0.0000  \Gamma
300 0.3333333333 0.333333333 0.0000  K
300 0.5000000000 0.500000000 0.0000  M
%endblock BandLines
```

%block BandPoints

writeKbands: false

writeBands: false

Calculate Total and Partial (projected) Density of States

Calculate Optical

Additional parameters

Make fdf

✓

Structure job was successfully created in ./calculations/Structure

[Do you want to download input file?](#)

Figure 5: Preprocessing tab of the GUI.

lation, information about band-gap value as well as a basic plot of energy band structure are presented. As it can be noticed, for graphene example, the resulting band-gap value is 0 and the band-structure plot remains very similar to that reported in previous studies [23-25].

4. Conclusion

SPIN is a new versatile tool for researchers who want to reduce the complexity of using DFT calculation code. Because it provides higher-level user interaction, it can also be used for educational purposes. SPIN is an Ipywidgets-based Interface that allows users to work efficiently in any operating system (Windows, Linux, and Mac) because it relies on Jupyter Notebooks. Within its environment, it is possible to work with standard SIESTA files and prepare figures of the atomic structure and other relevant features such as energy band spectrum, DOS, PDOS, and optical properties for publication. At the current stage, the core structure of SPIN deals with a completed pipeline using the SIESTA calculator. However, SPIN has been developed to add new functions and calculators easily. As the number of available new functionalities are added, SPIN will become an even more attractive toolbox contributing to the efficient development and utilization of electronic structure theory and molecular dynamics simulations. SPIN will also encourage and contribute to further collaborative efforts with the open exchange of data and results as well as efficient scripting to benefit the research community.


Declaration of competing interest

The authors declare that they have no known competing financial interests or personal relationships that could have appeared to influence the work reported in this paper.


Acknowledgments

The authors would like to thank Universidad de Medellín (UdeM) for supporting their work. JMV, EF, and JDC thank MINCIENCIAS, Colombia, for financial support of this research under contract 120680864729. MEMR acknowledges Mexican CONACYT for support through Grant CB 2017-2018 No. A1-S-8218.

a) # Press CTRL + ENTER or click run button
Calculations()



▼ SIESTA run



Select calculations folder (Default "Calculations"): No selection

Select calculations (Multiple values can be selected with shift + click):

<input type="text" value="CH3CH2O"/> <input type="text" value="Graphene"/>	<p>Select actions:</p> <input type="text" value="Graphene relax_structure"/> <input type="text" value="Graphene bands"/>
---	---

N° processors:

Siesta command:

Graphene: Relaxing Structure...

Job completed

Relax structure

System: Graphene Status:

Relaxed structure total energy: -308.093283 eV

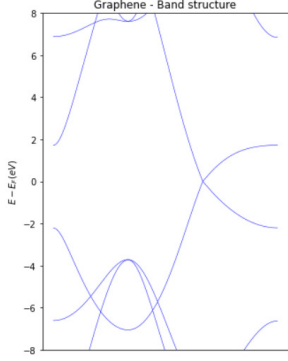
Graphene: Calculating bands Structure...

Job completed

Band structure

System: Graphene Status:

structure Band Gap value: 0



Graphene - Band structure

Kpoints

Figure 6: Calculations component of the GUI.

Data availability statement

The information here provided, together with the illustrative examples, can be found in the package for first version of SPIN. This version and possible newer ones can be downloaded from <https://github.com/JoseMVergara/SPIN>.

References

- [1] A. H. Larsen, J. J. Mortensen, J. Blomqvist, I. E. Castelli, R. Christensen, M. Dułak, J. Friis, M. N. Groves, B. Hammer, C. Hargus, et al., The atomic simulation environment—a python library for working with atoms, *Journal of Physics: Condensed Matter* 29 (27) (2017) 273002.
- [2] J. M. Soler, E. Artacho, J. D. Gale, A. García, J. Junquera, P. Ordejón, D. Sánchez-Portal, The SIESTA method for ab initio order-n materials simulation, *Journal of Physics: Condensed Matter* 14 (11) (2002) 2745–2779. doi:10.1088/0953-8984/14/11/302.
URL <https://doi.org/10.1088/0953-8984/14/11/302>
- [3] J. Enkovaara, C. Rostgaard, J. J. Mortensen, J. Chen, M. Dułak, L. Ferrighi, J. Gavnholt, C. Glinsvad, V. Haikola, H. Hansen, et al., Electronic structure calculations with gpaw: a real-space implementation of the projector augmented-wave method, *Journal of physics: Condensed matter* 22 (25) (2010) 253202.
- [4] P. Giannozzi, S. Baroni, N. Bonini, M. Calandra, R. Car, C. Cavazzoni, D. Ceresoli, G. L. Chiarotti, M. Cococcioni, I. Dabo, et al., Quantum espresso: a modular and open-source software project for quantum simulations of materials, *Journal of physics: Condensed matter* 21 (39) (2009) 395502.
- [5] G. Kresse, J. Furthmüller, Efficient iterative schemes for ab initio total-energy calculations using a plane-wave basis set, *Physical review B* 54 (16) (1996) 11169.
- [6] V. Wang, N. Xu, J.-C. Liu, G. Tang, W.-T. Geng, Vaspkit: a user-friendly interface facilitating high-throughput computing and analysis using vasp code, *Computer Physics Communications* (2021) 108033.

- [7] N. Papior, J. L. B., pfebrer, T. Frederiksen, S. S. Wuhl, zerothi/sisl: v0.11.0 (Feb. 2021). doi:10.5281/zenodo.4544334.
URL <https://doi.org/10.5281/zenodo.4544334>
- [8] T. Kluyver, B. Ragan-Kelley, F. Pérez, B. E. Granger, M. Bussonnier, J. Frederic, K. Kelley, J. B. Hamrick, J. Grout, S. Corlay, et al., Jupyter notebooks—a publishing format for reproducible computational workflows., in: ELPUB, 2016, pp. 87–90.
- [9] U. Herath, P. Tavadze, X. He, E. Bousquet, S. Singh, F. Muñoz, A. H. Romero, Pyprocar: A python library for electronic structure pre/post-processing, *Computer Physics Communications* 251 (2020) 107080.
- [10] S. P. Ong, W. D. Richards, A. Jain, G. Hautier, M. Kocher, S. Cholia, D. Gunter, V. L. Chevrier, K. A. Persson, G. Ceder, Python materials genomics (pymatgen): A robust, open-source python library for materials analysis, *Computational Materials Science* 68 (2013) 314–319.
- [11] S. Sozykin, Gui4dft—a siesta oriented gui, *Computer Physics Communications* 262 (2021) 107843.
- [12] S. B. Lisesivdin, B. Sarikavak-Lisesivdin, gpaw-tools—higher-level user interaction scripts for gpaw calculations and interatomic potential based structure optimization, *Computational Materials Science* 204 (2022) 111201.
- [13] F. Marchesin, P. Koval, Y. Pouillon, I. Lebedeva, A. García, M. García-Mota, A. Kimmel, Atomistic simulation advanced platform (asap) for materials modelling with ab initio methods, Psi-k conference 2022, Lausanne (Switzerland), abstract book. (2022).
- [14] N. Rego, D. Koes, 3dmol.js: molecular visualization with webgl, *Bioinformatics* 31 (8) (2015) 1322–1324.
- [15] H. Nguyen, D. A. Case, A. S. Rose, Ngview—interactive molecular graphics for jupyter notebooks, *Bioinformatics* 34 (7) (2018) 1241–1242.
- [16] N. M. O’Boyle, M. Banck, C. A. James, C. Morley, T. Vandermeersch, G. R. Hutchison, Open babel: An open chemical toolbox, *Journal of cheminformatics* 3 (1) (2011) 1–14.

- [17] A. C. Neto, F. Guinea, N. M. Peres, K. S. Novoselov, A. K. Geim, The electronic properties of graphene, *Reviews of modern physics* 81 (1) (2009) 109.
- [18] K. S. Novoselov, L. Colombo, P. Gellert, M. Schwab, K. Kim, et al., A roadmap for graphene, *nature* 490 (7419) (2012) 192–200.
- [19] J. Paul, A. Singh, Z. Dong, H. Zhuang, B. Revard, B. Rijal, M. Ashton, A. Linscheid, M. Blonsky, D. Gluhovic, et al., Computational methods for 2d materials: discovery, property characterization, and application design, *Journal of Physics: Condensed Matter* 29 (47) (2017) 473001.
- [20] J. P. Perdew, K. Burke, M. Ernzerhof, Generalized gradient approximation made simple, *Physical review letters* 77 (18) (1996) 3865.
- [21] E. Bitzek, P. Koskinen, F. Gähler, M. Moseler, P. Gumbsch, Structural relaxation made simple, *Physical review letters* 97 (17) (2006) 170201.
- [22] H. J. Monkhorst, J. D. Pack, Special points for brillouin-zone integrations, *Physical review B* 13 (12) (1976) 5188.
- [23] P. V. Medeiros, S. Stafström, J. Björk, Effects of extrinsic and intrinsic perturbations on the electronic structure of graphene: Retaining an effective primitive cell band structure by band unfolding, *Physical Review B* 89 (4) (2014) 041407.
- [24] D. Kienle, J. I. Cerda, A. W. Ghosh, Extended hückel theory for band structure, chemistry, and transport. i. carbon nanotubes, *Journal of applied physics* 100 (4) (2006) 043714.
- [25] G. Gui, J. Li, J. Zhong, Band structure engineering of graphene by strain: First-principles calculations, *Physical Review B* 78 (7) (2008) 075435.

4. Impact of different structural defects on fundamental properties of blue phosphorene nanotubes



Contents lists available at ScienceDirect

Computational Condensed Matter

journal homepage: www.elsevier.com/locate/cocom



Impact of different structural defects on fundamental properties of blue phosphorene nanotubes

J.M. Vergara^a, M.E. Mora-Ramos^b, J.D. Correa^{a,*}, E. Flórez^{a,*}

^a Facultad de Ciencias Básicas, Universidad de Medellín, Medellín, Colombia

^b Centro de Investigación en Ciencias-IICBA, Universidad Autónoma del Estado de Morelos, Av. Universidad 1001, C.P. 62209, Cuernavaca, Morelos, Mexico

ARTICLE INFO

Keywords:

Blue-phosphorene
DFT
Nanotubes
Optical response

ABSTRACT

Using density functional theory, we present the effect of different structural defects on electronic and optical properties of blue phosphorene nanotubes of both armchair and zigzag chirality. In addition, we have considered the influence of an applied electric field on the electronic states of either pristine and defect-laden structures. The main defective features considered are double vacancies and Stone–Wales defects, although results with these imperfections are, as well, compared with those arising when single vacancies of two types are regarded. The possible transition from semiconducting to metal-like behavior induced by the applied field for large enough zigzag nanotubes is predicted. Deviations of the optical response of defective systems compared to the pristine case are mainly revealed for the visible range and above, with an evident quantitative anisotropy related to the specific polarization of the incident light: parallel or perpendicular to the nanotube growth direction. This characterization of structural defects and their effects on the optoelectronic properties of blue phosphorene nanotubes is required to define how the surface of the nanotubes could be utilized to develop new optoelectronic devices.

1. Introduction

The successful isolation of graphene in 2004 [1] opened a broad field of research on two-dimensional (2D) materials so that today there is a large set of synthesized and theoretically proposed systems of this kind [2–4]. These have fascinating properties that endow them with great potential to be used in numerous industrial applications such as small molecule sensors, flexible/low power electronics, spintronic devices, optoelectronic applications in photonics, photovoltaics, and plasmonics, batteries, supercapacitors, and thermoelectric energy applications [5]. Among 2D materials, phosphorene, since its successful isolation in 2014, has unleashed enormous scientific activity in the field of materials due to its remarkable electronic properties [6,7]. Phosphorene has several allotropes as black phosphorene, red phosphorene, green phosphorene, and blue phosphorene (BP). In particular, BP is a single-layer allotrope of phosphorus that was predicted to be thermally and dynamically stable in 2014 [8], and was recently synthesized (2018) [9,10]. BP is a semiconductor of the indirect bandgap. Due to its characteristics and the possibility of tuning its electronic and dielectric properties, studies have been carried out to use them in applications such as optoelectronics and nanoscale devices that require of specific bandgap [11].

2D materials can be manipulated to form nanotubes (NTs). Nanotubes are a class of one-dimensional (1D) materials whose thickness varies depending on the 2D material from which they come. The nanotubes have unique properties, for example, high hardness, mechanical resistance, and flexibility. Also, nanotubes have optoelectronic properties that can be modulated through their diameter, allowing nanotubes to have potential applications in microelectronics, photovoltaic energy, gas detection, infrared photodetection, photocatalyst, and applications in biomedicine [12–28]. On the other hand, due to the importance of a better knowledge of the optical properties of the nanotubes and their possible use in new optoelectronic devices, several studies have been reported [29–32]. In the case of phosphorus nanotubes, they show asymmetric optical properties concerning the polarization direction. That is, zigzag tubes show very weak reflectivity for parallel polarization while, in contrast, the armchair tube displays high reflectivity. This shows a dependence between optical properties and chirality [30].

Two dimensional nanostructures as well as nanotubes usually suffer from various types of topological imperfections during their growth. Experiments and theory have demonstrated that the existence vacancies and Stone–Wales defects in the nanostructures have a significant influence on the mechanical and electronic properties, allowing to achieve new features and expand the range of applications for the material [33,

* Corresponding authors.

E-mail addresses: jcorrea@udemedellin.edu.co (J.D. Correa), elflorez@udemedellin.edu.co (E. Flórez).

<https://doi.org/10.1016/j.cocom.2022.e00701>

Received 1 March 2022; Received in revised form 21 April 2022; Accepted 30 May 2022

[34]. Expanding on some examples, Zhou et al. [35], investigated the effects of monovacancies, divacancies, Stone–Wales defects (SW), and octagon–pentagon pair defects in carbon nanotubes (CNTs) with zigzag chirality (ZZ). As a consequence of the presence of vacancies and the defect of the octagon–pentagon pair, the bandgap of the nanotube becomes reduced. In contrast, the SW defect induces an opening of the bandgap in CNTs. Besides, with the increasing defect concentration, there is a decrease in the bandgap, which causes CNTs to change from a semiconductor to a metallic system. Regarding phosphorene, Sorokin and Zhang studied the effect of monovacancies and divacancies on the mechanical properties of black phosphorene nanotubes (PNTs) [36]. According to their findings, vacancies in armchair (AM) PNTs and mono-vacant in zigzag(ZZ) PNTs have the lowest vacancy energy, decreasing with tube diameter in AMPNTs and increasing in ZZPNTs. Aierken et al. [37] showed in their work that blue phosphorene is advantageous to make small NTs. Research on phosphorene nanotubes is limited comparatively with carbon nanotubes. Nevertheless, these kinds of structures have attracted great interest in recent decades due to the urgent demand for tubular electronics, and their favorability towards adsorption and sensing of several molecules; for example, heptachlor, usually present in contaminated water [28]. This fact emphasizes the importance of research on phosphorene nanotubes, given their electronic and optical properties [38].

In our previous work [39], we investigated the effects of monovacancies (or single-vacancies) (SV) on the electronic structure of BPNTs. There, we considered two different types of SV in our calculation, called type A (SV-A) and type B (SV-B). Compared to blue phosphorene nanotubes, which exhibit fundamental bandgap values between one and two electron-volts, in the case of individual atomic vacancies (SV), the incorporation of spin polarization helps to identify the induction of localized mid-gap states in BPNTs. The energy difference between the highest near valence and lowest near conduction localized states is approximately 0.5 eV. Furthermore, increasing the concentration of individual vacancies leads to the formation of additional bands that change the energy gap of the system. This phenomenon would indicate that structural defects have a substantial impact on the electronic properties of nanotubes.

Another possibility to modulate the properties of nanosystems is the application of external electromagnetic probes on the structures. For example, Ospina et al. [40] investigated the effect of external electric fields in the optical and electronic properties of blue-phosphorene nanoribbons. They found that, for all systems, the energy band gap decreases as the electric field strength is augmented, and detected a transition of the electronic spectrum from semiconducting to metallic character. This phenomenon could be employed to develop new tunable optoelectronic devices. In addition, their theoretical results for the imaginary part of the dielectric function show that the interband linear optical response of blue phosphorene nanoribbons is also affected by changes in the electronic properties due to the influence of the applied electric field. For CNTs, Tien et al. [41] have shown that the bandgap modulation of semiconducting CNTs with monovacancy defect can be easily achieved by applying a transverse electric field, and found that the band structure of defective CNTs vary quite differently from that of the pristine nanotube, and strongly depends on the applied direction of the transverse electric field.

Despite great deals of theoretical efforts, there are still certain untreated aspects regarding the BPNTs. One of them is the influence of imperfections like divacancies and Stone–Wales defects on the electronic features of these nanosystems. Thus, in the present work, we aim to investigate such an influence and report on the properties of the energy states in the presence of defect sites in the BPNT structure. Besides, we investigate the effect of an external electric field in the properties of pristine BPNTs, BPNTs with monovacancies and double-vacancies, and BPNTs with Stone–Wales defects; and, secondly, we analyzed the optical properties of these nanosystems. Our study is based on first-principles density-functional theory (DFT) calculations.

To study the effect of an electric field on the electronic structure of the systems and to demonstrate the influence of atomic defects on the properties of BPNTs, we report the band structure and the band gaps of a semiconducting BPNT with a mono-vacancy, double-vacancy and Stone–Wales defect under a transverse electric field based on calculations. The reader will find some remarks on the methodology employed in the next section of the article. Then, Section 3 will contain the presentation and discussion of the obtained results, and, finally, the conclusions of the work will appear in Section 4.

2. Computational details and model constructing

The calculation of structural and electronic properties is performed within the framework of DFT, as it is implemented in the *ab initio* SIESTA package [42], where localized double- ζ and polarized atomic orbitals are employed as a basis set in addition to using norm-conserving pseudopotentials. We use a $1 \times 1 \times 5$ supercell. As exchange and correlation functional, we consider a GGA in the approximation of Perdew, Burke, and Ernzerhof (PBE) [43]. All structures are relaxed using the FIRE minimization algorithm until the forces on the atoms are less than 0.04 eV/\AA [44]. The Brillouin zone is sampled using a $1 \times 1 \times 2$ Monkhorst–Pack grid. A MeshCutoff value of 350 Ry is taken. Besides, the study is carried out without the inclusion of spin polarization for DV and SW defects.

The optical properties are determined within the framework of the independent particle approximation, through the imaginary part of the dielectric function, which is given by [45]:

$$\epsilon_{2,\sigma}(\omega) = \left(\frac{2\pi e}{m\omega} \right)^2 \sum_{c,v} |M_{(c,\sigma),(v,\sigma)}|^2 \delta(E_{c,\sigma} - E_{v,\sigma} - \hbar\omega), \quad (1)$$

where, the indices c and v represent the respective sets of quantum numbers associated with the energy state of the conduction and valence band, respectively, including $\sigma = \uparrow, \downarrow$ for the z component of the spin. $M_{(c,\sigma),(v,\sigma)}$ describes the corresponding element of the electric dipole moment matrix. In practice, the energy conservation is guaranteed with a Gaussian function with HWHM equal to 0.06 eV . We considered two polarization of the incident light: x and z directions (perpendicular and parallel to nanotube growth direction, respectively). In order to ensure the convergence of the optical absorption spectrum we have used a k -grid points of $1 \times 1 \times 101$.

The total imaginary part of the dielectric function is given finally by

$$\epsilon_2 = \epsilon_{2,\uparrow} + \epsilon_{2,\downarrow} \quad (2)$$

Having obtained ϵ_2 , with the use of the Kramers–Krönig relations, its real part, $\epsilon_1(\omega)$, is evaluated. With the knowledge of the entire dielectric function, it is possible to derive other optical properties as functions of frequency. A relevant quantity in this sense, given the feasibility of its experimental measurement, is the index of refraction. It can be evaluated from:

$$n(\omega) = \frac{1}{\sqrt{2}} \left[\epsilon_1(\omega) + \sqrt{\epsilon_1^2(\omega) + \epsilon_2^2(\omega)} \right]^{1/2}. \quad (3)$$

BPNT structures can be seen as rolled up blue-phosphorene monolayer (BPML) and, in a similar way to carbon nanotubes [46], can be twined on different directions. In this report, we consider the so-called achiral nanotubes, on which the rolling line goes along the zigzag and armchair direction of the monolayer. In addition, the unit cell of the BPNTs is determined by the chiral and translation vectors, which are given by $\vec{C}_h = n\vec{a}_1 + m\vec{a}_2$, and $\vec{T} = u\vec{a}_1 + v\vec{a}_2$ respectively; where \vec{a}_1 and \vec{a}_2 are the BPML unit cell vectors –Details about the determination of geometric structure of BPML and BPNTs are given in the supplementary material–. The geometric and electronic structure of BPNTs is characterized by a couple of indices, (n, m) . In accordance, for achiral zigzag blue-phosphorene nanotubes (ZZ-BPNTs) $m = 0$, while for armchair blue-phosphorene nanotubes (AM-BPNTs) $n = m$ (see panel (a)

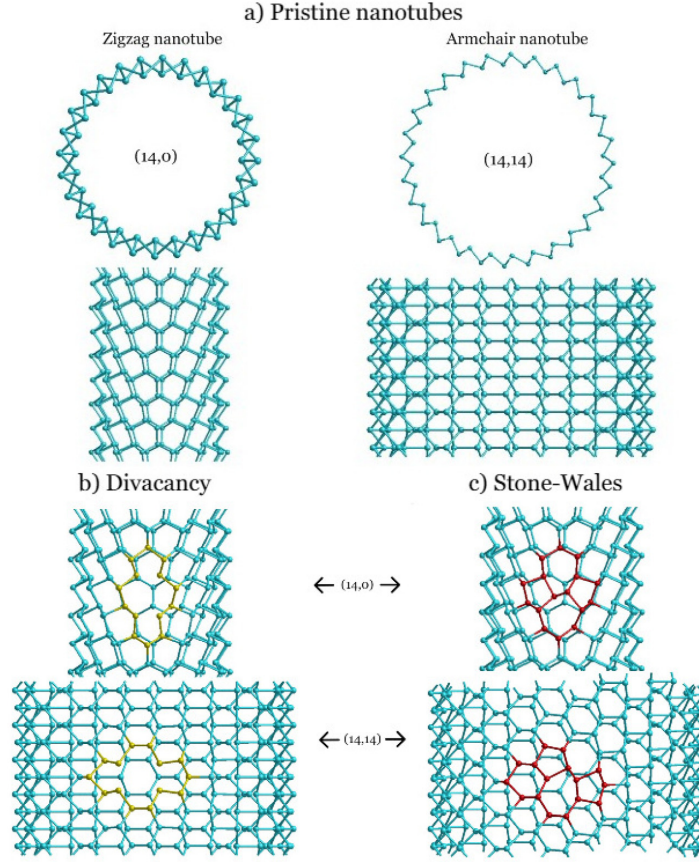


Fig. 1. Panel (a) contains transversal (top) and longitudinal (bottom) views of the (14,14) armchair and (14,0) zigzag pristine BPNTs. Panels (b) and (c) show a schematic view of double-vacancy and Stone-Wales defects of (14,0) and (14,14) BPNTs, respectively.

from Fig. 1). As n and m increase, the diameter of the BPNTs augments. Unlike carbon nanotubes, BPNTs have two radii, determined by the buckling of phosphorus atoms in the original BPML.

As mentioned, we investigate the effects of structural defects in the nanostructures. In particular, we shall study both double-vacancies (DVs) -which can be constructed by removing a pair of adjacent atoms-, and Stone-Wales defects (SWs) -which is formed by rotating a $P-P$ bond in the hexagonal network by 90° . A graphical view of these imperfections is seen in panels (b) and (c) of Fig. 1. Our previous results on pristine BPNTs and BPNTs with two different single vacancies [39] will be presented as well, in order to contrast and identify the influence that such defects have on the electronic properties of the material. Eight different nanotube sizes for both armchair and zigzag configurations, going from $n = 7$ to $n = 14$ are considered, for all studied systems.

3. Results and discussion

3.1. Electronic properties

The value of formation energy (see Table S1) for all defects considered is obtained from the equation $E_F = E_{\text{defect-total}} - n_p E_p$, where $E_{\text{defect-total}}$ is the total energy of the defective structure, and E_p is the total energy of the perfect nanotube divided by the total number of atoms in it. Besides, n_p is the number of phosphorus atoms in defective BPNT. Single vacancies' formation energies are between 2.526 and

2.013 eV, depending on the size of BPNT radius. These values are in agreement with previous results for the formation energy of SV on a blue phosphorene monolayer, with a formation energy of 2.380 eV [33]. For DV, the formation energy lies between 2.888 and 1.901. These values are in concordance with the report for BP of 2.850 eV [33]. For SW defect, the formation energies are between 0.159 and 1.353 eV. This energy range is rather long and suggests that SW defect is the most favorable from the energetic point of view, similar to the case of BP where formation energy of SW defect is 1.600 eV.

For pristine BPNTs are structurally optimized and their electronic band structure is calculated [39]. Then, defects of the single-vacancy (SV) [39], double-vacancy (DV), and Stone-Wales types are assumed. In each of the cases, energy dispersion relations are obtained for a $1 \times 1 \times 5$ supercell, such that the Brillouin Zone is folded. To analyze the effect of DV and SW defects on the electronic properties of BPNTs, we present in Fig. 2 the energy band structures for pristine (panels (a) and (b)) BPNTs to contrast with the energy band structures of DV (panels (c) and (d)) and SW (panels (e) and (f)) for both, armchair and zigzag systems with n varying between 7 and 14. To complement the analysis of electronic structure of pristine and defective SW BPNTs, Fig. 3 shows the projected density of states (PDOS) for pristine and DV SW BPNTs. The PDOS is considered over the s , p_x , and p_z orbitals. For all BPNTs, it is possible to observe that, for valence states, the contribution of p_x orbital to the density of states is more significant than the other ones; which is expected since p_x and p_y orbitals are

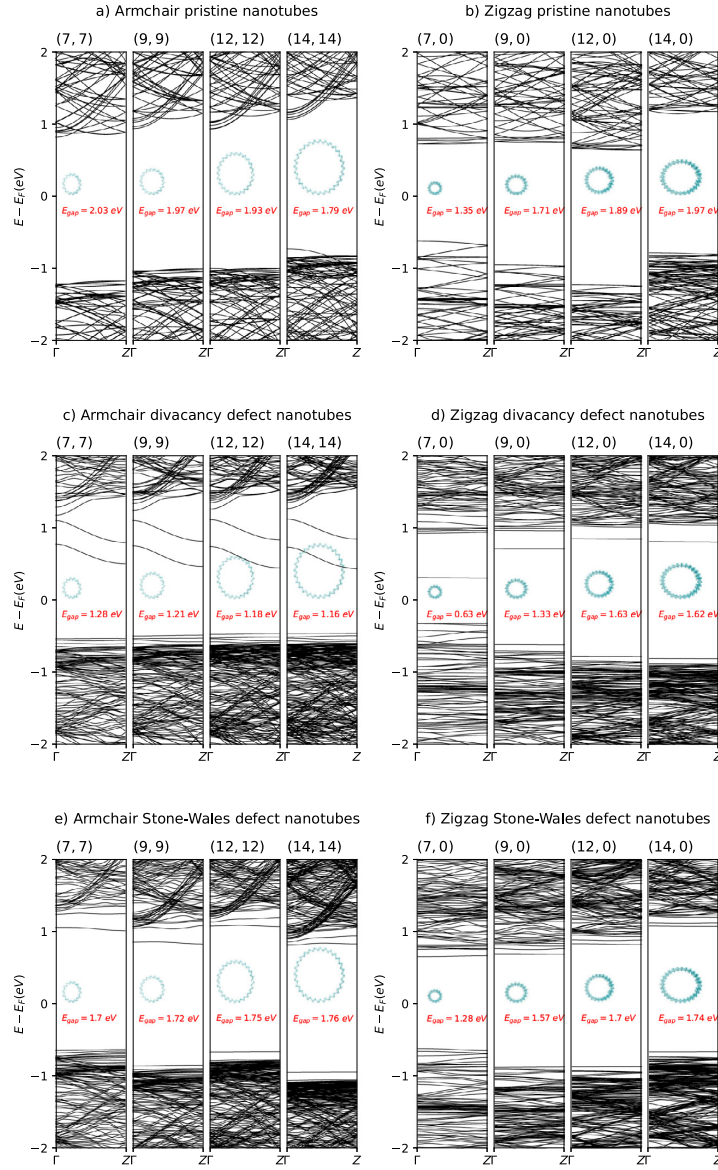


Fig. 2. Band structure of a–b Pristine c–d DV and e–f SW BPNTs for n equal to 7, 9, 12 and 14 for armchair and zigzag chiralities. The red label corresponds to band-gap value. (For interpretation of the references to color in this figure legend, the reader is referred to the web version of this article.)

the leading causes of the atomic bonds. However, for the conduction states, one may observe matched contributions from p_x and p_z ones. This behavior is probably due to the hybridization of p orbitals, induced by the buckling present in blue-phosphorene. Besides, the curvature of BPNTs could increase orbital hybridization, which is observed for small diameters nanotube. This behavior is independent of the nanotube chirality. For defective nanotubes, for example, nanotube with a DV, the PDOS show similar nature to the pristine case, but some contributions coming from localized states induced into the energy gap are observed, in concordance with the band structure in Fig. 2.

All the calculated BP nanotubes showed indirect band-gaps, which is consistent with the planar monolayer BP characteristics. It can be noticed that, for both SW and DV defects for ZZ-BPNTs the induced

band-gap states are dispersionless, indicating their local nature. In the case of AM-BPNTs, for DV systems, the associated states appearing within the original band-gap show strong dispersion for conduction bands, together with quasi-flat valence band ones. This has to do with the smaller size of the translation vector in the structure geometry (recall that is approximately half of the ZZ-BPNT translation vector one). In SW case, AM-BPNTs show a small dispersion, which is very similar to what was observed in ZZ chirality. Another fact we can observe is that the band structures of SW systems remain very similar to the pristine ones.

About size of the nanotubes (see Figs. 2 and 4), it can be observed that there is not a noticeable influence on the band structure of any of the defects analyzed (DV and SW) since, as long as the radius of

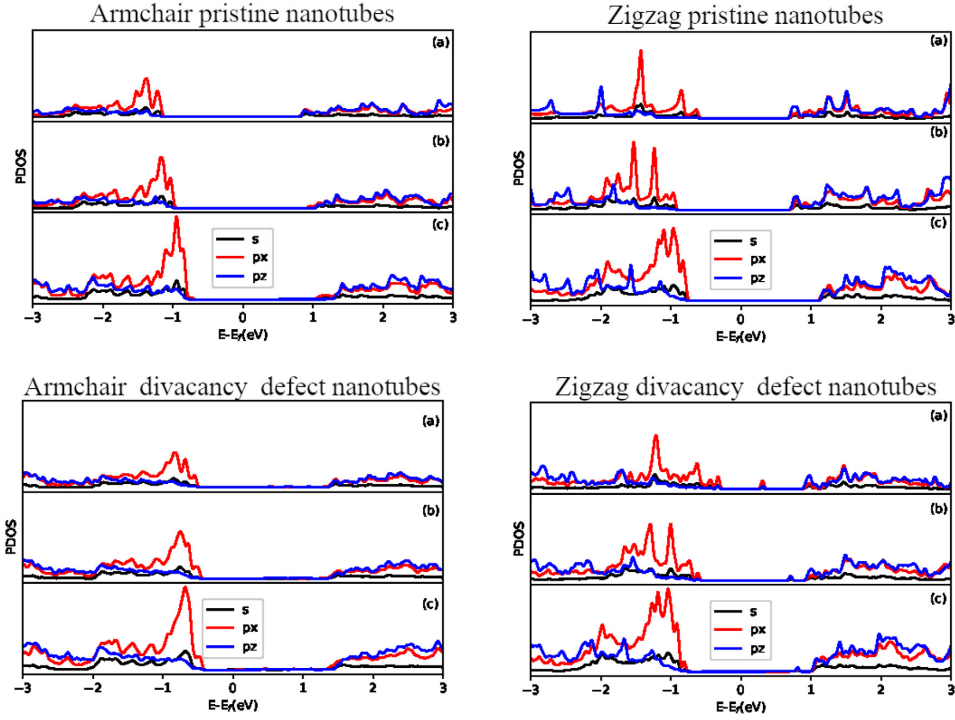


Fig. 3. Project density of states of pristine and DV SW BPNTs phosphorene nanotubes for n equal to 7 (a), 9(b), and 14(c) for armchair and zigzag chiralities. The s , p_x , and p_z orbitals are considered.

the nanotube increases, the band structure remains very similar to the previous one, a phenomenon observed in both chiralities (AM and ZZ), the smaller ZZ-BPNTs being the only notable exception.

The dependence of band gap on size and chirality for BPNTs with various structural defects is shown in Fig. 4. Interestingly, the band gap of the zigzag systems progressively increases with the increase of radius. It can be seen that for almost all systems (except SV-A) the band gap is rapidly increasing until a determined size, above which we observe smaller changes with the increase of radius. However, the armchair systems exhibit a different trend, the band gap values remain almost constant in all systems and have minimal changes – in one sense or the other –, which points to no significant dependence between size and band gaps for these particular systems.

Analyzing the band gap values for the different types of structural imperfections, we can observe that all defects have some effect on the band gap value. Actually, all structures have a smaller band gap compared to pristine BPNTs with the same radius and chirality. One may conclude that SW defects have the least effect, since these systems present the least change with respect to pristine nanotubes. In DV defects case, the band gap values for AM systems are approximately 50% lower while they lead to an average decrease of 18% in ZZ systems. The most notable effect on the band gap values is the one coming from structures having single-vacancies of both types, A and B, whose presence reduces them significantly as we can see from Fig. 4. We can conclude, then, that vacancies induce a decreasing of band gap. The same effect can be seen in the study carried out by Zhou, et al. [35] on (8, 0) and (14, 0) zigzag carbon nanotubes. Like the results obtained for the BPNTs, the systems with SW type defects undergo smaller changes in the band gap with respect to the pristine nanotubes. However, a difference can be seen in the influence of each point defect on the band gap of these systems: in the case of carbon nanotubes, structures with DV defects experienced a greater reduction in their band

gap than systems with SV, a phenomenon contrary to that observed for BPNTs.

“The strain engineering significantly modifies the optical absorption in the visible light, while the effect of the external electric field on the optical properties is weak. Our results will be helpful to design the electro-optical devices based on monolayer materials with MH band”. “Such significant changes in the electronic properties under external excitations show that multilayered GaN shows promise in configurable nanoelectronic devices” Furthermore, its charge carrier mobilities are significantly higher than the other popular 2D semiconductors, e.g., MoS2 and phosphorene. Therefore, this 2D-BN material could have huge application potentials in the electronics and solar energy conversion fields Compared to the isolated arsenene and SnS2 monolayers, the arsenene/SnS2 heterostructure has the enhanced optical absorption from visible to ultraviolet region, especially possessing the absorption peak up to 35.1

3.2. Effect of external electric field on electronic properties

Due that the general form of the band structure of BPNT is not stronger affected by the radius of the nanotube, as was discussed in the previous section, it was decided to present only the results corresponding to the smallest and biggest nanotubes in all the studied systems; i.e., NTs with $n = 7$ and $n = 14$. In order to study the effect of external electric field on blue-phosphorene nanotubes, band structure calculations were performed under various transverse electric field – oriented along the $+x$ direction, specifically – intensities, ranging between 0.1 V/\AA and 0.6 V/\AA . In Figs. 5 and 6 we show the obtained electronic band structure and the related density of states for the cases of biggest AM and ZZ pristine, type-A and type-B SV, DV, and SW defect. Calculations for both SV types were performed with the

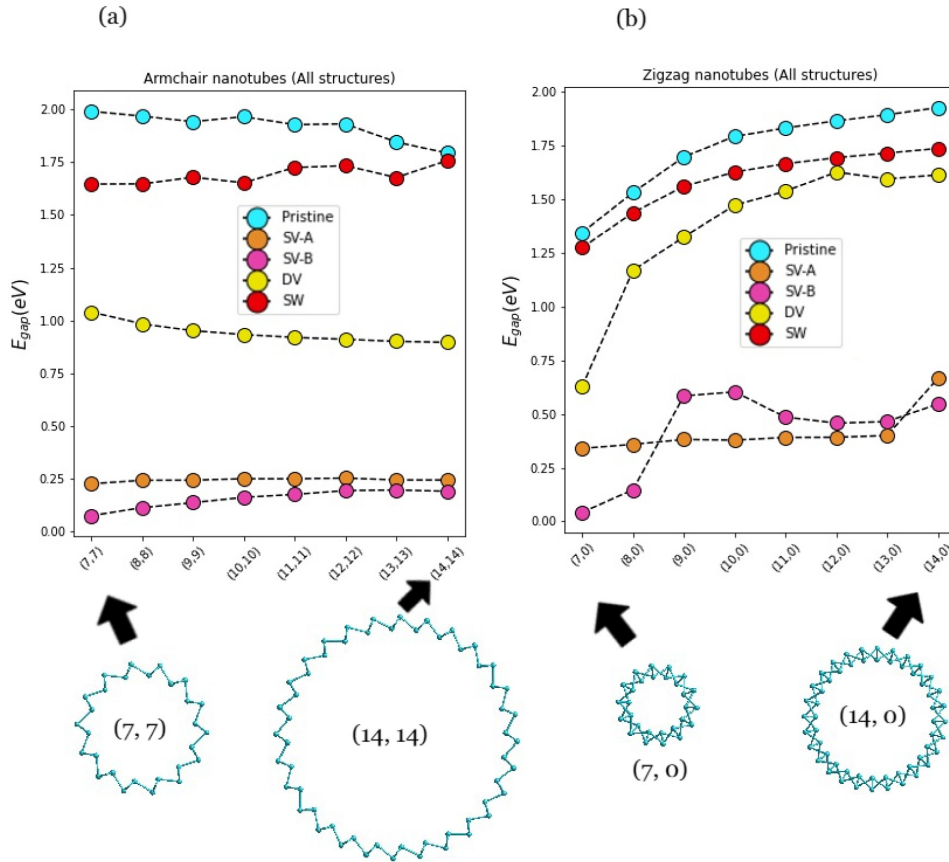


Fig. 4. Variation of the band-gap in blue phosphorene nanotubes of both armchair and zigzag geometries, calculated as a function of the size for: pristine (cyan) [39], and type-A single-vacancy (orange) [39], type-B single-vacancy (magenta) [39], double-vacancy (yellow) and Stone–Wales defect (red) imperfect structures. (For interpretation of the references to color in this figure legend, the reader is referred to the web version of this article.)

inclusion of spin-polarization, as can be realized by observing the spin-resolved DOS in each case. We left the analogous results for smallest nanotube size to be presented on supporting material (figures S1 and S2)

According to what is shown in the band structure plots for pristine and defect-laden systems (see Figs. 5 and 6), there is a trend towards a semiconductor-to-metal transition – indicated by a significant reduction of the energy band gap – induced by the strengthening electric field. The conclusions derived from results obtained for the largest NT radii, with regard to the effect of this external probe on their electronic properties, can be extended for all systems: There exists a great dependence with the size and chirality of nanotube. It has been seen that the biggest structures, i.e., systems with $n = 14$ require lower field strength to approach the semiconductor–metal transition, in comparison with smaller structures. In fact, either pristine or imperfect AMBPNTs reach the metallic condition for sufficiently intense applied field, with the pristine, DV and SW cases becoming metals already at relatively small probe strength; and SV-laden systems needing stronger fields for the transition. In contrast, structures with ZZ chirality require higher fields to reduce the energy band gap close to zero. Actually, in neither of the smaller ZZ systems a transition of that kind was reached; that is, the systems remained as semiconductors.

The above mentioned effect of an applied electric field on energy band gap of BPNTs can be better noticed by observing Fig.S3. There, we plot the calculated gaps for the cases with smallest and largest NT radii,

considering pristine and the distinct defect-laden structures involved. Some particular phenomena can be observed:

- The semiconductor–metal transition in armchair structures (panels (a) and (b)) takes place regardless the vacancy or defect type. Transitions to a metallic system occur, in general, at lower values of field intensity. Smaller NTs with ZZ chirality (panels (c) and (d)) do not become metallic even for the highest field strengths, no matter the kind of imperfection considered. Band gaps have little variation, with a slight decrease in the pristine, SW and DV cases; and a very weak growth when SVs are included. Zigzag BPNTs having $n = 14$ show a trend towards metallic character for high enough applied fields, except for those bearing SV-A. For the latter complex, a minimum close to zero appears at the value of 0.5 V/\AA , and then the band gap increases. Nevertheless, such particular behavior does not prevent us from concluding that the degree of band gap modification under the same electric field is more significant when nanotubes radii increase, similar to results obtained for zigzag Boron nitride nanotubes (BNNTs) reported by Chegel and Behzad [47].
- The band gap variations are quite different between the systems. For pristine, and defective nanotubes with DV and SW imperfections, when the applied field grows stronger, the variations of energy gaps are very similar from a given field strength. However, for SV-A and SV-B, the decay of this quantity with the increase

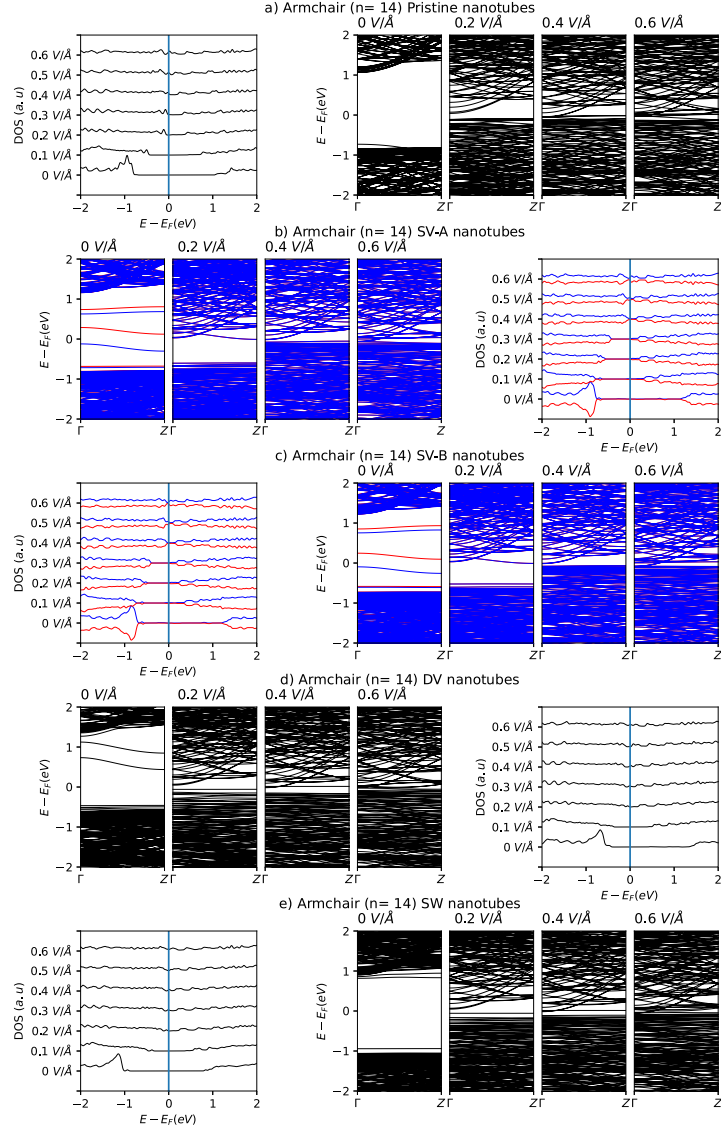


Fig. 5. Effect of electric field on energy band structure and density of states of pristine and different structural defect types on blue-phosphorene nanotubes for the biggest Armchair nanotube ($n = 14$) system. For band structure plots, values of 0, 0.2, 0.4 and 0.6 $\text{V}/\text{\AA}$ electric field intensity are considered.

of field strength is faster than for the other systems, indicating a strong effect associated to the vacancy defect. Furthermore, the band-gap changes for the two single-vacancy models share a similar trend, even though the exact values of the band gaps under various strengths of the external transverse field are different indeed. This behavior, observed in pristine and single vacancy BP nanotubes is similar to that shown by CNTs when an external electric field is applied along the $+x$ direction, according to the results obtained by Tien et al. [41], in a study carried out for (10,0) zigzag CNTs, as well as the results shown by Kim et al. [48] in (5,5) armchair CNTs.

In general, the electric field effect on the energy gap of defective BPNTs resembles – in some cases, closely – the corresponding behavior of pristine NTs. The results come closer as long as the applied field

intensity grows enough. In all, it is possible to say that a strong enough electric field acts in a way that changes the coupling between atomic orbitals responsible for the energy spectrum of the structures, with this interaction to be somewhat affected by the presence of defects in the system.

3.3. Optical properties

The analysis of optical response of the systems under consideration goes through the calculation of the frequency-dependent dielectric function $\epsilon(\omega) = \epsilon_1(\omega) + i\epsilon_2(\omega)$. It is an essential quantity to understand the various optical properties. To provide a view on this phenomenon, calculations were performed for the largest and smallest structures involved: AM and ZZ type nanotubes with $n = 7$ and $n = 14$, always

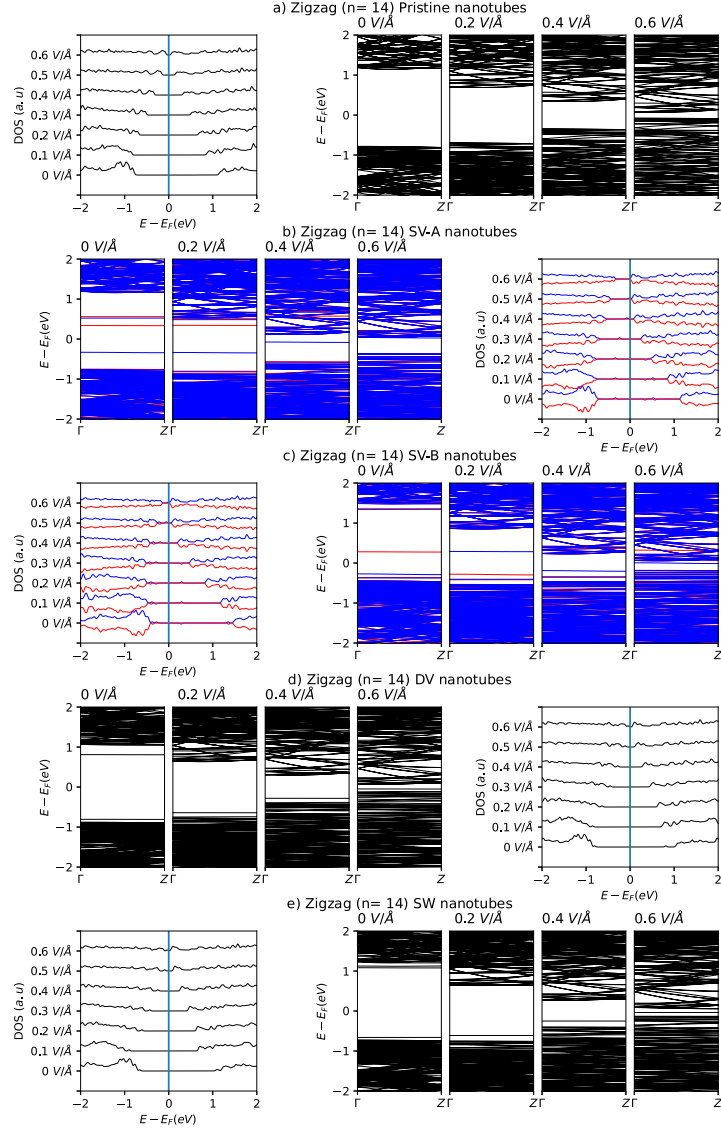


Fig. 6. Effect of electric field on energy band structure and density of states of pristine and different structural defect types on blue-phosphorene nanotubes for the biggest Zigzag nanotube ($n = 14$) system. For band structure plots, values of 0, 0.2, 0.4 and 0.6 V/Å electric field intensity are considered.

comparing with the corresponding quantity in the pristine NT case. Two different polarizations of the incident light were considered: one is perpendicular to NT growth direction, and the other is parallel to it. In accordance, Fig. 7 show the imaginary part of the frequency-dependent dielectric function (for corresponding real part see Fig. S6 in supplementary material).

Distinctions regarding the particular incident polarization can be readily observed. They appear to be more pronounced in the case of ZZ-BPNTs. However, noticeable changes from one kind of system to another cannot be observed, except for pristine NTs, for which both minima and resonant peaks at energies $\gtrsim 3$ eV exhibit quite different amplitudes, something that will reflect in the index of refraction as will be commented below. It is worth to highlight a low-energy feature that the SV-B produces in the armchair structure under perpendicular

incident polarization. It clearly departs from the remaining cases, indicating the contribution from valence-to-conduction band transitions around the main energy band gap, as can be noticed from Fig. 6(a,b). Comments along the same lines can be given when analyzing the real part of the dielectric function.

To provide a more detailed discussion, we choose as representative system the case of $\epsilon_2(\omega)$ with light field oriented along the z -axis. In the parallel (\parallel) direction for pristine BPNTs, a rather wide absorption band in the region from ~ 2 eV to > 6 eV is observed (see cyan curve in Fig. 7), this implies that the light within such an energy range will be strongly absorbed by the pristine case. After introducing defects, the absorption edges are shifted to a lower energy range compared with that of pristine BPNTs. That is, single vacancies (SV-A and SV-B), divacancies and Stone–Wales defect systems (with smaller changes) all make the optical absorption edges generate a slight redshift phenomenon. For the $\epsilon_2(\omega)$

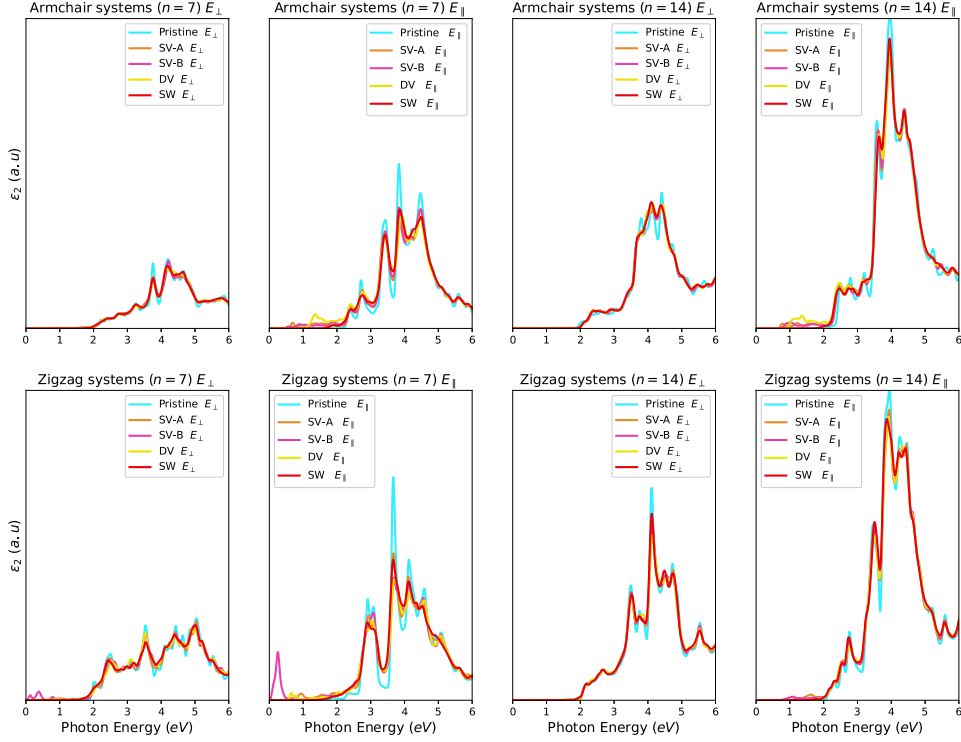


Fig. 7. The imaginary part of the dielectric function of smallest and biggest ($n = 7$ and $n = 14$ respectively) pristine and defective blue phosphorene nanotubes systems as a function of the incident photon energy. The calculation includes two distinct polarizations of the incident photons: E_{\parallel} corresponds to light polarized along the direction parallel to, and E_{\perp} to light polarized perpendicular to the BPNT growth direction. Curves for the different defective systems are identified.

spectra along the perpendicular x direction, the absorption edges of SV-A, SV-B and DV in the smallest zigzag systems ($n = 7$) are below 1.5 eV, indicating a redshift phenomenon. Nevertheless, the edges of all other evaluated systems are nearly the same as each other for ~ 2 eV. In all cases, the response for parallel and perpendicular polarizations of the incident light show the main peaks in the ultraviolet region (above 3.3 eV) which denotes the inter-band optical transitions between remote conduction and valence bands. Besides, in all defective systems considered, absorption peaks become weaker in both, perpendicular and parallel polarization configurations.

Fig. 8 contains the refractive index calculated, as a function of the incident photon energy, from the real and imaginary parts of the dielectric function. Again, the two previously mentioned light polarizations are considered. There is a clear quantitative anisotropy between the components of this measurable quantity belonging to parallel and perpendicular orientations of the light field, with the greater values associated to the parallel one. In addition, results for defective BPNTs differ from their values in the pristine case mostly in the energy range above 2 eV, where oscillations in $n(\omega)$ reveal larger amplitude for pristine structures. Values of refraction index are higher for the bigger ($n = 14$) NTs and they are largest in the particular AM chirality.

By focusing attention on the low-energy interval, it is seen that there are practically no quantitative differences between the defective and pristine cases, except for the DV case – for energies below 2 eV – in the AM structures (for which the static value $n(0)$ is essentially the same in all cases)-, and for SV-B systems in the ZZ ones, which raise $n(0)$ above the pristine and other defect-laden BPNTs. The latter situation appears only in the $n = 7$ size and is more pronounced for parallel light polarization; but, in general, values of the static index of refraction tend to coincide for all structures when their size is larger.

The effect of the external electric field on the optical properties of pristine and defective BPNTs has been considered as well. In supplementary material Figs S4 and S5, the imaginary part of the dielectric function appears depending on the field intensity for all studied cases. Results suggest that the external electric field only significantly affects the optical response of the AMBPNT $n=14$ with parallel polarization of the incident light. This reveals through a field-induced transition on the infrared region of the spectrum, just for the highest values of field strength considered. This behavior is in accordance with the observed electronic structure of all investigated systems. One of the forms to characterize the optical response is to evaluate the refractive index. In Table S2, the static refractive index is reported together with its value at 2.1 eV—energy that corresponds to the yellow line of sodium, which is a usual reference in optical measurements. Our results suggest that the refractive index shows variation concerning the polarization of incident light, but the presence of structural defects does not induce significant changes in this quantity. In general, when an external electric field is applied, values of static refractive index and frequency-dependent indices of refraction show small changes. The exception is found, however, for AMBPNT $n=14$, for which static refractive index shows a rather large increase as the external electric field strengthens. This behavior is especially observed for incident light polarized parallel to the BPNT growth direction, and may be related with a field-induced enhancement of the expected value of interband electric dipole moment under near-zero gap conditions.

4. Conclusion

We have investigated electronic structures of $n = 7$ to $n = 14$ armchair and zigzag blue phosphorene nanotubes with various types

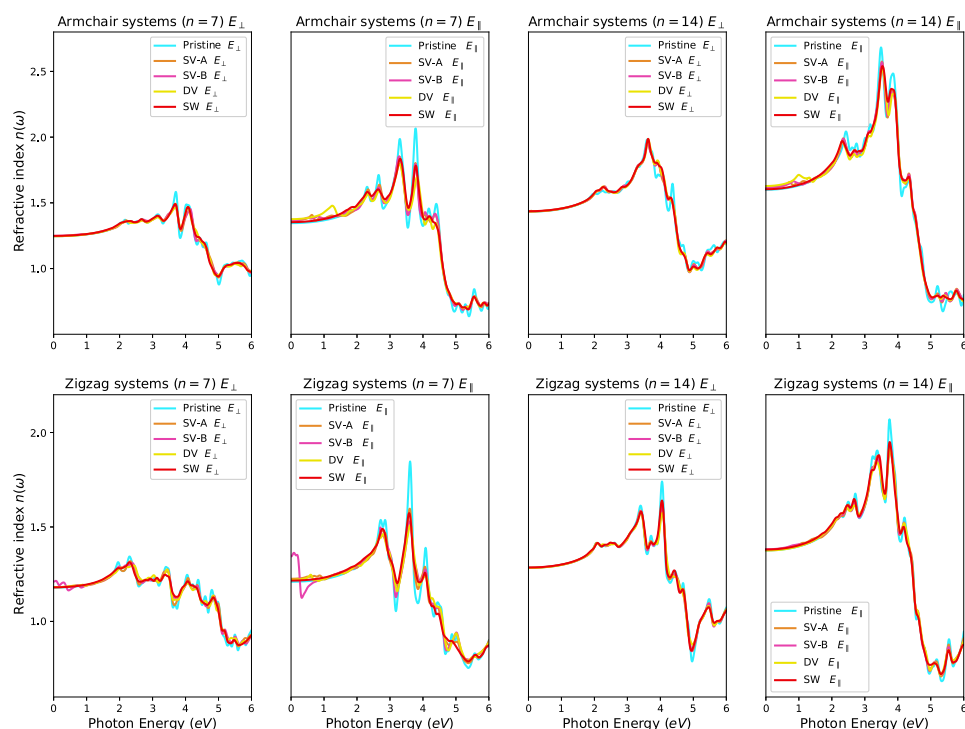


Fig. 8. The refractive index of smallest and biggest ($n = 7$ and $n = 14$ respectively) pristine and defective blue phosphorene nanotubes as a function of the incident photon energy. The calculation includes two distinct polarizations of the incident photons: E_{\parallel} corresponds to light polarized along the direction parallel to, and E_{\perp} to light polarized perpendicular to the BPNT growth direction. Curves for the different defective systems are identified.

of defects, including, double-vacancy and Stone-wales defect, and the effect of applied external electric field on it, by using the first-principles calculations in the density-function theory. Our results indicate that all vacancy defect types induce a decreasing in the BPNTs band gap. Besides, the effect of single-vacancies in reducing the system band gap is stronger in both, zigzag and armchair, compared to other types of defects, reaching a value 90% lower in the armchair systems compared with pristine nanotubes and 65% in those of the zigzag types.

When an external electric field is applied on the structures, we have observed that bigger systems requires lower field strengths to reach the semiconductor-metal transition. This transition does exist regardless of the vacancy defect type on armchair systems, which makes the armchair chirality more favorable to achieve it. We can also conclude that both single-vacancy systems (type-A and type-B) require lower electric field values to become a metallic material, compared with other all systems.

With regard to the optical properties, we have revealed an anisotropy linked to the particular incident light polarization to be either parallel or perpendicular to the nanotube growth direction. Besides, the differences in values of the calculated index of refraction, related with the presence or absence of defects, are noticeable mainly within the visible range and above, whilst static values remain practically the same for larger nanotubes and only show deviations in smaller zigzag nanotubes laden with type B single vacancies.

Declaration of competing interest

The authors declare that they have no known competing financial interests or personal relationships that could have appeared to influence the work reported in this paper.

Data availability

Data will be made available on request.

Acknowledgments

Authors thanks Minciencias to financial support of this research by contract 120680864729. MEMR is grateful to Mexican Conacyt for support through Grant A1-S-8218 (Ciencia Básica 2017–2018).

Appendix A. Supplementary data

Supplementary material related to this article can be found online at <https://doi.org/10.1016/j.cocom.2022.e00701>.

References

- [1] K.S. Novoselov, A.K. Geim, S.V. Morozov, D. Jiang, Y. Zhang, S.V. Dubonos, I.V. Grigorieva, A.A. Firsov, Electric field effect in atomically thin carbon films, *Science* 306 (5696) (2004) 666–669.
- [2] G.R. Bhimanapati, Z. Lin, V. Meunier, Y. Jung, J. Cha, S. Das, D. Xiao, Y. Son, M.S. Strano, V.R. Cooper, et al., Recent advances in two-dimensional materials beyond graphene, *ACS Nano* 9 (12) (2015) 11509–11539.
- [3] L. Wang, P. Hu, Y. Long, Z. Liu, X. He, Recent advances in ternary two-dimensional materials: synthesis, properties and applications, *J. Mater. Chem. A* 5 (44) (2017) 22855–22876.
- [4] B. Xu, S. Qi, M. Jin, X. Cai, L. Lai, Z. Sun, X. Han, Z. Lin, H. Shao, P. Peng, et al., 2020 Roadmap on two-dimensional materials for energy storage and conversion, *Chin. Chem. Lett.* 30 (12) (2019) 2053–2064.
- [5] N.R. Glavin, R. Rao, V. Varshney, E. Bianco, A. Apte, A. Roy, E. Ringe, P.M. Ajayan, Emerging applications of elemental 2D materials, *Adv. Mater.* 32 (7) (2020) 1904302.

- [6] J. Pang, A. Bachmatiuk, Y. Yin, B. Trzebicka, L. Zhao, L. Fu, R.G. Mendes, T. Gemming, Z. Liu, M.H. Rummeli, Applications of phosphorene and black phosphorus in energy conversion and storage devices, *Adv. Energy Mater.* 8 (8) (2018) 1702093.
- [7] A. Yang, D. Wang, X. Wang, D. Zhang, N. Koratkar, M. Rong, Recent advances in phosphorene as a sensing material, *Nano Today* 20 (2018) 13–32.
- [8] Z. Zhu, D. Tománek, Semiconducting layered blue phosphorus: a computational study, *Phys. Rev. Lett.* 112 (17) (2014) 176802.
- [9] W. Zhang, H. Enriquez, Y. Tong, A. Bendounan, A. Kara, A.P. Seitsonen, A.J. Mayne, G. Dujardin, H. Oughaddou, Epitaxial synthesis of blue phosphorene, *Small* 14 (51) (2018) 1804066.
- [10] J.L. Zhang, S. Zhao, S. Sun, H. Ding, J. Hu, Y. Li, Q. Xu, X. Yu, M. Telychko, J. Su, et al., Synthesis of monolayer blue phosphorus enabled by silicon intercalation, *ACS Nano* 14 (3) (2020) 3687–3695.
- [11] R. Swaroop, P. Ahluwalia, K. Tankeshwar, A. Kumar, Ultra-narrow blue phosphorene nanoribbons for tunable optoelectronics, *RSC Adv.* 7 (5) (2017) 2992–3002.
- [12] V.N. Popov, Carbon nanotubes: properties and application, *Mater. Sci. Eng. R* 43 (3) (2004) 61–102.
- [13] V.V. Pokropivny, Non-carbon nanotubes (review). Part 2. Types and structure, *Powder Metall. Metal Ceram.* 40 (11–12) (2001) 582–594.
- [14] A.L. Ivanovskii, Non-carbon nanotubes: synthesis and simulation, *Russ. Chem. Rev.* 71 (3) (2002) 175–194.
- [15] M. Endo, T. Hayashi, Y.A. Kim, H. Muramatsu, Development and application of carbon nanotubes, *Japan. J. Appl. Phys.* 45 (6R) (2006) 4883.
- [16] N. Govindaraju, R. Singh, Chapter 8—synthesis and properties of boron nitride nanotubes, in: *Nanotube superfiber materials*, William Andrew Publishing, Oxford, 2014.
- [17] N.M. Bardhan, 30 Years of advances in functionalization of carbon nanomaterials for biomedical applications: a practical review, *J. Mater. Res.* 32 (1) (2017) 107–127.
- [18] Z. He, Y. Jiang, J. Zhu, Y. Li, L. Dai, W. Meng, L. Wang, S. Liu, Phosphorus doped multi-walled carbon nanotubes: An excellent electrocatalyst for the VO₂⁺/VO₂⁺ redox reaction, *ChemElectroChem* 5 (17) (2018) 2464–2474.
- [19] E. Kianfar, Recent advances in synthesis, properties, and applications of vanadium oxide nanotube, *Microchem. J.* 145 (2019) 966–978.
- [20] F. Dvorak, R. Zazpe, M. Krbal, H. Sopha, J. Prikryl, S. Ng, L. Hromadko, F. Bures, J.M. Macak, One-dimensional anodic TiO₂ nanotubes coated by atomic layer deposition: Towards advanced applications, *Appl. Mater. Today* 14 (2019) 1–20.
- [21] E.S. Goda, M. Gab-Allah, B.S. Singu, K.R. Yoon, Halloysite nanotubes based electrochemical sensors: A review, *Microchem. J.* 147 (2019) 1083–1096.
- [22] G. Rahman, Z. Najaf, A. Mehmood, S. Bilal, S.A. Mian, G. Ali, et al., An overview of the recent progress in the synthesis and applications of carbon nanotubes, *C—J. Carbon Res.* 5 (1) (2019) 3.
- [23] V. Sorkin, Y. Zhang, Mechanical properties of phosphorene nanotubes: a density functional tight-binding study, *Nanotechnology* 27 (39) (2016) 395701.
- [24] J. Hao, Z. Wang, Q. Jin, DFT Study of structural, elastic, electronic and dielectric properties of blue phosphorus nanotubes, *Sci. Rep.* 9 (1) (2019) 1–8.
- [25] R. Bhuvaneshwari, V. Nagarajan, R. Chandiramouli, Molecular interaction of oxytetracycline and sulfapyridine on blue phosphorene nanotubes: A first-principles insight, *Phys. Lett. A* 394 (2021) 127198.
- [26] J. Hao, Z. Wang, Y. Wang, Computational investigation of lithium intercalation in single-walled zigzag blue phosphorene nanotubes, *Chem. Phys.* 550 (2021) 111297.
- [27] M. Jyothi, V. Nagarajan, R. Chandiramouli, Interaction studies of dichlobenil and isoproturon on square-octagon phosphorene nanotube based on DFT frame work, *Chem. Phys. Lett.* 778 (2021) 138773.
- [28] J.P. Maria, V. Nagarajan, R. Chandiramouli, Chemosensing nature of black phosphorene nanotube towards C₁₄H₉Cl₅ and C₁₀H₅Cl₇ molecules—A first-principles insight, *Comput. Theor. Chem.* 1196 (2021) 113109.
- [29] C. Li, Z. Xie, Z. Chen, N. Cheng, J. Wang, G. Zhu, Tunable bandgap and optical properties of black phosphorene nanotubes, *Materials* 11 (2) (2018) 304.
- [30] T. Hu, A. Hashmi, J. Hong, Geometry, electronic structures and optical properties of phosphorus nanotubes, *Nanotechnology* 26 (41) (2015) 415702.
- [31] H. Kataura, Y. Kumazawa, Y. Maniwa, I. Umezu, S. Suzuki, Y. Ohtsuka, Y. Achiba, Optical properties of single-wall carbon nanotubes, *Synth. Met.* 103 (1–3) (1999) 2555–2558.
- [32] X. Wan, J. Dong, D. Xing, Optical properties of carbon nanotubes, *Phys. Rev. B* 58 (11) (1998) 6756.
- [33] M. Sun, J.-P. Chou, A. Hu, U. Schwingenschlogl, Point defects in blue phosphorene, *Chem. Mater.* 31 (19) (2019) 8129–8135.
- [34] F. Safari, M. Fathipour, A.Y. Goharizi, Electronic and transport properties of blue phosphorene in presence of point defects: A first-principles study, *Physica E* 118 (2020) 113938.
- [35] Q.-X. Zhou, C.-Y. Wang, Z.-B. Fu, Y.-J. Tang, H. Zhang, Effects of various defects on the electronic properties of single-walled carbon nanotubes: A first principle study, *Front. Phys.* 9 (2) (2014) 200–209.
- [36] V. Sorkin, Y. Zhang, Effect of vacancies on the mechanical properties of phosphorene nanotubes, *Nanotechnology* 29 (23) (2018) 235707.
- [37] Y. Aierken, O. Leenaerts, F.M. Peeters, Defect-induced faceted blue phosphorene nanotubes, *Phys. Rev. B* 92 (10) (2015) 1–7.
- [38] C. Li, Z. Xie, Z. Chen, N. Cheng, J. Wang, G. Zhu, Tunable bandgap and optical properties of black phosphorene nanotubes, *Materials* 11 (2) (2018) 304.
- [39] J. Vergara, E. Flórez, M. Mora-Ramos, J. Correa, Effects of single vacancy on electronic properties of blue-phosphorene nanotubes, *Mater. Res. Express* 7 (1) (2020) 015042.
- [40] D. Ospina, C. Duque, M. Mora-Ramos, J. Correa, Effects of external electric field on the optical and electronic properties of blue phosphorene nanoribbons: A DFT study, *Comput. Mater. Sci.* 135 (2017) 43–53.
- [41] L.-G. Tien, C.-H. Tsai, F.-Y. Li, M.-H. Lee, Band-gap modification of defective carbon nanotubes under a transverse electric field, *Phys. Rev. B* 72 (24) (2005) 245417.
- [42] J.M. Soler, E. Artacho, J.D. Gale, A. Garcia, J. Junquera, P. Ordejón, D. Sánchez-Portal, The SIESTA method for ab initio order-n materials simulation, *J. Phys.: Condens. Matter* 14 (11) (2002) 2745–2779.
- [43] J.P. Perdew, K. Burke, M. Ernzerhof, Generalized gradient approximation made simple, *Phys. Rev. Lett.* 77 (18) (1996) 3865.
- [44] E. Bitzek, P. Koskinen, F. Gähler, M. Moseler, P. Gumbsch, Structural relaxation made simple, *Phys. Rev. Lett.* 97 (17) (2006) 170201.
- [45] E.A. Zuluaga-Hernández, E. Flórez, L. Dorkis, M.E. Mora-Ramos, J.D. Correa, Opto-electronic properties of blue phosphorene oxide with and without oxygen vacancies, *Int. J. Quantum Chem.* 120 (2) (2020) e26075.
- [46] M. Dresselhaus, G. Dresselhaus, R. Saito, Physics of carbon nanotubes, *Carbon* 33 (7) (1995) 883–891.
- [47] R. Chegel, S. Behzad, Effects of an electric field on the electronic and optical properties of zigzag boron nitride nanotubes, *Solid State Commun.* 151 (3) (2011) 259–263.
- [48] C. Kim, B. Kim, S.M. Lee, C. Jo, Y.H. Lee, Effect of electric field on the electronic structures of carbon nanotubes, *Appl. Phys. Lett.* 79 (8) (2001) 1187–1189.

5. Adsorption affinity of Sulfonamides onto Blue-phosphorene nanotubes

Adsorption affinity of Sulfonamides onto Blue-phosphorene nanotubes

J. M. Vergara^a, J. D. Correa^{a,*}, E. Flórez^{a,*}

^a*Facultad de Ciencias Básicas, Universidad de Medellín, Medellín-Colombia*

Abstract

The efficiency of (14, 14) armchair and (14, 0) zigzag based blue phosphorene nanotube (BPNT) to identify and remove three popular toxic antibiotics – Sulfanilamide (SAM), Sulfadimethoxine (SMX), and Sulfadiazine (SDZ) – from the water bodies were studied using density functional theory calculations. Analyzed molecules are weakly adsorbed on the pristine BPNTs with adsorption energy of about $-0,312$, $-0,285$ and $-0,377$ eV. Further, the electronic properties of the fundamental and antibiotics-adsorbed BPNT are investigated. The effect of single-vacancy BPNTs on the adsorption affinity of antibiotic molecules was studied. Compared with pristine systems, despite the increase in the reactivity of the zigzag BPNTs to the sulfonamides, armchair configurations show a transition from bipolar-magnetic semiconductor to not magnetic metallic system, suggesting that defective armchair BPNTs also can be employed as a sensor for antibiotic molecules, besides single-vacancies increases the E_{ads} values of all evaluated systems by up to 89% indicating an improvement in the capacity of BPNTs to adsorbed biologically active sulfonamide-based compounds like SAM, SDZ, and SMX.

Keywords: Blue-phosphorene nanotubes, Antibiotics, Sulfonamides, Density functional theory, Adsorption affinity

*Corresponding author

Email addresses: jcorrea@udemedellin.edu.co (J. D. Correa),
elflorez@udemedellin.edu.co (E. Flórez)

1. Introduction

Sulfonamide molecules constitute an important class of drugs, comprising several types of pharmacological agents that possess antibacterial, antiviral, anticonvulsant, diuretic, protease inhibitors, cyclooxygenase 2 (COX2) inhibitor, anticancer activities, and others [1]. Sulfonamide antibiotics are produced in large quantities and are widely used in human therapy and livestock production. As a result, more and more pharmaceutical residues from sewage effluents, hospital effluents, and other untreated wastewater will seep into the surface and groundwater, then migrate and transform into the aquatic environment. It should be noted that this type of residual substance present in aqueous environments generates great concern due to its potential risk to the environment and biological survival, because it represents a high risk to human health and can affect the evolutionary structure of the bacterial community, strengthening bacterial resistance to these products [2–4].

Currently, many techniques have been used to remove antibiotics, including biological processes, and advanced oxidation processes (AOPs), and an alternative is to take advantage of the potential of some structures and nanosystems as adsorbents of organic pollutants, such as emerging pollutants, present in bodies of water. Some materials, such as carbonaceous materials, are used in efficient techniques for removing antibiotics from wastewater due to their properties. In particular, it has been shown that nanotubes of this material have potential application in the removal of antibiotics from aqueous solutions [3–6]. For example, Liu *et al.* [7] investigated how sulfonamide adsorption behaves on multiwalled carbon nanotubes. Among the sulfonamides evaluated are Sulfanilamide (SAM), Sulfamerazine (SMR), Sulfadimethoxine (SMX), Sulfadiazine (SDZ), Sulfamethazine (SMT), and Sulfamethoxydiazine (SMD). Their results indicate that CNTs have potential applications in the removal of sulfonamides from aqueous solutions by adsorption process, which can reach a high efficiency (in a pH adsorption range of 3 to 9). However, the adsorption mechanisms need further investigation to guide engineering applications because the removal of antibiotics is incomplete [8].

Taking into account the profitable benefits of carbon nanotubes and the adsorption strategy, we are inspecting the efficiency of nanotubes formed by blue phosphorene, one of the four main allotropes of phosphorus (black, red, green, and blue) which was predicted to be thermal and dynamically stable in (2014) [9] and was recently synthesized (2018) [10, 11]. Regarding

Blue-phosphorene nanotubes (BPNTs), Bhuvanewari *et al* [12], studied the molecular interaction of armchair-type blue phosphorene nanotubes (10, 10) with Sulfapyridine (SP) which is an antibacterial drug Sulfanilamide (SAM), found that the interaction properties of the BPNTs that interact with the antibiotic, such as the remarkable Bader charge transfer, the significant adsorption energy, and the prominent average band gap variation, indicate a high efficiency of the BPNT to eliminate toxic antibiotics from water bodies. One of the strategies used to modulate the properties of systems is to generate artificial defects in the structures by irradiation of ions or electrons [13]. It would be interesting to analyze and compare the effect that these modifications in BPNTs would have on the adsorption capacities of these antibiotics.

Despite theoretical efforts, there are still untreated aspects regarding the capabilities of blue phosphorene nanotubes in the removal of antibiotics. For this reason, in the present work the behavior of blue phosphorene nanotubes has been evaluated in the adsorption of antibiotics and the effect that the inclusion of structural defects such as single-vacancies could have in this type of applications, specifically in the adsorption of Sulfanilamide molecule as a model sulfonamide antibiotic.

2. Computational details and model constructing

Generally, to activate the surface of nanotubes, whether carbon or other material, it is necessary to induce defects, dope, decorate, or functionalize the nanotube wall to achieve an increase in its adsorption capacity [14–18].

Therefore, in this work, we analyze the adsorption of a sulfanilamide molecule (SAM) on pristine and defective single vacancy (SV) blue phosphorene nanotubes. So that it is possible to contrast and identify the incidence of SV in the adsorption capacity of the BPNT. Our analyses consider BPNTs of type AM and ZZ, characterized by the chiral numbers (14, 14) and (14, 0), respectively. A supercell of $1 \times 1 \times 5$ guarantees that the SAM molecule do not interact with their images. The analyzed adsorption sites for SAM can be seen in figure 1.

The calculation of structural and electronic properties is performed within the framework of DFT, as it is implemented in the *ab initio* SIESTA package [19] where localized double- ζ polarized atomic orbitals are employed as basis set, together with conserved norm pseudopotentials. For the exchange and correlation functional used, the one proposed by Dion *et al* [20] and whose

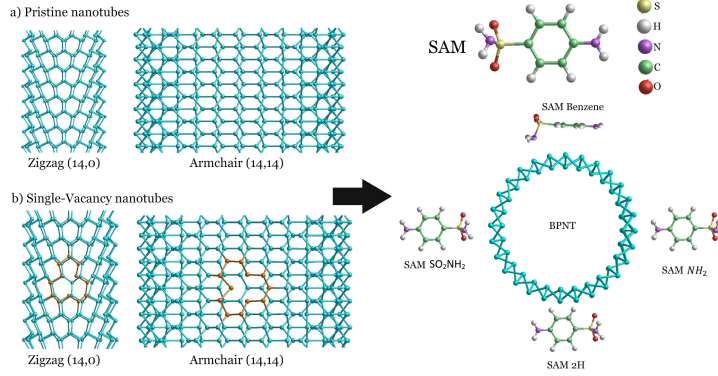


Figure 1: Schematic view of all evaluated SAM adsorption sites for both, pristine and single-vacancy nanotubes.

exchange was modified by Klimes *et al* [21]. This functional include van der Waals interactions and is labeled as (KBM). All structures are relaxed through the FIRE minimization algorithm, until the force on the atoms is smaller than $0.04 \text{ eV}/\text{\AA}$ [22]. The Brillouin zone sampling is carried out via Monkroost-Pack-grid of $1 \times 1 \times 2$. A Mesh cutoff value of $350 R_y$ was used. The study was carried out with the inclusion of collinear spin-polarization for SV systems and without spin-polarization for pristine BPNT structures.

The adsorption energy between the molecule and the BPNT is characterized by evaluating the adsorption Energy (E_{ads}), which is defined as:

$$E_{ads} = E_{Total} - E_{BPNT} - E_{Adsorbate}, \quad (1)$$

where $E_{Adsorbate}$ is the total energy of SAM, E_{Total} is the total energy of the system composed of the BPNT and the adsorbate and E_{BPNT} is the BPNT total energy.

Further, conventional transition state theory is adopted to determine the recovery time of BPNTs from the interaction of the toxic antibiotics [23, 24]. The following equation, which encompasses the attempt frequency θ_0 , adsorption energy from eq. 1, Boltzmann's constant (k_B), and the temperature (T), is employed to reckon the recovery time of the blue-phosphorene nanotube. Recovery time captures the time cost for the desorption of a target molecule from the sensing material's surface [25] and could be obtained according to

System	Initial SAM positions	Final SAM positions	E_{ads}	System	Initial SAM positions	Final SAM positions	E_{ads}
Pristine ZZ	Benzene	Benzene	-0.279	SV ZZ	Benzene	Benzene	-0.509
	NH_2	NH_2	-0.191		$2H$	$2H$	-0.497
	SO_2NH_2	SO_2NH_2	-0.130		NH_2	NH_2	-0.380
	$2H$	$2H$	-0.094		SO_2NH_2	SO_2NH_2	-0.272
Pristine AM	Benzene	Benzene	-0.312	SV AM	Benzene	Benzene	-0.373
	$2H$	$2H$	-0.205		$2H$	$2H$	-0.221
	NH_2	NH_2	-0.053		NH_2	NH_2	-0.161
	SO_2NH_2	SO_2NH_2	-0.028		SO_2NH_2	SO_2NH_2	-0.122

Table 1: Results interaction of pristine and single-vacancy (SV) with SAM molecule; Adsorption energy (E_{ads}) is presented in eV .

the transition state theory and Van't Hoff–Arrhenius explanation:

$$\tau = \theta_0^{-1} \exp\left(\frac{-E_{ads}}{k_B T}\right), \quad (2)$$

where the frequency factor θ_0 is assume to be $10^{12} Hz$ and $10^{16} Hz$, under visible and UV light conditions, respectively [25–27], k_B is approximately $8,617 \times 10^{-5} eV/K$ [25] and T is evaluated in 300 (ambient temperature), 310, 320 and, 330 K .

3. Results and discussion

3.1. Geometric structures of Sulfonamides on pristine and single-vacancy BPNTs

The adsorption of SAM molecule on the Pristine and SV Blue-Phosphorene nanotubes for both armchair and zigzag configurations have been analyzed over four different adsorption sites, indicated in Figure 1. The crucial property, which supports us in verifying the kind of interaction taking place between the SAM antibiotics and the BPNT, thereby highlighting the use of the designed base nanotube is adsorption energy (E_{ads}) [28, 29]. The measured E_{ads} results are given in table 1, it evidence that while SAM adsorption on $2H$, NH_2 , and SO_2NH_2 sites is possible, Benzene position is the most outstanding in the results, since it obtained the highest adsorption energy within its respective groups (same chirality and same type of vacancy), i.e. is the most stable in all evaluated systems. This is attributed to the presence of polar groups and aromatic rings offering $\pi - \pi$ interactions between target contaminants and BPNTs [3, 4, 30–32]. The polarity of the adsorption/interaction energy (negative) suggests that the adsorption process of the molecule is stable and signifies the easy attraction of the SAM antibiotic towards both pristine and SV BPNT. In the case of SV systems, there is an increment in the E_{ads} value in comparison with pristine system in all studied positions, the

Molecule	Position	System	E_{ads}	System	E_{ads}
SAM	Benzene	Pristine ZZ	-0,279	SV ZZ	-0,509
		Pristine AM	-0,312	SV AM	-0,373
SDZ	Benzene	Pristine ZZ	-0,217	SV ZZ	-0,382
		Pristine AM	-0,285	SV AM	-0,537
SMX	Benzene	Pristine ZZ	-0,207	SV ZZ	-0,372
		Pristine AM	-0,248	SV AM	-0,322

Table 2: Results interaction of Benzene sites for pristine and single-vacancy (SV) with SAM, SDZ and SMX molecules; Adsorption energy (E_{ads}) is presented in eV .

above indicates that structural defects, in this case, single vacancies, slightly improve the ability of BPNTs for SAM molecule adsorption. Besides, in SV system, it can be note that ZZ chirality is most favorable than AM, since the adsorption energy of the molecule is superior to that of its equivalent position with AM because in all evaluated systems the E_{ads} had a percentage increase of almost 40%, which indicates that for these systems the chirality of the ZZ type is possibly more active than the AM type and therefore, it benefits the adsorption of the SAM molecule.

Additionally, the adsorption of SDZ and SMX antibiotics was studied on benzene position as it can be seen in figure 2. According to the obtained results in table 2, pristine BPNTs shows a similar behavior in all evaluated molecules, that is, the AM BPNTs presents superior E_{ads} than ZZ systems. These results indicate that AM configurations should be a better option, and is important to remark that AM phosphorene nanotubes present significant stable nature in comparison to the zigzag phosphorene nanotubes [33]. It could be observed from Table 2 that the order of maximum adsorption capacity of the three sulfonamides were SAM > SDZ > SMX for pristine systems and ZZ SV. In SV AM-BPNTs SDZ molecule presents higher E_{ads} than SAM and SMX (SDZ > SAM > SMX). In comparison with results obtained in previous studies for BPTNs [29], SAM, SDZ, and SMX molecules have a smaller E_{ads} than another antibiotics like oxytetracycline (OC) and sulfapyridine (SP) ($< -1,25$ approximately). Regarding CNTs, previously reported absorption affinities depends on initial conditions, that is, the order of adsorption efficiency of some sulfonamides was SMD > SMT > SDZ > SMX > SMR > SAM obtained by Liu *et al* [7], SMT > SMR > SP > SDZ obtained by Zhao *et al* [4] and SMX > SMT obtained by Wei *et al* [34]. Furthermore, according to the values obtained, single vacancies improve ad-

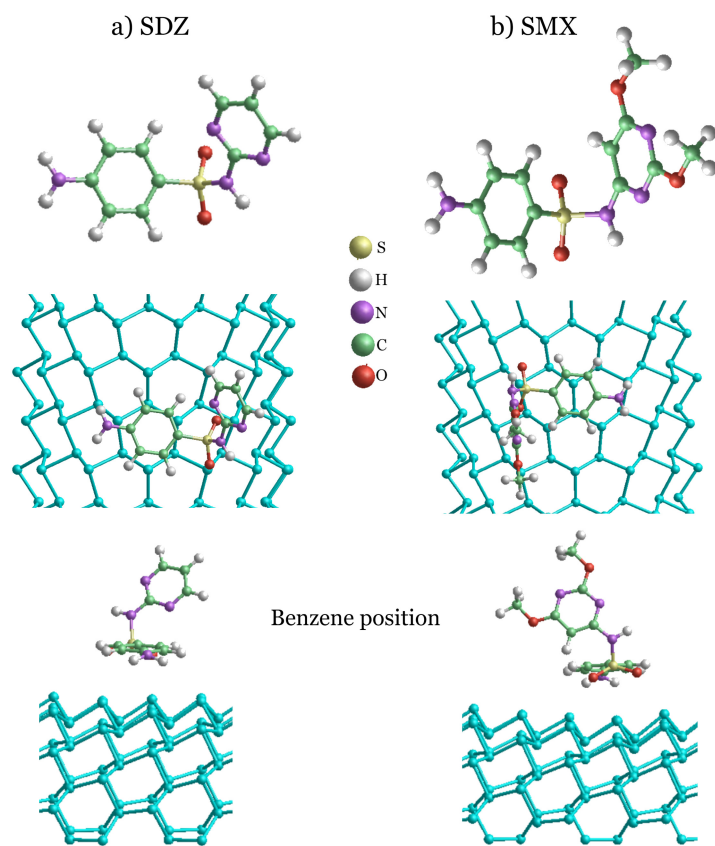


Figure 2: Schematic view of evaluated Benzene position for SDZ and SMX adsorption sites for both, pristine and single-vacancy nanotubes.

sorption energy of the SAM, SDZ, and SMX molecules, that is, the increase in E_{ads} are found in percentage increase ranges that go from 20% to 89% for the AM SAM (smaller increase) and AM SDZ (larger increase) systems. This indicates that structural defects, in this case, single vacancies, improve the capacity of BPNTs for adsorption of these toxic antibiotics.

3.2. *Electronic properties*

The electronic structure of the system can be inspected through band structure. The band structure for Benzene sites (most stable in all systems) is present in Fig. 3. The electronic band structure shows that the inclusion of SV vacancy on ZZ and AM BPNT induces localized states into the nanotube band gap. Besides, the SV vacancy induced the magnetization of the system, which we observed as different bands for each spin component. The band gaps measured reckoned for the pristine BPNTs are 1,793 for AM and 1,927 for ZZ configurations [35]. Results indicate that SV induces a reduction in band-gap value and transforms the ZZ and AM BPNTs systems into a small gap magnetic bipolar semiconductor. These results are according to previous results [35, 36]. However, when a SAM and SMX molecule is adsorbed, AM BPNT shows a transition from a bipolar-magnetic semiconductor to not magnetic metallic system. This suggests that defective AM BPNTs also can be employed as a sensor for these antibiotics.

3.3. *Recovery time*

The adsorption energies observed for the interaction of antibiotics on BPNTs influences the recovery time taken by the BPNT to come to its original state. From Table 3, it can be seen than from all molecules the initial form of the BPNTs in both, pristine and SV can be attained quickly. In particular, it would take little time for the BPNT to be retrieved back to its premier position. However, it is important to highlight that both values of τ that are too long and too short are unfavorable for detection in real experiments [25].

4. **Conclusion**

Electronic response of Zigzag and Armchair BPNTs to biologically active sulfonamide-based compounds were studied using DFT calculations. Results indicate that analyzed molecules SAM, SDZ, SMX are weakly adsorbed on the pristine BPNTs with adsorption energy of about $-0,312$, $-0,285$ and

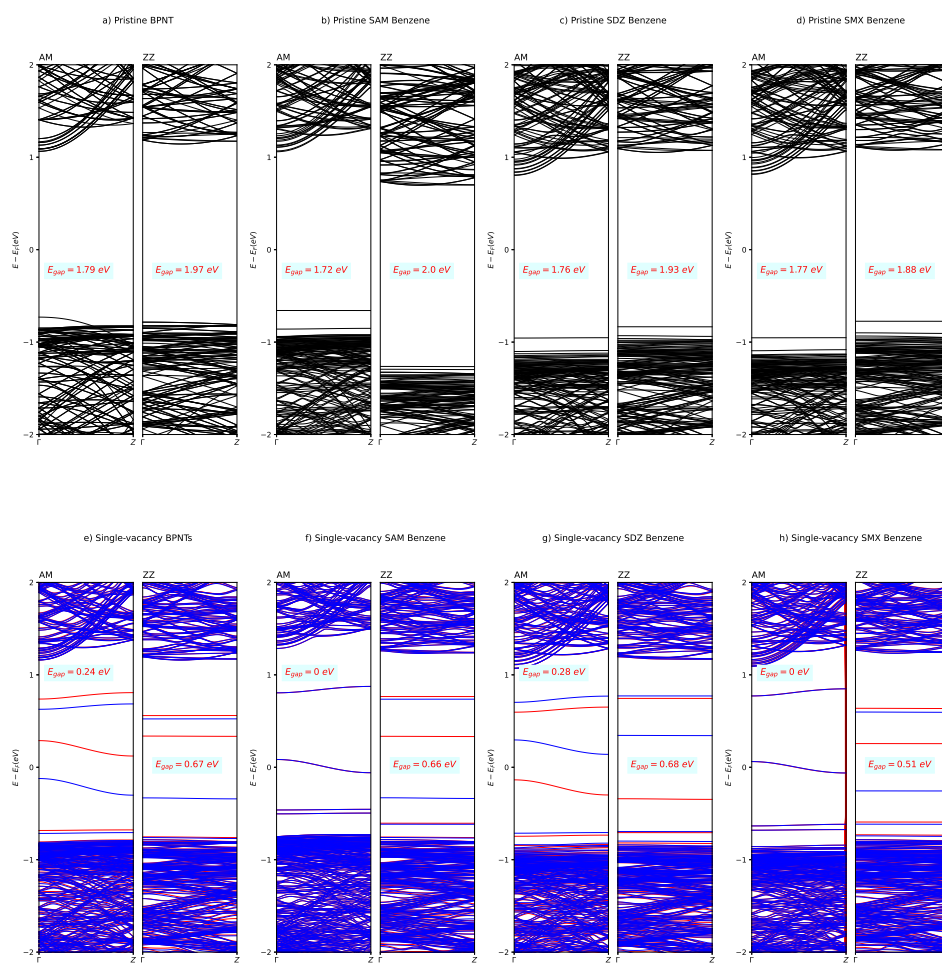


Figure 3: Band structure of Benzene sites for SAM, SDZ and SMX molecules.

			$\theta_0 = 10^{12}$ (Visible light)			
Molecule	Position	System	τ 300K	τ 310K	τ 320K	τ 330K
SAM	Benzene	Pristine ZZ	$4,9 \times 10^{-08}$	$3,4 \times 10^{-08}$	$2,5 \times 10^{-08}$	$1,8 \times 10^{-08}$
		Pristine AM	$1,8 \times 10^{-07}$	$1,2 \times 10^{-07}$	$8,3 \times 10^{-08}$	$5,9 \times 10^{-08}$
		SV ZZ	$4,8 \times 10^{-04}$	$2,5 \times 10^{-04}$	$1,4 \times 10^{-04}$	$7,8 \times 10^{-05}$
		SV AM	$1,9 \times 10^{-06}$	$1,2 \times 10^{-06}$	$7,6 \times 10^{-07}$	$5,0 \times 10^{-07}$
SDZ	Benzene	Pristine ZZ	$4,4 \times 10^{-09}$	$3,3 \times 10^{-09}$	$2,6 \times 10^{-09}$	$2,0 \times 10^{-09}$
		Pristine AM	$6,0 \times 10^{-08}$	$4,2 \times 10^{-08}$	$3,0 \times 10^{-08}$	$2,2 \times 10^{-08}$
		SV ZZ	$2,6 \times 10^{-06}$	$1,6 \times 10^{-06}$	$1,0 \times 10^{-06}$	$6,8 \times 10^{-07}$
		SV AM	$1,1 \times 10^{-03}$	$5,5 \times 10^{-04}$	$2,9 \times 10^{-04}$	$1,6 \times 10^{-04}$
SMX	Benzene	Pristine ZZ	$3,0 \times 10^{-09}$	$2,3 \times 10^{-09}$	$1,8 \times 10^{-09}$	$1,4 \times 10^{-09}$
		Pristine AM	$1,5 \times 10^{-08}$	$1,1 \times 10^{-08}$	$8,2 \times 10^{-09}$	$6,2 \times 10^{-09}$
		SV ZZ	$1,8 \times 10^{-06}$	$1,1 \times 10^{-06}$	$7,3 \times 10^{-07}$	$4,8 \times 10^{-07}$
		SV AM	$2,6 \times 10^{-07}$	$1,7 \times 10^{-07}$	$1,2 \times 10^{-07}$	$8,2 \times 10^{-08}$
			$\theta_0 = 10^{16}$ (UV light)			
Molecule	Position	System	τ 300K	τ 310K	τ 320K	τ 330K
SAM	Benzene	Pristine ZZ	$4,9 \times 10^{-12}$	$3,4 \times 10^{-12}$	$2,5 \times 10^{-12}$	$1,8 \times 10^{-12}$
		Pristine AM	$1,8 \times 10^{-11}$	$1,2 \times 10^{-11}$	$8,3 \times 10^{-12}$	$5,9 \times 10^{-12}$
		SV ZZ	$4,8 \times 10^{-08}$	$2,5 \times 10^{-08}$	$1,4 \times 10^{-08}$	$7,8 \times 10^{-09}$
		SV AM	$1,9 \times 10^{-10}$	$1,2 \times 10^{-10}$	$7,6 \times 10^{-11}$	$5,0 \times 10^{-11}$
SDZ	Benzene	Pristine ZZ	$4,4 \times 10^{-13}$	$3,3 \times 10^{-13}$	$2,6 \times 10^{-13}$	$2,0 \times 10^{-13}$
		Pristine AM	$6,0 \times 10^{-12}$	$4,2 \times 10^{-12}$	$3,0 \times 10^{-12}$	$2,2 \times 10^{-12}$
		SV ZZ	$2,6 \times 10^{-10}$	$1,6 \times 10^{-10}$	$1,0 \times 10^{-10}$	$6,8 \times 10^{-11}$
		SV AM	$1,1 \times 10^{-07}$	$5,5 \times 10^{-08}$	$2,9 \times 10^{-08}$	$1,6 \times 10^{-08}$
SMX	Benzene	Pristine ZZ	$3,0 \times 10^{-13}$	$2,3 \times 10^{-13}$	$1,8 \times 10^{-13}$	$1,4 \times 10^{-13}$
		Pristine AM	$1,5 \times 10^{-12}$	$1,1 \times 10^{-12}$	$8,2 \times 10^{-13}$	$6,2 \times 10^{-13}$
		SV ZZ	$2,6 \times 10^{-11}$	$1,7 \times 10^{-11}$	$1,2 \times 10^{-11}$	$8,2 \times 10^{-12}$
		SV AM	$1,8 \times 10^{-10}$	$1,1 \times 10^{-10}$	$7,3 \times 10^{-11}$	$4,8 \times 10^{-11}$

Table 3: Results interaction of Benzene sites for pristine and single-vacancy (SV) with SAM, SDZ and SMX molecules; recovery time (τ) is presented in *s*.

$-0,248\text{ eV}$, Besides,for SAM molecule, Benzene position is the most outstanding in the results, since it obtained the highest adsorption energy within its respective groups (same chirality and same type of vacancy). To improve the adsorption, a P atom of the BPNT has been removed given a single-vacancy defect. SV increase the reactivity of the BPNTs so that the adsorption energies increased for all evaluated systems to about a percentage ranges that go from 20% to 89% for the AM SAM (smaller increase) and AM SDZ (larger increase) systems, respectively. This indicates that structural defects, improve the capacity of BPNTs for adsorption of these toxic antibiotics. The orders of E_{ads} of three sulfonamides were as follows: SAM > SDZ > SMX for pristine systems and ZZ SV. In SV AM-BPNTs SDZ molecule presents higher E_{ads} than SAM and SMX (SDZ > SAM > SMX). The calculations results demonstrate that despite the increase in the reactivity of the ZZ SV BPNT to the sulfonamides, AM configurations show a transition from bipolar-magnetic semiconductor to not magnetic metallic system, suggesting that defective AM BPNTs also can be employed as a sensor for antibiotic molecules like SAM, SDZ, and SMX.

Declaration of competing interest

The authors declare that they have no known competing financial interests or personal relationships that could have appeared to influence the work reported in this paper.

Acknowledgments

The authors would like to thank Universidad de Medellín (UdeM) for supporting their work. Authors thanks MINCIENCIAS to financial support of this research by contract 120680864729.

References

- [1] F. Carta, A. Scozzafava, C. T. Supuran, Sulfonamides: a patent review (2008–2012), Expert opinion on therapeutic patents 22 (7) (2012) 747–758.
- [2] W.-Q. Guo, H.-S. Zheng, S. Li, J.-S. Du, X.-C. Feng, R.-L. Yin, Q.-L. Wu, N.-Q. Ren, J.-S. Chang, Removal of cephalosporin antibiotics 7-aca

from wastewater during the cultivation of lipid-accumulating microalgae, *Bioresource technology* 221 (2016) 284–290.

- [3] L. Ji, W. Chen, S. Zheng, Z. Xu, D. Zhu, Adsorption of sulfonamide antibiotics to multiwalled carbon nanotubes, *Langmuir* 25 (19) (2009) 11608–11613.
- [4] H. Zhao, X. Liu, Z. Cao, Y. Zhan, X. Shi, Y. Yang, J. Zhou, J. Xu, Adsorption behavior and mechanism of chloramphenicols, sulfonamides, and non-antibiotic pharmaceuticals on multi-walled carbon nanotubes, *Journal of hazardous materials* 310 (2016) 235–245.
- [5] S. A. Mousavi, H. Janjani, Antibiotics adsorption from aqueous solutions using carbon nanotubes: a systematic review, *Toxin Reviews* (2018).
- [6] S. Kurwadkar, T. V. Hoang, K. Malwade, S. R. Kanel, W. F. Harper, G. Struckhoff, Application of carbon nanotubes for removal of emerging contaminants of concern in engineered water and wastewater treatment systems, *Nanotechnology for Environmental Engineering* 4 (1) (2019) 1–16.
- [7] Y. Liu, Y. Peng, B. An, L. Li, Y. Liu, Effect of molecular structure on the adsorption affinity of sulfonamides onto cnts: Batch experiments and dft calculations, *Chemosphere* 246 (2020) 125778.
- [8] S. Tian, C. Zhang, D. Huang, R. Wang, G. Zeng, M. Yan, W. Xiong, C. Zhou, M. Cheng, W. Xue, et al., Recent progress in sustainable technologies for adsorptive and reactive removal of sulfonamides, *Chemical Engineering Journal* 389 (2020) 123423.
- [9] Z. Zhu, D. Tománek, Semiconducting layered blue phosphorus: a computational study, *Physical review letters* 112 (17) (2014) 176802.
- [10] W. Zhang, H. Enriquez, Y. Tong, A. Bendounan, A. Kara, A. P. Seitsonen, A. J. Mayne, G. Dujardin, H. Oughaddou, Epitaxial synthesis of blue phosphorene, *Small* 14 (51) (2018) 1804066.
- [11] J. L. Zhang, S. Zhao, S. Sun, H. Ding, J. Hu, Y. Li, Q. Xu, X. Yu, M. Telychko, J. Su, et al., Synthesis of monolayer blue phosphorus enabled by silicon intercalation, *ACS nano* 14 (3) (2020) 3687–3695.

- [12] R. Bhuvaneshwari, V. Nagarajan, R. Chandiramouli, Molecular interaction of oxytetracycline and sulfapyridine on blue phosphorene nanotubes: A first-principles insight, *Physics Letters A* 394 (2021) 127198.
- [13] M. Sun, J.-P. Chou, A. Hu, U. Schwingenschlogl, Point defects in blue phosphorene, *Chemistry of Materials* 31 (19) (2019) 8129–8135.
- [14] M. R. Mananghaya, Hydrogen adsorption of nitrogen-doped carbon nanotubes functionalized with 3d-block transition metals, *Journal of Chemical Sciences* 127 (4) (2015) 751–759.
- [15] D. Gehringer, T. Dengg, M. N. Popov, D. Holec, Interactions between a h₂ molecule and carbon nanostructures: A dft study, *C—Journal of Carbon Research* 6 (1) (2020) 16.
- [16] M. F. Fellah, Pt doped (8, 0) single wall carbon nanotube as hydrogen sensor: A density functional theory study, *International Journal of Hydrogen Energy* 44 (49) (2019) 27010–27021.
- [17] K. Tada, S. Furuya, K. Watanabe, Ab initio study of hydrogen adsorption to single-walled carbon nanotubes, *Physical Review B* 63 (15) (2001) 155405.
- [18] H. J. Kwon, Y. Kwon, T. Kim, Y. Jung, S. Lee, M. Cho, S. Kwon, Enhanced competitive adsorption of co₂ and h₂ on graphyne: A density functional theory study, *AIP Advances* 7 (12) (2017) 125013.
- [19] J. M. Soler, E. Artacho, J. D. Gale, A. García, J. Junquera, P. Ordejón, D. Sánchez-Portal, The SIESTA method for ab initio order-n materials simulation, *Journal of Physics: Condensed Matter* 14 (11) (2002) 2745–2779. doi:10.1088/0953-8984/14/11/302.
URL <https://doi.org/10.1088/0953-8984/14/11/302>
- [20] M. Dion, H. Rydberg, E. Schröder, D. C. Langreth, B. I. Lundqvist, Van der waals density functional for general geometries, *Physical review letters* 92 (24) (2004) 246401.
- [21] J. Klimeš, D. R. Bowler, A. Michaelides, Chemical accuracy for the van der waals density functional, *Journal of Physics: Condensed Matter* 22 (2) (2009) 022201.

- [22] E. Bitzek, P. Koskinen, F. Gähler, M. Moseler, P. Gumbsch, Structural relaxation made simple, *Physical review letters* 97 (17) (2006) 170201.
- [23] D. Ma, W. Ju, T. Li, G. Yang, C. He, B. Ma, Y. Tang, Z. Lu, Z. Yang, Formaldehyde molecule adsorption on the doped monolayer mos2: a first-principles study, *Applied Surface Science* 371 (2016) 180–188.
- [24] D. Ma, Q. Wang, T. Li, C. He, B. Ma, Y. Tang, Z. Lu, Z. Yang, Repairing sulfur vacancies in the mos 2 monolayer by using co, no and no 2 molecules, *Journal of Materials Chemistry C* 4 (29) (2016) 7093–7101.
- [25] A. Aasi, E. Aasi, S. Mehdi Aghaei, B. Panchapakesan, Green phosphorene as a promising biosensor for detection of furan and p-xylene as biomarkers of disease: A dft study, *Sensors* 22 (9) (2022) 3178.
- [26] J. Du, G. Jiang, First-principle study on monolayer and bilayer snp3 sheets as the potential sensors for no2, no, and nh3 detection, *Nanotechnology* 31 (32) (2020) 325504.
- [27] I. G. Pitt, R. G. Gilbert, K. R. Ryan, Application of transition-state theory to gas-surface reactions: Barrierless adsorption on clean surfaces, *The Journal of Physical Chemistry* 98 (49) (1994) 13001–13010.
- [28] A. S. Rad, O. R. Kashani, Adsorption of acetyl halide molecules on the surface of pristine and al-doped graphene: ab initio study, *Applied Surface Science* 355 (2015) 233–241.
- [29] R. Bhuvanewari, V. Nagarajan, R. Chandiramouli, Molecular interaction studies of cumene and toluene on δ -arsenene nanosheet—a first-principles outlook, *Molecular Physics* 119 (3) (2021) e1800853.
- [30] M. Jyothi, V. Nagarajan, R. Chandiramouli, Interaction studies of dichlobenil and isoproturon on square-octagon phosphorene nanotube based on dft frame work, *Chemical Physics Letters* 778 (2021) 138773.
- [31] A. N. M. Nasir, N. Yahaya, N. N. M. Zain, V. Lim, S. Kamaruzaman, B. Saad, N. Nishiyama, N. Yoshida, Y. Hirota, Thiol-functionalized magnetic carbon nanotubes for magnetic micro-solid phase extraction of sulfonamide antibiotics from milks and commercial chicken meat products, *Food chemistry* 276 (2019) 458–466.

- [32] Z. Rahmani, L. Edjlali, E. Vessally, A. Hosseinian, P. D. K. Nezhad, A density functional theory outlook on the possible sensing ability of boron nitride nanotubes and their al-and si-doped derivatives for sulfonamide drugs, *Journal of Sulfur Chemistry* 41 (1) (2020) 82–95.
- [33] H. Guo, N. Lu, J. Dai, X. Wu, X. C. Zeng, Phosphorene nanoribbons, phosphorus nanotubes, and van der waals multilayers, *The Journal of Physical Chemistry C* 118 (25) (2014) 14051–14059.
- [34] J. Wei, W. Sun, W. Pan, X. Yu, G. Sun, H. Jiang, Comparing the effects of different oxygen-containing functional groups on sulfonamides adsorption by carbon nanotubes: experiments and theoretical calculation, *Chemical Engineering Journal* 312 (2017) 167–179.
- [35] J. Vergara, E. Flórez, M. Mora-Ramos, J. Correa, Effects of single vacancy on electronic properties of blue-phosphorene nanotubes, *Materials Research Express* 7 (1) (2020) 015042.
- [36] J. Vergara, M. Mora-Ramos, J. Correa, E. Flórez, Impact of different structural defects on fundamental properties of blue phosphorene nanotubes, *Computational Condensed Matter* (2022) e00701.

6. Impact of single Pt atom adsorption on fundamental properties of blue phosphorene and its activity toward hydrogen evolution reaction

Impact of single Pt atom adsorption on fundamental properties of blue phosphorene and its activity toward hydrogen evolution reaction

J. M. Vergara^a, J. D. Correa^a, A.A Koverga^{b*}, E. Flórez^{a*}

^aFacultad de Ciencias Básicas, Universidad de Medellín, Medellín-Colombia

^bDepartment of Chemistry, Division of Fundamental Sciences (IEFQ), Technological Institute of Aeronautics (ITA), São Jose dos Campos, São Paulo CEP:12228-900, Brazil

Abstract

The adsorption of single H atom and H₂ on blue phosphorene monolayer with and without Pt atom adsorbed on the surface has been investigated using density functional theory with the Perdew-Burke-Ernzerhof exchange correlation functional. With H adsorption energy as a descriptor, catalytic activity of evaluated systems for hydrogen evolution reaction was estimated. Obtained results evidence the impact of Pt atom on fundamental properties of the blue phosphorene monolayer such as its electronic structure, work function and charge distribution in the system. As the result catalytic activity toward hydrogen evolution reaction is affected as well. These data, potentially, can be a useful basis for designing and developing novel functional materials with predetermined catalytic properties.

Keywords: Platinum, blue phosphorene, HER, DFT

1. Introduction

With the growing demand and use of fossil fuels as an energy source, their significant disadvantage has become evident, stemming from their finite nature. Furthermore, their combustion results in “greenhouse” effect, significantly affecting the climate [1]. Thus, alternative means of energy production and storage are required. Hydrogen presents a viable option for carbon-free energy storage because of its high energy density and ecologically-friendly products of its combustion.

However, employing hydrogen for energy conversion and storage solutions has potential only has a good prospect if its production can be carried out in a “green” and low-cost way. These requirements are fulfilled by the electrocatalytic hydrogen evolution reaction (HER) given by



Currently, the best known electrocatalysts for HER are based on noble metals such as platinum. [2–4] It, however,

is very scarce, and, thus, has a high cost, which limits its application in industry [2,5–8]. For this reason, the exploration and development of alternative new catalysts with low cost and high efficiency is highly desirable for practical implementation of HER [9-12].

In recent years, the interest in two-dimensional materials has been growing, sparked by their unique properties that have potential use in numerous applications, electrocatalysis among them. [13–24] Among 2D materials, black phosphorene (also named phosphorene), since its successful isolation, drew attention as a potential electrocatalyst for HER due to its remarkable electronic properties, large surface area, high carrier mobility, and long carrier diffusion distance [25-29]. However, HER activity of pristine black phosphorene is much lower than that of Pt [30] and is not satisfactory for practical applications. [31]

In that sense, several strategies have been implemented in order to optimize HER activity of black phosphorene, such as the introduction of extrinsic active sites by metal doping, for example, Co, [27] Au, [32] Pd [33] and Pt, [34–36] doping and decoration with functional groups like NH_2 and OH. [37] Another alternative is to alter the catalytic HER on phosphorene by the creation of optimal active sites with system defects, [30, 38, 39] system strain modulation, [40] and functionalization. [41] In this regard, recent study [42] analyzed the catalytic properties of metal-doped phosphorene toward HER. The results indicated that the free energies of hydrogen adsorption ΔG_{H^*} (a typical HER activity descriptor) for Co-doped system is very close to the optimal value of 0 eV, suggesting high expected HER activity.

Another allotrope of phosphorus is blue phosphorene (BP). It was theoretically predicted to be thermally and dynamically stable [43], and was later synthesized. [44, 45] Because of its characteristics like a buckled semiconductor structure, a carrier mobility in excess of $10^3 \text{ cm}^2 \text{V}^{-1} \text{s}^{-1}$ [46] and the possibility of tuning its electronic and dielectric properties, the BP presents a significant interest in applications such as optoelectronics and nanoscale devices that require a specific bandgap [47]. This gave a further impulse to investigate the catalytic properties of BP, and it was found that blue phosphorene nanotubes are promising candidates for photocatalytic oxygen evolution reaction. [48] Also it has been shown that doped BP has excellent photocatalytic potential for NH_3 production and electrocatalytic oxygen reduction reaction which points that BP can be potentially used to design practical applications for water molecule splitting. [49–51] Moreover, various studies of hetero-structures and engineering band gap of BP by functionalization have been performed [52–54] offering an interesting possibility for designing efficient photocatalysts. Interestingly, while decorating blue phosphorene with a single atom of another material, active for HER, such as Pt, could be another strategy to optimize HER activity of the resulting system, [55] there are no studies available on complex systems, comprised of Pt supported on BP monolayer.

Here fundamental properties of BP, modified with a single Pt atom (BP–Pt), are investigated using density functional theory (DFT). Changes in the charge distribution, electron and band structure of the BP-Pt system are

discussed in the context of their consequent impact on catalytic properties of the overall system.

2. Computational details

Periodic density functional calculations were performed using the Vienna ab initio simulation package (VASP) [56] within the generalized gradient approximation, utilizing Perdew, Burke and Ernzerhof for the exchange-correlation energy functional. [57] The kinetic energy cut-off of 500 eV for the plane wave basis set was selected. Integration of the reciprocal space for all surfaces was carried out using $5 \times 5 \times 1$ grids of special k-points within Monkhorst-Pack scheme for the geometry optimization procedures, [58] while $17 \times 17 \times 1$ grid was used for the Density of States calculations. Blue phosphorene monolayer was represented by a 4×4 single-layer supercell in all performed calculations. All systems were fully relaxed employing the conjugate gradient algorithm until the variation in the total forces was smaller than 0.001 eV/\AA at the current and previous step. A vacuum of 18 \AA along the z direction was included to avoid possible interactions between repeating cell images.

Adsorption of a single hydrogen and platinum atoms on various top, bridge, fcc, and hcp sites were studied first to define the preferable adsorption locations on the BP monolayer (Fig. 1). Additionally, the adsorption energies of a single H atom and H_2 molecule on BP and BP-Pt surfaces were evaluated. For the H_2 molecule, three initial orientations were considered, parallel, perpendicular, and tilted to the plane of the surface, as can be seen in Fig. 1.

The adsorption energies on clean BP and Pt-modified BP surfaces were calculated from the following expression:

$$E_{\text{Ads}} = E_{\text{Surf+Adsorbate}} - (E_{\text{Surf}} - E_{\text{Adsorbate}}) \quad (2)$$

where E_{Surf} correspond to the energy of the pure BP or BP-Pt and $E_{\text{Adsorbate}}$ the energy of the adsorbate (atomic H, H_2 or Pt) in a vacuum, respectively. For H, atomic H energy in gas phase was used as reference.

The effect of van der Waals corrections, as implemented by Grimme et al., [59] on adsorption energies was tested and because of the closeness of the results with and without dispersion corrections, most calculations have been carried out without the corrections, unless specifically stated otherwise.

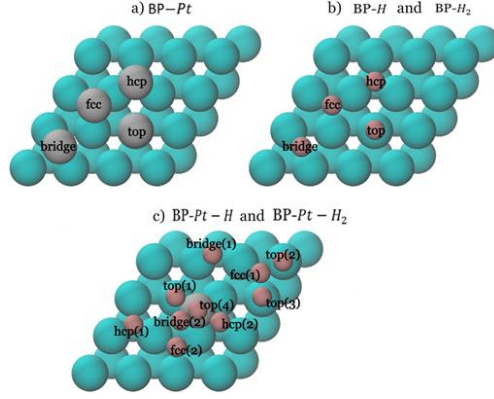


Figure 1: Adsorption sites available on BP surface (panels a and b) and on BP surface decorated with platinum atom (panel c). Blue, silver and brown spheres correspond to atoms of P, Pt and H, respectively.

To construct a volcano curve, hydrogen adsorption energies have been obtained for the 12 metals used in work of Nørskov et al., [60] employing 4×4 supercells with 4 atomic layers and 18 \AA of vacuum. In electrocatalysis instead of using energy of a single H atom as in eq. 2, it is common to employ half of the energy of H_2 in the gas phase as the reference. Thus, HBE values for the volcano curve were obtained using the following expression:

$$E_{\text{Ads,H}} = E_{\text{Surf+H}} - \left(E_{\text{Surf}} + \frac{1}{2} E_{\text{H}_2,\text{g}} \right) \quad (3)$$

The numeric difference between the $E_{\text{H,g}}$ and $\frac{1}{2} E_{\text{H}_2,\text{g}}$ is 2.25 eV, thus, if HBEs were calculated using eq. 2, the whole curve would have shifted to the left for a value of 2.25 eV, without affecting the trends of activity. Experimental values for HER exchange current were taken from the works of Nørskov et al.[60] and Trasatti[3] and were plotted versus the corresponding HBEs.

3. Results and discussion

3.1. Effect of platinum atom on fundamental properties of BP monolayer

The adsorption of a platinum atom on the BP 4×4 monolayer has been analyzed over four different adsorption sites, indicated in Fig. 1 (a). The results evidence that while adsorption on hcp and top sites is possible, fcc position is the most stable. Initially being placed onto bridge site Pt atom also converges to the fcc position with strong adsorption

energy of -4.2 eV (see Tab. S1 in Supplementary Information).

The electronic coupling effects between BP monolayer and Pt atom were analyzed employing the 2D cross sections of charge density difference shown in Fig. 2.

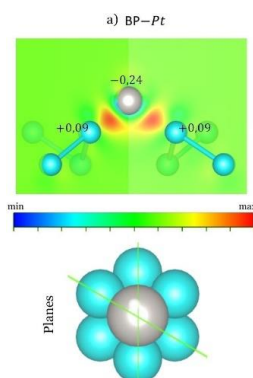


Figure 2: Cross sections of charge density difference in BP-Pt system. Red and yellow colors denote regions of charge buildup, while blue and green – of charge depletion. Blue and silver spheres correspond to atoms of phosphorus and platinum. Cross planes, normal to the surfaces, are shown from the top view on the systems.

It is evident that formation of electron-rich region between Pt and nearest P atoms is present, pointing to P→Pt charge transfer taking place in the system. As the result, accumulation of $-0.23 e$ negative charge on Pt atom is seen while P atoms in direct contact with the adatom become slightly positively charged. This observation is in line with previously reported charge transfer from the surface to adsorbate in system, comprised of black phosphorene decorated with Pt atom. [61] From the electronic localization function (ELF) in Fig. S1 it also can be seen that the P-Pt bond has a mixed metallic-covalent nature.

Band structure data, illustrated in Fig. 3, show that BP monolayer is a semiconductor material. Also, in the same Figure it can be seen that the d -states of the Pt atom are located close to the Fermi level, *i.e.*, the density of states starts at the bottom of the valence band and fills up to the Fermi level, in agreement with the charge transfer from P to Pt, described above.

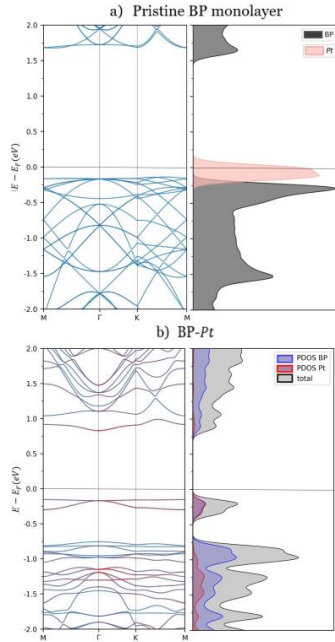


Figure 3: Band structure and DOS of BP pristine monolayer (panel a); band structure, DOS and PDOS of BP with Pt atom present in the system (panel b). DOS plots correspond to average of all atoms in the system, besides, PDOS in panel b represent the sum of s and p states for BP and d states for Pt. For each system, the Fermi level (horizontal line) is indicated.

3.2. H adsorption on BP and BP-Pt surfaces

Adsorption of a single H atom on BP monolayer was studied in a similar way to Pt atom, *i.e.* the same adsorption sites, seen in Fig. 1 were considered. Here it must be mentioned that the obtained $E_{\text{Ads,H}}$ values with and without van der Waals corrections were very close. Specifically, hydrogen adsorption energy on the most stable top site without dispersion corrections is -1.84 eV, while if the Grimme-D3 scheme was used, the adsorption energy becomes slightly more negative ($E_{\text{Ads,H}} = -1.89$ eV). For this reason, the results presented in this study are based on the calculations carried out without the van der Waals corrections. Previous results for black-phosphorene [62] indicate H atom preferably occupies the top site, as well, however on black phosphorene its adsorption is less stable, judging from adsorption energy value of -1.29 eV. Also, the shorter optimized P – H distance on black-phosphorene, of 1.45 Å compared to 0.76 Å on blue phosphorene further confirms stronger adsorption on the latter phase.

To assess the effect of a single Pt atom presence on fcc site of the BP on atomic hydrogen stability on the same surface, adsorption of H atom was analyzed on ten different sites of the BP-Pt system located on various distances from the Pt adatom (Fig. 1(c)). On the Pt-modified BP surface the adsorption at a distance from Pt atom was less stable than in its

vicinity (-1.84 eV vs. -2.86 eV), suggesting a local nature of Pt atom on stability of other adsorbates on the same surface, in agreement with observed changes in charge distribution and electron localization, described above.

The band structure in Fig. 4 panel (a) shows that H atom induces a semiconductor-metal transition in both surfaces - with and without Pt atom, since an overlap of valence and conduction bands in both systems, takes place.

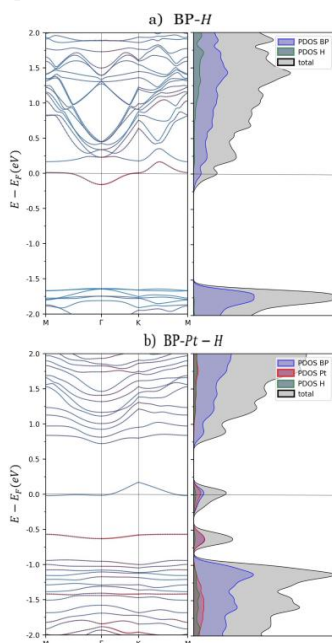


Figure 4: Effect of Pt in electronic structure of BP-H; panels a) and b) shows band structure, PDOS and DOS of BP with H atom and BP-Pt with H atom, respectively. DOS/PDOS plots correspond to average of all atoms in the system, besides, PDOS represent the sum of s and p states for BP and d states for Pt. For each system, the Fermi level (horizontal line) is indicated.

Furthermore, in Fig. 5 can be seen that presence of the H atom leads to surface dipole formation, that can alter the chemical properties of the sites in the vicinity of the adsorbate. Also on a more fundamental level, the band structure, and the DOS and PDOS for BP system with H atom, show breaking of some generation around the Γ -point and that the resulting electronic states close to the Fermi level stem from a hybridization of BP and H in both, s , and p states. A good catalyst usually has a band extending across the Fermi level, which interacts with the reactant [63] on the surface. When the interaction is weak, the level is just broadened, and when the interaction is strong, the level is split into bonding and antibonding orbital. When the overall reaction is in equilibrium, the orbital is half-filled at the transition state and the part of the density of states that lies below the Fermi level reduces the energy of activation [64]. When Pt atom is present on the BP surface the adsorption of H induces the breaking of many degenerations,

given to more accessible states than the pristine BP surface. Overlapping between the BP, and Pt orbitals (s+p and d, respectively) occurs around the Fermi energy level, i.e., from 0,25 eV to -0,75 eV. These findings indicate that there are far more orbital hybrids in the BP-Pt-H system than in the unmodified BP system.

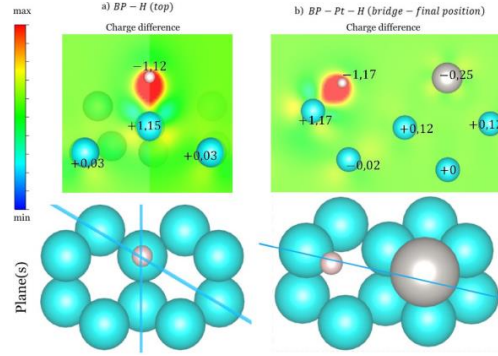


Figure 5: Cross sections of charge density difference in BP and BP-Pt systems with atomic hydrogen. Red and yellow colors denote regions of charge buildup, while blue and green – of charge depletion. White spheres indicate position of hydrogen atom, the rest of the color coding is the same as in Fig. 2 Cross planes, normal to the surfaces, are shown from the top view on the systems.

Table 1: Adsorption energies E_{Ads} , hydrogen-nearest surface atom distance $d(P - H_{(n)})$, distance between hydrogen atoms $d(H - H)$ and if there was dissociation in the systems with H_2 . On the most stable site for each evaluated system.

System	Initial site	Final site	E_{Ads} (eV)	Normal	Normal	$d(H - H)$ (Å)	Dissociation?
				$d(P - H_{(1)})$ (Å)	$d(P - H_{(2)})$ (Å)		
BP-Pt	fcc	fcc	-4.20	1.37	-	-	-
BP-H	top	top	-1.84	0.76	-	-	-
BP-Pt - H	hcp ₍₁₎	bridge _(away Pt)	-2.87	0.91	-	-	-
BP-H ₂	top	top	-0.52	2.92	3.67	0.75	No
Tilted 45°							
BP-Pt - H ₂	top ₍₄₎	bridge _(near Pt)	-0.73	2.68	2.68	2.08	Yes
Tilted 45°		bridge _(near Pt)					

3.3. H_2 adsorption on BP and BP-Pt surfaces

The adsorption behavior of H_2 molecules, parallel and perpendicular to the surface, and in intermediate, tilted configuration (with the angle between the surface and the H-H bond close to 45°) was evaluated on various sites of BP (4×4) monolayer (the site and orientation indications are given in Fig. 1). It can be seen from the values in Table 2 that top site is the most preferable for H_2 adsorption on pristine BP. It is noteworthy, that the geometry obtained from tilted initial orientation after the relaxation is very close to that where H_2 was initially perpendicular to the surface

plane, and more stable than of the system where H₂ was oriented parallel to the surface plane.

Table 2: Initial and final locations, adsorption energy values (E_{Ads}) and optimized geometries for BP-H₂ and BP-Pt-H₂. The most stable sites in each system are highlighted with bold font.

System	Initial site	Final site	E_{Ads} (eV)	Normal	Normal	$d(H-H)$ (Å)	Dissociation?	
				$d(P-H_{(1)})$ (Å)	$d(P-H_{(2)})$ (Å)			
BP-H ₂	top	top	-0.52	2.92	3.67	0.75	No	
	hcp	hcp	-0.49	3.31	3.40	0.75	No	
Tilted 45°	fcc	bridge-hcp	0.59	0.54	0.85	5.83	Yes	
	bridge	bridge-hcp	0.64	0.57	0.97	6.74	Yes	
BP-Pt-H ₂	top(4)	bridge_(near-Pt)-bridge_(near-Pt)	-0.73	2.68	2.68	2.08	Yes	
	fcc(2)	bridge _(near-Pt) -top _(away-Pt)	0.01	0.81	2.44	8.25	Yes	
	top(1)	bridge _(near-Pt) -bridge _(away-Pt)	0.03	0.16	2.43	5.09	Yes	
	top(2)	bridge _(far away-Pt) -bridge _(far away-Pt)	0.42	0.20	0.98	3.88	Yes	
	top(3)	bridge _(far away-Pt) -bridge _(far away-Pt)	0.50	0.13	0.97	3.86	Yes	
	Tilted 45°	fcc(1)	bridge _(far away-Pt) -top _(far away-Pt)	0.61	0.54	0.95	4.26	Yes
	hcp(1)	bridge _(near-Pt) -bridge _(far away-Pt)	0.63	0.73	2.06	8.21	Yes	
	bridge(2)	bridge _(away-Pt) -top _(far away-Pt)	0.74	0.55	0.97	6.08	Yes	
	hcp(2)	bridge _(near-Pt) -hcp _(near-Pt)	0.78	0.90	1.55	5.10	Yes	
	bridge(1)	bridge _(away-Pt) -top _(away-Pt)	0.94	0.40	0.91	5.47	Yes	

Then, the absorption of a tilted H₂ molecule was studied on ten different sites of BP-Pt surface to define the preferable adsorption location. According to the obtained results in Tab. 1 H₂ adsorbs weakly on the pristine BP (-0.52 eV). Presence of Pt atom on the surface does not change significantly adsorption characteristics of molecular hydrogen on top(4) site with an $E_{Ads,H}=-0.73$ eV (Tab. 2). It should be noted that in all systems a dissociation of H₂ molecule is possible as it can be seen in Tab. 1.

Interestingly, H₂ interaction with certain sites of BP-PT, such as hcp(1) and fcc(2) could result in a dissociation of hydrogen with resulting two atoms of hydrogen adsorbed on opposite sides of the BP ML plane (see Fig. S2 of the Supplementary Information). This phenomenon resembles hydrogen spillover process which consists of four steps: 1). molecular hydrogen interaction with the surface; 2). H₂ dissociation; 3). atomic hydrogen migration from hydrogen-rich surface to the hydrogen-poor substrate; 4). atomic hydrogen diffusion into the substrate. Hydrogen spillover has been reported for other 2D substrates, such as graphene, carbon nanotubes and C₆₀ fullerene [65-67], thus, the obtained results suggest that this process may take place in the BP-Pt system as well.

Importantly, from band structure and DOS in Fig. 6, it can be seen that interaction of BP with H_2 molecule does not induce changes in the electronic structure of the BP because the H_2 molecule states are mixed with the BP states, over and under minimal conduction band and maximal valence band. Besides, it can be seen that Pt atom in BP with H_2 causes the induction of additional bands near the Fermi level and lowers the conduction band minimum, as was discussed previously. Finally, ELF plots evidence separation of electron densities of H_2 and the surface atoms in case of intact H_2 adsorption, pointing to its physisorption. In case of the dissociative hydrogen molecule adsorption an electron-rich regions around H and P atoms are formed, evidencing formation of chemical bond.

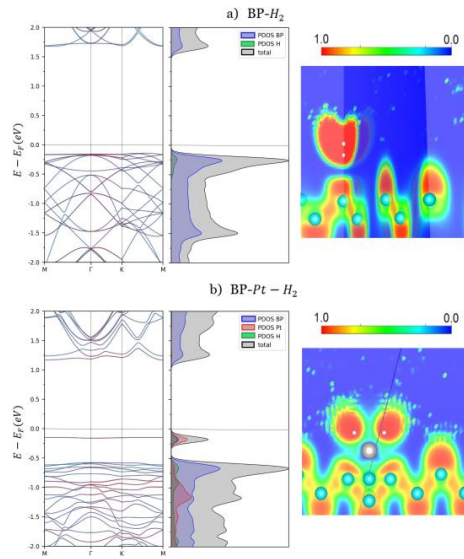
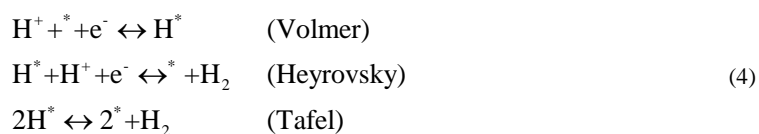


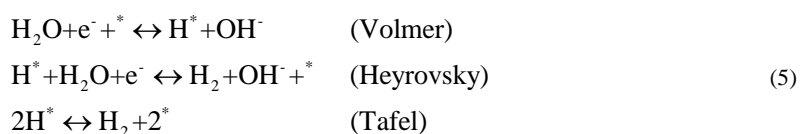
Figure 6: Effect of Pt in electronic structure of BP- H_2 ; panels a) and b) shows band structure, PDOS, DOS and ELF of BP- H_2 and BP-Pt - H_2 respectively. red lines in band structure represent the contribution of nearest P atoms to H_2 and Pt - H_2 . DOS/PDOS plots correspond to average of all atoms in the system, besides, PDOS represent the sum of s and p states for BP and d states for Pt. For each system, the Fermi level (horizontal line) is indicated.

3.4. Theoretically estimated BP and BP-Pt activities toward hydrogen evolution reaction

Depending on whether it takes place in acidic or alkaline media, HER is schematically expressed by 1. In acidic media the process starts with Volmer reaction, followed by either Heyrovsky or Tafel reaction, that in acid media can be expressed as:



Here * corresponds to surface adsorption site. Thus, the only reaction intermediate interacting with catalyst's surface is adsorbed hydrogen, and atomic hydrogen binding energy (HBE) on the material of interest has been the most common activity descriptor for HER in acidic media [68-72]. In alkaline media water is the expected reacting species, the HER mechanism is also comprised of three possible steps:



The reaction can proceed either by Volmer–Heyrovsky or Volmer-Tafel steps, but in either of the mechanisms atomic hydrogen is the only reaction intermediate adsorbed directly on the surface, similarly to the situation in acidic media. Therefore, an optimal HBE is still an important factor maintaining the balance between adsorption and desorption of H* intermediate in alkaline media.

Other factors may additionally define characteristics of HER, such as its rate. In general terms the rate of H⁺ and OH⁻ adsorption on the surface is the rate determining step for the HER in the acidic and alkaline media, respectively. During adsorption, the charge has to move through the interfacial double layer (H⁺ in acid and OH⁻ in alkaline) and its rate depends on the extent to which electrolyte, i.e. water, can accommodate this charge migration. If the interfacial water is easily reorganized, charge transfer through the double layer will be rapid; if the interfacial water is rigid and difficult to reorganize, charge transfer through the double layer will be slow.[73] Within the model, used in the present work, it is impossible to draw a conclusion about the impact of Pt atom presence on the BP surface on the near-surface water structure, and this question will be addressed in the future studies.

Therefore, using theoretically calculated values of hydrogen bond energy (HBE) it is possible to approximately estimate HER activity of BP and BP–Pt systems, since HBE is often used as an activity descriptor.[2, 3, 60, 74] Practically, HER exchange current density is a commonly used experimental criterion for evaluating catalytic activity of a material towards HER. Plotting it against the value of HBE, a volcano-type curve is obtained, on which the materials with the best catalytic properties for HER are located in the proximity of its apex. Although underlying principles are not completely clear yet, HER volcano plot is a useful tool for screening potential new catalysts and is used throughout the literature.

Thus, two branches of volcano curve were fitted with linear functions and the resulting curve can be seen in Fig. 7. For the sake of comparison, previously obtained data on HER activity of composite systems, comprised of Pt ML,

supported on polar terminations of tungsten and molybdenum carbide, is shown as well. **¡Error! No se encuentra el origen de la referencia.** It is important to keep in mind that $E_{\text{Ads,H}}$ values, presented in this figure, were obtained using half of the total energy of H_2 in gas phase as the reference.

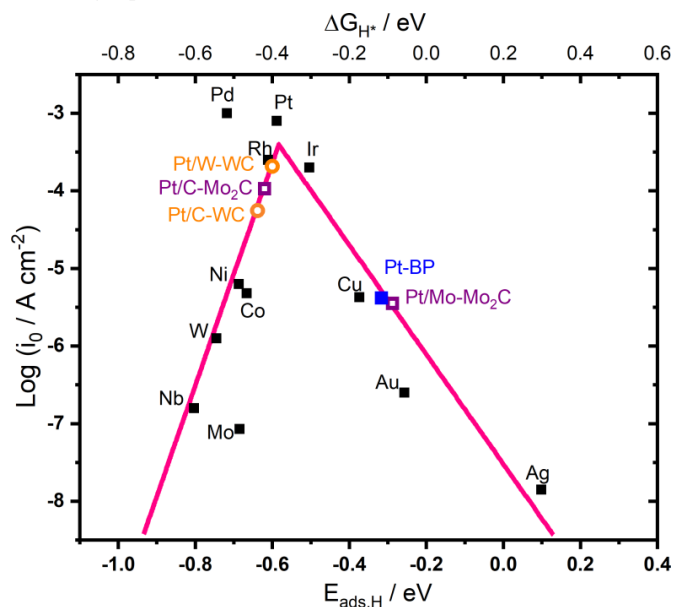


Figure 7: Volcano curve showing the correlation between theoretically calculated adsorption energy of atomic hydrogen and experimentally obtained HER exchange currents for selected metallic catalysts. Predictions on the HER activity for BP–Pt system is indicated with blue square. Value for the activity of the pristine BP system is outside of the scale of the plot and, therefore, is not indicated. Free energies for hydrogen adsorption, ΔG_{H^*} calculated as $E_{\text{Ads,H}} + 0.24\text{eV}$ [49], are indicated as well.

As it can be seen hydrogen binds too weakly to the surface of pristine BP ($\text{HBE} = 0.41\text{ eV}$), and, therefore is outside of the scale of the plot. However, adding a single Pt atom to the surface, affects significantly its electronic properties in the vicinity of the modification site, as it was discussed above. As the result a noticeable shift in the predicted activity is seen, suggesting that BP-Pt system performance for HER would be comparable to that of Ni.

Thus, similarly to other systems comprising Pt supported on various material (see Table S4 of the Supplementary Information), the resulting activity of BP-Pt system is lower than that of pure Pt, but noticeably higher than of unmodified BP. Compared to activity of Pt supported on SnO , TiSe_2 , CoS_2 and $\text{W}_2\text{B}_2\text{O}_2$ nanosheets [75-78] the BP-Pt system is expected to be more active. At the same time, as it is seen in Figure 7 and Table S4, transition metal carbides (TMC), employed as the support, are expected to be more active toward HER than BP-Pt. However, the direct comparison of the Pt/TMC and BP-Pt systems is not possible at the moment, since the mentioned Pt/TMC systems

consisted of a full platinum monolayer, supported on the carbides, while the present work focuses on the single Pt atom interacting with the BP monolayer. This analysis, however, is outside of the scope of the present work and could present an interest topic for a future study.

Indeed, in a realistic system low Pt coverage of 1/16 ML, described in the present work, is rarely attainable, and the coverage of Pt adatoms will play a twofold important role: i). at higher coverages more surface atoms of the BP will be affected by the presence of platinum, consequently affecting the average HBE on these surfaces; ii). at high Pt coverages most of the BP surface sites will become unavailable, and hydrogen adsorption will take place mostly on sites formed by the adatoms and their electronic structure would play an increasingly important role [12]. Therefore, an important next step would be to consider higher Pt coverages on BP ML to bring the model closer to actual practical catalytic system.

The stability under the working conditions is an important characteristic for potential catalysts. Using the method proposed by Anićijević et al. [79] the stability of BP-Pt systems was evaluated (See Section S1 of the Supporting Information). The obtained results indicated that a single Pt atom would not be very stable under the conditions of HER. This model, however, does not account for factors such as presence of electrolyte and possible formation of 3D Pt structures on the BP monolayer, therefore must be further expanded in the future to bring the theoretical model closer to the practical systems.

Nonetheless, the obtained information opens possibilities for fine tuning of the catalytic properties of 2D phosphorus-based systems and present an important first step toward further systematic approach to designing catalytically active materials, tailored for specific target processes.

Conclusions

Periodic DFT calculations have been performed on systems comprised of blue phosphorene monolayer with and without Pt atom present on the surface to study their interactions with atomic and molecular hydrogen. The obtained results evidence that in these systems presence of Pt atom causes charge transfer from the surface to the adsorbate. Also, Pt atom induces band transformation and state occupation, producing states near the Fermi level, all of which will promote the semiconductor properties of BP, and affect its interaction with species, adsorbed on the BP surface, in particular atomic and molecular hydrogen.

As the result of these changes the activity of BP-Pt systems toward HER sees an improvement, compared to that of the unmodified BP surface. Better understanding of the origins of the HER activity of the BP materials may offer a theoretical basis for a systematic and controlled design and development of new inexpensive catalysts for the hydrogen evolution reaction.

Acknowledgments

The authors would like to thank Universidad de Medellín (UdeM) for supporting their work. Authors thank MINCIENCIAS to financial support of this research by contract 120680864729.

References

- [1] Pera-Titus M. Porous inorganic membranes for CO_2 capture: present and prospects. *Chemical reviews*. 2014;114(2):1413-92.
- [2] Conway BE, Bockris JO. Electrolytic Hydrogen Evolution Kinetics and Its Relation to the Electronic and Adsorptive Properties of the Metal. *The Journal of Chemical Physics*. 1957 mar;26(3):532-41.
- [3] Trasatti S. Work function, electronegativity, and electrochemical behaviour of metals. *Journal of Electroanalytical Chemistry and Interfacial Electrochemistry*. 1972;39(1):163-84.
- [4] Skúlason E, Tripkovic V, Bjorketun ME, Gudmundsdóttir S, Karlberg G, Rossmeisl J, et al. Modeling the electrochemical hydrogen oxidation and evolution reactions on the basis of density functional theory calculations. *The Journal of Physical Chemistry C*. 2010;114(42):18182-97.
- [5] McCrum IT, Koper M. The role of adsorbed hydroxide in hydrogen evolution reaction kinetics on modified platinum. *Nature Energy*. 2020;5(11):891-9.
- [6] Cheng N, Stambula S, Wang D, Banis MN, Liu J, Riese A, et al. Platinum single-atom and cluster catalysis of the hydrogen evolution reaction. *Nature communications*. 2016;7(1):1-9.
- [7] Bockris J, Ammar I, Huq A. The mechanism of the hydrogen evolution reaction on platinum, silver and tungsten surfaces in acid solutions. *The Journal of Physical Chemistry*. 1957;61(7):879-86.
- [8] Zheng Y, Jiao Y, Zhu Y, Li LH, Han Y, Chen Y, et al. Hydrogen evolution by a metal-free electrocatalyst. *Nature communications*. 2014;5(1):1-8.
- [9] Zeng L, Li G, Zhang S, Xiao S, Zhao N, Chen BH, et al. Highly dispersed platinum on LaNi nanoparticles/nanoporous carbon for highly efficient electrocatalytic hydrogen evolution. *International Journal of Hydrogen Energy*. 2022.

- [10] Vasilchenko D, Zhurenok A, Saraev A, Gerasimov E, Cherepanova S, Kovtunova L, et al. Platinum deposition onto $g-C_3N_4$ with using of labile nitratocomplex for generation of the highly active hydrogen evolution photocatalysts. *International Journal of Hydrogen Energy*. 2022;47(21):11326-40.
- [11] Akter A, Pietras J, Gopalan S. Heavily neodymium doped ceria as an effective barrier layer in solid oxide electrochemical cells. *International Journal of Hydrogen Energy*. 2022;47(78):33429-38.
- [12] Koverga AA, Flórez E, Jimenez-Orozco C, Rodriguez JA. Not all platinum surfaces are the same: Effect of the support on fundamental properties of platinum adlayer and its implications for the activity toward hydrogen evolution reaction. *Electrochimica Acta*. 2021;368:137598.
- [13] Bhimanapati GR, Lin Z, Meunier V, Jung Y, Cha J, Das S, et al. Recent advances in two-dimensional materials beyond graphene. *ACS nano*. 2015;9(12):11509-39.
- [14] Wang L, Hu P, Long Y, Liu Z, He X. Recent advances in ternary two-dimensional materials: synthesis, properties and applications. *Journal of Materials Chemistry A*. 2017;5(44):22855-76.
- [15] Glavin NR, Rao R, Varshney V, Bianco E, Apte A, Roy A, et al. Emerging applications of elemental 2D materials. *Advanced Materials*. 2020;32(7):1904302.
- [16] Jeong GH, Sasikala SP, Yun T, Lee GY, Lee WJ, Kim SO. Nanoscale assembly of 2D materials for energy and environmental applications. *Advanced Materials*. 2020;32(35):1907006.
- [17] Shifa TA, Wang F, Liu Y, He J. Heterostructures based on 2D materials: A versatile platform for efficient catalysis. *Advanced Materials*. 2019;31(45):1804828.
- [18] Ao KL, Shao Y, Chan IN, Shi X, Kawazoe Y, Yang M, et al. Design of novel pentagonal 2D transitional-metal sulphide monolayers for hydrogen evolution reaction. *International Journal of Hydrogen Energy*. 2020;45(32):16201-9.
- [19] Qin B, Zhang Q, Li YH, Yang G, Peng F. Formation of lattice-dislocated zinc oxide via anodic corrosion for electrocatalytic CO_2 reduction to syngas with a potential-dependent CO: H_2 ratio. *ACS applied materials & interfaces*. 2020;12(27):30466-73.
- [20] Wang E, Zhang B, Zhou J, Sun Z. High catalytic activity of MBenes supported single atom catalysts for oxygen reduction and oxygen evolution reaction. *Applied Surface Science*. 2022;604:154522.
- [21] Ren Y, Zhai Q, Wang B, Hu L, Ma Y, Dai Y, et al. Synergistic Adsorption Electrocatalysis of 2D/2D

- heterostructure toward high performance Li-S batteries. *Chemical Engineering Journal*. 2022;439:135535.
- [22] Jin H, Yu H, Li H, Davey K, Song T, Paik U, et al. MXene Analogue: A 2D Nitridene Solid Solution for High-Rate Hydrogen Production. *Angewandte Chemie International Edition*. 2022:e202203850.
- [23] Lu Y, Zhong H, Li J, Dominic AM, Hu Y, Gao Z, et al. sp-Carbon Incorporated Conductive Metal-Organic Framework as Photocathode for Photoelectrochemical Hydrogen Generation. *Angewandte Chemie International Edition*. 2022:e202208163.
- [24] Hu R, Jiang H, Xian J, Mi S, Wei L, Fang G, et al. Microwave-pulse sugarblowing assisted synthesis of 2D transition metal carbides for sustainable hydrogen evolution. *Applied Catalysis B: Environmental*. 2022;317:121728.
- [25] Pang J, Bachmatiuk A, Yin Y, Trzebicka B, Zhao L, Fu L, et al. Applications of phosphorene and black phosphorus in energy conversion and storage devices. *Advanced Energy Materials*. 2018;8(8):1702093.
- [26] Yang A, Wang D, Wang X, Zhang D, Koratkar N, Rong M. Recent advances in phosphorene as a sensing material. *Nano Today*. 2018;20:13-32.
- [27] Zhang Wl, Zhang K, Wu Xj. Enhanced catalytic hydrogen evolution reaction in phosphorene nanosheet via cobalt intercalation. *Chinese Journal of Chemical Physics*. 2019;32(5):572.
- [28] Srivastava R, Nouseen S, Chattopadhyay J, Woi PM, Son DN, Bastakoti BP. Recent Advances in Electrochemical Water Splitting and Reduction of CO_2 into Green Fuels on 2D Phosphorene-Based Catalyst. *Energy Technology*. 2021;9(1):2000741.
- [29] Dinh KN, Zhang Y, Zhu J, Sun W. Phosphorene-Based Electrocatalysts. *Chemistry –A European Journal*. 2020;26(29):6437-46.
- [30] Cai Y, Gao J, Chen S, Ke Q, Zhang G, Zhang YW. Design of phosphorene for hydrogen evolution performance comparable to platinum. *Chemistry of Materials*. 2019;31(21):8948-56.
- [31] Shao L, Sun H, Miao L, Chen X, Han M, Sun J, et al. Facile preparation of NH_2 -functionalized black phosphorene for the electrocatalytic hydrogen evolution reaction. *Journal of Materials Chemistry A*. 2018;6(6):2494-9.
- [32] Wu Q, Liang M, Zhang S, Liu X, Wang F. Development of functional black phosphorus nanosheets with remarkable catalytic and antibacterial performance. *Nanoscale*. 2018;10(22):10428-35.

- [33] Wu T, Ma Y, Qu Z, Fan J, Li Q, Shi P, et al. Black phosphorus–graphene heterostructure-supported Pd nanoparticles with superior activity and stability for ethanol electro-oxidation. *ACS applied materials & interfaces*. 2019;11(5):5136-45.
- [34] Bai L, Wang X, Tang S, Kang Y, Wang J, Yu Y, et al. Black phosphorus/platinum heterostructure: a highly efficient photocatalyst for solar-driven chemical reactions. *Advanced Materials*. 2018;30(40):1803641.
- [35] Wang X, Bai L, Lu J, Zhang X, Liu D, Yang H, et al. Rapid activation of platinum with black phosphorus for efficient hydrogen evolution. *Angewandte Chemie*. 2019;131(52):19236-42.
- [36] Kovalska E, Luxa J, Melle-Franco M, Wu B, Marek I, Roy PK, et al. Single step synthesis of platinum-decorated phosphorene: perspectives for catalysis, gas sensing, and energy storage. *ACS applied materials & interfaces*. 2020;12(45):50516-26.
- [37] Gan Y, Xue XX, Jiang XX, Xu Z, Chen K, Yu JF, et al. Chemically modified phosphorene as efficient catalyst for hydrogen evolution reaction. *Journal of Physics: Condensed Matter*. 2019;32(2):025202.
- [38] Lu J, Zhang X, Liu D, Yang N, Huang H, Jin S, et al. Modulation of phosphorene for optimal hydrogen evolution reaction. *ACS applied materials & interfaces*. 2019;11(41):37787-95.
- [39] Wang M, Song R, Zhang X, Liu G, Xu S, Xu Z, et al. Defects engineering promotes the electrochemical hydrogen evolution reaction property of phosphorene surface. *international journal of hydrogen energy*. 2021;46(2):1913-22.
- [40] Liu F, Huang Z, Liu H, Liao Y, Qi X, Zhong J. Strain Modulation of Black Phosphorene for the Hydrogen Evolution Reaction Activity. *physica status solidi (b)*. 2021;258(11):2100195.
- [41] Vishnoi P, Gupta U, Pandey R, Rao CN. Stable functionalized phosphorenes with photocatalytic HER activity. *Journal of Materials Chemistry A*. 2019;7(12):6631-7.
- [42] Liu D, Wang J, Lu J, Ma C, Huang H, Wang Z, et al. Direct synthesis of metal-doped phosphorene with enhanced electrocatalytic hydrogen evolution. *Small Methods*. 2019;3(7):1900083.
- [43] Zhu Z, Tománek D. Semiconducting layered blue phosphorus: a computational study. *Physical review letters*. 2014;112(17):176802.
- [44] Zhang W, Enriquez H, Tong Y, Bendounan A, Kara A, Seitsonen AP, et al. Epitaxial synthesis of blue phosphorene. *Small*. 2018;14(51):1804066.
- [45] Zhang JL, Zhao S, Sun S, Ding H, Hu J, Li Y, et al. Synthesis of Monolayer Blue Phosphorus Enabled

- by Silicon Intercalation. *ACS nano*. 2020;14(3):3687-95.
- [46] Sun M, Chou JP, Hu A, Schwingenschlogl U. Point defects in blue phosphorene. *Chemistry of Materials*. 2019;31(19):8129-35.
- [47] Swaroop R, Ahluwalia P, Tankeshwar K, Kumar A. Ultra-narrow blue phosphorene nanoribbons for tunable optoelectronics. *RSC advances*. 2017;7(5):2992-3002.
- [48] Ju L, Dai Y, Wei W, Liang Y, Huang B. Potential of one-dimensional blue phosphorene nanotubes as a water splitting photocatalyst. *Journal of Materials Chemistry A*. 2018;6(42):21087-97.
- [49] Cheng Y, Song Y, Zhang Y. The doping and oxidation of 2D black and blue phosphorene: a new photocatalyst for nitrogen reduction driven by visible light. *Physical Chemistry Chemical Physics*. 2019;21(44):24449-57.
- [50] Maibam A, Das SK, Samal PP, Krishnamurty S. Enhanced photocatalytic properties of a chemically modified blue phosphorene. *RSC Advances*. 2021;11(22):13348-58.
- [51] Xiao Y, Wang J, Wang Y, Zhang W. A new promising catalytic activity on blue phosphorene nitrogen-doped nanosheets for the ORR as cathode in nonaqueous Li-air batteries. *Applied Surface Science*. 2019;488:620-8.
- [52] Li C, Xu Y, Sheng W, Yin WJ, Nie GZ, Ao Z. A promising blue phosphorene/ C_2N van der Waals type-II heterojunction as a solar photocatalyst: a first-principles study. *Physical Chemistry Chemical Physics*. 2020;22(2):615-23.
- [53] Wang BJ, Li XH, Zhao R, Cai XL, Yu WY, Li WB, et al. Electronic structures and enhanced photocatalytic properties of blue phosphorene/BSe van der Waals heterostructures. *Journal of Materials Chemistry A*. 2018;6(19):8923-9.
- [54] Maibam A, Chakraborty D, Joshi K, Krishnamurty S. Exploring edge functionalised blue phosphorene nanoribbons as novel photocatalysts for water splitting. *New Journal of Chemistry*. 2021;45(7):3570-80.
- [55] Zhu J, Cai L, Yin X, Wang Z, Zhang L, Ma H, et al. Enhanced electrocatalytic hydrogen evolution activity in single-atom Pt-decorated VS_2 nanosheets. *ACS nano*. 2020;14(5):5600-8.
- [56] Kresse G, Furthmüller J. Efficient iterative schemes for ab initio total energy calculations using a plane-wave basis set. *Physical review B*. 1996;54(16):11169.

- [57] Perdew JP, Burke K, Ernzerhof M. Generalized gradient approximation made simple. *Physical review letters*. 1996;77(18):3865.
- [58] Monkhorst HJ, Pack JD. Special points for Brillouin-zone integrations. *Physical review B*. 1976;13(12):5188.
- [59] Grimme S, Antony J, Ehrlich S, Krieg H. A consistent and accurate ab initio parametrization of density functional dispersion correction (DFT-D) for the 94 elements H-Pu. *The Journal of chemical physics*. 2010;132(15):154104.
- [60] Nørskov JK, Bligaard T, Logadottir A, Kitchin JR, Chen JG, Pandelov S, et al. Trends in the Exchange Current for Hydrogen Evolution. *Journal of The Electrochemical Society*. 2005;152(3):J23.
- [61] Sun X, Luan S, Shen H, Lei S. Effect of metal doping on carbon monoxide adsorption on phosphorene: a first-principles study. *Superlattices and Microstructures*. 2018;124:168-75.
- [62] Kulish VV, Malyi OI, Persson C, Wu P. Adsorption of metal adatoms on single-layer phosphorene. *Physical Chemistry Chemical Physics*. 2015;17(2):992-1000.
- [63] Santos E, Quaino P, Schmickler W. Theory of electrocatalysis: hydrogen evolution and more. *Physical Chemistry Chemical Physics*. 2012;14(32):11224-33.
- [64] Quaino P, Santos E, Soldano G, Schmickler W. Recent Progress in Hydrogen Electrocatalysis. *Advances in Physical Chemistry*. 2011.
- [65] Sihag A, Xie ZL, Thang HV, Kuo CL, Tseng FG, Dyer MS, et al. DFT insights into comparative hydrogen adsorption and hydrogen spillover mechanisms of Pt_4 /graphene and Pt_4 /anatase (101) surfaces. *The Journal of Physical Chemistry C*. 2019;123(42):25618-27.
- [66] Ambrusi R, Orazi V, Marchetti J, Juan A, Pronsato M. Hydrogen storage by spillover on Ni_4 cluster embedded in three vacancy graphene. A DFT and dynamics study. *Journal of Physics and Chemistry of Solids*. 2022;167:110706.
- [67] Moyal AM, Paz-Tal O, Ben-Yehuda E, Moretto P, Bielewski M, Napolitano E, et al. Insights on hydrogen spillover on carbonaceous supports. *Nanoscale*. 2022;14(25):9068-77.
- [68] Zheng J, Sheng W, Zhuang Z, Xu B, Yan Y. Universal dependence of hydrogen oxidation and evolution reaction activity of platinum-group metals on pH and hydrogen binding energy. *Science advances*.

- 2016;2(3):e1501602.
- [69] Bhowmik T, Kundu MK, Barman S. Palladium nanoparticle–graphitic carbon nitride porous synergistic catalyst for hydrogen evolution/oxidation reactions over a broad range of pH and correlation of its catalytic activity with measured hydrogen binding energy. *Acs Catalysis*. 2016;6(3):1929-41.
- [70] Tian X, Zhao P, Sheng W. Hydrogen evolution and oxidation: mechanistic studies and material advances. *Advanced Materials*. 2019;31(31):1808066.
- [71] Dubouis N, Grimaud A. The hydrogen evolution reaction: from material to interfacial descriptors. *Chemical Science*. 2019;10(40):9165-81.
- [72] Rebollar L, Intikhab S, Oliveira NJ, Yan Y, Xu B, McCrum IT, et al. “Beyond adsorption” descriptors in hydrogen electrocatalysis. *ACS Catalysis*. 2020;10(24):14747-62.
- [73] Ledezma-Yanez I, Wallace W D Z, Sebastián-Pascual P, Climent V, Feliu JM, Koper M. Interfacial water reorganization as a pH-dependent descriptor of the hydrogen evolution rate on platinum electrodes. *Nature Energy*. 2017;2(4):1-7.
- [74] Michalsky R, Zhang YJ, Peterson AA. Trends in the Hydrogen Evolution Activity of Metal Carbide Catalysts. *ACS Catalysis*. 2014;4(5):1274-8.
- [75] Sun Z, Gao Z, Zhang C, Guan L, Tao J. Atomically dispersed low-cost transition metals catalyze efficient hydrogen evolution on two-dimensional SnO nanosheets. *International Journal of Hydrogen Energy*. 2021;46(56):28602- 12.
- [76] Li B, Wu Y, Li N, Chen X, Zeng X. Arramel; Zhao, X.; Jiang, J. Single Metal Atoms Supported on MBenes for Robust Electrochemical Hydrogen Evolution *ACS Appl Mater Interfaces*. 2020;12(8):9261-7.
- [77] Song Z, Yi J, Qi J, Zheng Q, Zhu Z, Tao L, et al. Line defects in monolayer $TiSe_2$ with adsorption of Pt atoms potentially enable excellent catalytic activity. *Nano Research*. 2022;15(5):4687-92.
- [78] Shi J, Chen T, Sun X. The effect of heteroatom doping on the active metal site of CoS_2 for hydrogen evolution reaction. *RSC Advances*. 2022;12(27):17257-63.
- [79] Aničijević DDV, Nikolić VM, Marčeta-Kaninski MP, Pašti IA. Is platinum necessary for efficient hydrogen evolution? –DFT study of metal mono-layers on tungsten carbide. *International journal of hydrogen*

energy. 2013;38(36):16071-9.

7. Conclusions

7.1. SPIN: [S]imple [P]ython [I]pywidgets [N]otebook Interface to obtain the optoelectronic properties of materials employing DFT

SPIN is a new versatile tool for researchers who want to reduce complexity of using SIESTA software in their studies. Because it provides higher-level user interaction, it can be also used for educational purposes. SPIN is a Ipywidgets based Interface which allow users to work easily in any operating system (Windows, Linux and Mac), because it works on Jupyter Notebooks. This new tools allow the users to work with standard SIESTA files and prepare figures of the atomic structure and properties such band structure, DOS, PDOS and optical properties for publication.

What can be expected from SPIN in the future? At the current stage, the core structure of SPIN deals with completed pipeline using SIESTA calculator, however, SPIN has been developed to easily add new functions and calculators, in that sense, for future we expected to add functionalities for other calculators, for example, GPAW, among others. As the number of available calculators increases and new functionality is added, SPIN will hopefully become an even more attractive toolbox contributing to efficient development and utilization of electronic structure theory and molecular dynamics simulations. We hope that SPIN will also encourage and contribute to further collaborative efforts with open exchange of not only data and results but also efficient scripting to the benefit of the research community.

7.2. Impact of different structural defects on fundamental properties of blue phosphorene nanotubes

We have investigated electronic structures of $n = 7$ to $n = 14$ armchair and zigzag blue phosphorene nanotubes with various types of defects, including, double-vacancy

and Stone-wales defect, and the effect of applied external electric field on it, by using the first-principles calculations in the density-function theory. Our results indicate that all vacancy defect types induce a decreasing in the BPNTs band gap. Besides, the effect of single-vacancies in reducing the system band gap is stronger in both, zigzag and armchair, compared to other types of defects, reaching a value 90% lower in the armchair systems compared with pristine nanotubes and 65% in those of the zigzag types.

When a external electric field is applied on the structures, we have observed that bigger systems requires lower field strengths to reach the semiconductor-metal transition. This transition does exist regardless of the vacancy defect type on armchair systems, which makes the armchair chirality more favorable to achieve it. We can also conclude that both single-vacancy systems (type-A and type-B) require lower electric field values to become a metallic material metal, compared with other all systems.

With regard to the optical properties, we have revealed an anisotropy linked to the particular incident light polarization to be either parallel or perpendicular to the nanotube growth direction. Besides, the differences in values of the calculated index of refraction, related with the presence or absence of defects, are noticeable mainly within the visible range and above, whilst static values remain practically the same for larger nanotubes and only show deviations in smaller zigzag nanotubes laden with type B single vacancies.

This characterization of structural defects and their effects on the optoelectronic properties of blue phosphorene nanotubes is required to define how the surface of the nanotubes could be utilized to develop new optoelectronic devices.

7.3. Adsorption affinity of sulfonamides onto Blue-phosphorene nanotubes

Electronic response of Zigzag and Armchair BPNTs to biologically active sulfonamide-based compounds were studied using DFT calculations. Results indicate that analyzed molecules SAM, SDZ, SMX are weakly adsorbed on the pristine BPNTs with adsorption energy of about $-0,312$, $-0,285$ and $-0,248$ eV, Besides, for SAM molecule, Benzene position is the most outstanding in the results, since it obtained the highest adsorption energy within its respective groups (same chirality and same type of vacancy). To improve the adsorption, a P atom of the BPNT has been removed given a single-vacancy defect. SV increase the reactivity of the BPNTs so that the adsorption energies increased for all evaluated systems to about a percentage ranges that go from 20% to 89% for the AM SAM (smaller increase) and AM SDZ (larger increase) systems, respectively. This indicates that structural defects, improve the capacity of BPNTs for adsorption of these toxic antibiotics. The orders of E_{ads} of three sulfonamides were as follows: SAM > SDZ > SMX for pristine systems and ZZ SV. In SV AM-BPNTs SDZ molecule presents higher E_{ads} than SAM and SMX (SDZ > SAM > SMX). The calculations results demonstrate that despite the increase in the reactivity of the ZZ SV BPNT to the sulfonamides, AM configurations show a transition from bipolar-magnetic semiconductor to not magnetic metallic system, suggesting that defective AM BPNTs also can be employed as a sensor for antibi-

otic molecules like SAM, SDZ, and SMX.

7.4. Modulation of Blue-Phosphorene for *Pt* atom adsorption by hydrogen evolution reaction

Periodic DFT calculations have been performed on systems comprised of blue phosphorene monolayer with and without Pt atom present on the surface to study their interactions with atomic and molecular hydrogen. The obtained results evidence that in these systems presence of Pt atom causes charge transfer from the surface to the adsorbate. Also, Pt atom induces band transformation and state occupation, producing states near the Fermi level, all of which will promote the semiconductor properties of BP, and affect its interaction with species, adsorbed on the BP surface, in particular atomic and molecular hydrogen.

As the result of these changes the activity of BP–Pt systems toward HER sees an improvement, compared to that of the unmodified BP surface. Better understanding of the origins of the HER activity of the BP materials may offer a theoretical basis for a systematic and controlled design and development of new inexpensive catalysts for the hydrogen evolution reaction.

Bibliography

- [1] A. H. Larsen, J. J. Mortensen, J. Blomqvist, I. E. Castelli, R. Christensen, M. Dułak, J. Friis, M. N. Groves, B. Hammer, C. Hargus, et al., “The atomic simulation environment—a python library for working with atoms,” *Journal of Physics: Condensed Matter*, vol. 29, no. 27, p. 273002, 2017.
- [2] J. M. Soler, E. Artacho, J. D. Gale, A. García, J. Junquera, P. Ordejón, and D. Sánchez-Portal, “The SIESTA method for ab initio order-n materials simulation,” *Journal of Physics: Condensed Matter*, vol. 14, pp. 2745–2779, mar 2002.
- [3] J. Enkovaara, C. Rostgaard, J. J. Mortensen, J. Chen, M. Dułak, L. Ferrighi, J. Gavnholt, C. Glinsvad, V. Haikola, H. Hansen, et al., “Electronic structure calculations with gpaw: a real-space implementation of the projector augmented-wave method,” *Journal of physics: Condensed matter*, vol. 22, no. 25, p. 253202, 2010.
- [4] P. Giannozzi, S. Baroni, N. Bonini, M. Calandra, R. Car, C. Cavazzoni, D. Ceresoli, G. L. Chiarotti, M. Cococcioni, I. Dabo, et al., “Quantum espresso: a modular and open-source software project for quantum simulations of materials,” *Journal of physics: Condensed matter*, vol. 21, no. 39, p. 395502, 2009.
- [5] G. Kresse and J. Furthmüller, “Efficient iterative schemes for ab initio total-energy calculations using a plane-wave basis set,” *Physical review B*, vol. 54, no. 16, p. 11169, 1996.
- [6] N. Papior, J. L. B. Pfeiffer, T. Frederiksen, and S. S. Wuhl, “zeroth/isl: v0.11.0,” Feb. 2021.
- [7] V. Wang, N. Xu, J.-C. Liu, G. Tang, and W.-T. Geng, “Vaspkit: a user-friendly interface facilitating high-throughput computing and analysis using vasp code,” *Computer Physics Communications*, p. 108033, 2021.
- [8] T. Kluyver, B. Ragan-Kelley, F. Pérez, B. E. Granger, M. Bussonnier, J. Frederic, K. Kelley, J. B. Hamrick, J. Grout, S. Corlay, et al., “Jupyter notebooks—a publishing format for reproducible computational workflows,” in *ELPUB*, pp. 87–90, 2016.

-
- [9] U. Herath, P. Tavadze, X. He, E. Bousquet, S. Singh, F. Muñoz, and A. H. Romero, “Pyprocar: A python library for electronic structure pre/post-processing,” *Computer Physics Communications*, vol. 251, p. 107080, 2020.
- [10] S. P. Ong, W. D. Richards, A. Jain, G. Hautier, M. Kocher, S. Cholia, D. Gunter, V. L. Chevrier, K. A. Persson, and G. Ceder, “Python materials genomics (pymatgen): A robust, open-source python library for materials analysis,” *Computational Materials Science*, vol. 68, pp. 314–319, 2013.
- [11] S. Sozykin, “Gui4dft—a siesta oriented gui,” *Computer Physics Communications*, vol. 262, p. 107843, 2021.
- [12] S. B. Lisesivdin and B. Sarikavak-Lisesivdin, “gpaw-tools—higher-level user interaction scripts for gpaw calculations and interatomic potential based structure optimization,” *Computational Materials Science*, vol. 204, p. 111201, 2022.
- [13] F. Marchesin, P. Koval, Y. Pouillon, I. Lebedeva, A. García, M. García-Mota, A. Kimmel “Atomistic Simulation Advanced Platform (ASAP) for materials modelling with ab initio methods”, Psi-k conference 2022, Lausanne (Switzerland), abstract book.
- [14] P. R. Wallace, “The band theory of graphite,” *Physical review*, vol. 71, no. 9, p. 622, 1947.
- [15] K. S. Novoselov, A. K. Geim, S. V. Morozov, D. Jiang, Y. Zhang, S. V. Dubonos, I. V. Grigorieva, and A. A. Firsov, “Electric field effect in atomically thin carbon films,” *science*, vol. 306, no. 5696, pp. 666–669, 2004.
- [16] R. Raccichini, A. Varzi, S. Passerini, and B. Scrosati, “The role of graphene for electrochemical energy storage,” *Nature materials*, vol. 14, no. 3, pp. 271–279, 2015.
- [17] G. R. Bhimanapati, Z. Lin, V. Meunier, Y. Jung, J. Cha, S. Das, D. Xiao, Y. Son, M. S. Strano, V. R. Cooper, et al., “Recent advances in two-dimensional materials beyond graphene,” *ACS nano*, vol. 9, no. 12, pp. 11509–11539, 2015.
- [18] L. Wang, P. Hu, Y. Long, Z. Liu, and X. He, “Recent advances in ternary two-dimensional materials: synthesis, properties and applications,” *Journal of Materials Chemistry A*, vol. 5, no. 44, pp. 22855–22876, 2017.
- [19] B. Xu, S. Qi, M. Jin, X. Cai, L. Lai, Z. Sun, X. Han, Z. Lin, H. Shao, P. Peng, et al., “2020 roadmap on two-dimensional materials for energy storage and conversion,” *Chinese Chemical Letters*, vol. 30, no. 12, pp. 2053–2064, 2019.
- [20] N. R. Glavin, R. Rao, V. Varshney, E. Bianco, A. Apte, A. Roy, E. Ringe, and P. M. Ajayan, “Emerging applications of elemental 2d materials,” *Advanced Materials*, vol. 32, no. 7, p. 1904302, 2020.
-

- [21] J. Pang, A. Bachmatiuk, Y. Yin, B. Trzebicka, L. Zhao, L. Fu, R. G. Mendes, T. Gemming, Z. Liu, and M. H. Rummeli, "Applications of phosphorene and black phosphorus in energy conversion and storage devices," *Advanced Energy Materials*, vol. 8, no. 8, p. 1702093, 2018.
- [22] A. Yang, D. Wang, X. Wang, D. Zhang, N. Koratkar, and M. Rong, "Recent advances in phosphorene as a sensing material," *Nano Today*, vol. 20, pp. 13–32, 2018.
- [23] P. Bridgman, "Two new modifications of phosphorus.," *Journal of the American Chemical Society*, vol. 36, no. 7, pp. 1344–1363, 1914.
- [24] L. Donarelli, Maurizio; Ottaviano, "2d materials for gas sensing applications: A review on graphene oxide, mos₂, ws₂ and phosphorene," *Sensors*, vol. 18, 10 2018.
- [25] H. Liu, A. T. Neal, Z. Zhu, Z. Luo, X. Xu, D. Tománek, and P. D. Ye, "Phosphorene: an unexplored 2d semiconductor with a high hole mobility," *ACS nano*, vol. 8, no. 4, pp. 4033–4041, 2014.
- [26] A. Castellanos-Gomez, L. Vicarelli, E. Prada, J. O. Island, K. Narasimha-Acharya, S. I. Blanter, D. J. Groenendijk, M. Buscema, G. A. Steele, J. Alvarez, et al., "Isolation and characterization of few-layer black phosphorus," *2D Materials*, vol. 1, no. 2, p. 025001, 2014.
- [27] S. Bagheri, N. Mansouri, and E. Aghaie, "Phosphorene: a new competitor for graphene," *International Journal of Hydrogen Energy*, vol. 41, no. 7, pp. 4085–4095, 2016.
- [28] R. Nourbakhsh, Zahra; Asgari, "Phosphorene as a nanoelectromechanical material," *Physical Review B*, vol. 98, 9 2018.
- [29] L. Kou, C. Chen, and S. C. Smith, "Phosphorene: fabrication, properties, and applications," *The journal of physical chemistry letters*, vol. 6, no. 14, pp. 2794–2805, 2015.
- [30] Y. Aierken, O. Leenaerts, and F. M. Peeters, "Defect-induced faceted blue phosphorene nanotubes," *Physical Review B*, vol. 92, no. 10, p. 104104, 2015.
- [31] K. N. Alnassar, M. Roknabadi, M. Behdani, and B. Shohany, "Theoretical study of electronic properties of nanostructures composed of blue phosphorene and graphene sheet," vol. 871, no. 1, p. 012084, 2020.
- [32] V. Sorkin, Y. Cai, Z. Ong, G. Zhang, and Y.-W. Zhang, "Recent advances in the study of phosphorene and its nanostructures," *Critical Reviews in Solid State and Materials Sciences*, vol. 42, no. 1, pp. 1–82, 2017.

-
- [33] R. Pica, Monica; D'Amato, "Chemistry of phosphorene: Synthesis, functionalization and biomedical applications in an update review," *Inorganics*, vol. 8, 04 2020.
- [34] Z. Zhu and D. Tománek, "Semiconducting layered blue phosphorus: a computational study," *Physical review letters*, vol. 112, no. 17, p. 176802, 2014.
- [35] W. Zhang, H. Enriquez, Y. Tong, A. Bendounan, A. Kara, A. P. Seitsonen, A. J. Mayne, G. Dujardin, and H. Oughaddou, "Epitaxial synthesis of blue phosphorene," *Small*, vol. 14, no. 51, p. 1804066, 2018.
- [36] J. L. Zhang, S. Zhao, S. Sun, H. Ding, J. Hu, Y. Li, Q. Xu, X. Yu, M. Telychko, J. Su, et al., "Synthesis of monolayer blue phosphorus enabled by silicon intercalation," *ACS nano*, vol. 14, no. 3, pp. 3687–3695, 2020.
- [37] R. Swaroop, P. Ahluwalia, K. Tankeshwar, and A. Kumar, "Ultra-narrow blue phosphorene nanoribbons for tunable optoelectronics," *RSC advances*, vol. 7, no. 5, pp. 2992–3002, 2017.
- [38] M. Sun, W. Tang, Q. Ren, S.-k. Wang, J. Yu, and Y. Du, "A first-principles study of light non-metallic atom substituted blue phosphorene," *Applied Surface Science*, vol. 356, pp. 110–114, 2015.
- [39] G. A. Shaikh, D. Raval, B. Babariya, S. K. Gupta, and P. Gajjar, "An ab-initio study of blue phosphorene monolayer: Electronic, vibrational and optical properties," *Materials Today: Proceedings*, 2020.
- [40] F. Safari, M. Fathipour, and A. Y. Goharrizi, "Electronic and transport properties of blue phosphorene in presence of point defects: a first-principles study," *Physica E: Low-dimensional Systems and Nanostructures*, vol. 118, p. 113938, 2020.
- [41] X. Wang, G. Sun, N. Li, and P. Chen, "Quantum dots derived from two-dimensional materials and their applications for catalysis and energy," *Chemical Society Reviews*, vol. 45, no. 8, pp. 2239–2262, 2016.
- [42] A. Carvalho, A. Rodin, and A. C. Neto, "Phosphorene nanoribbons," *EPL (Europhysics Letters)*, vol. 108, no. 4, p. 47005, 2014.
- [43] D. Drumm, J. Smith, M. Per, A. Budi, L. Hollenberg, and S. Russo, "Ab initio electronic properties of monolayer phosphorus nanowires in silicon," *Physical review letters*, vol. 110, no. 12, p. 126802, 2013.
- [44] F. Bachhuber, J. von Appen, R. Dronskowski, P. Schmidt, T. Nilges, A. Pfitzner, and R. Wehrich, "The extended stability range of phosphorus allotropes," *Angewandte Chemie International Edition*, vol. 53, no. 43, pp. 11629–11633, 2014.
- [45] C. Li, Z. Xie, Z. Chen, N. Cheng, J. Wang, and G. Zhu, "Tunable bandgap and optical properties of black phosphorene nanotubes," *Materials*, vol. 11, no. 2, p. 304, 2018.

- [46] V. N. Popov, "Carbon nanotubes: properties and application," *Materials Science and Engineering: R: Reports*, vol. 43, no. 3, pp. 61–102, 2004.
- [47] V. V. Pokropivny, "Non-carbon nanotubes (review). part 2. types and structure," *Powder Metallurgy and Metal Ceramics*, vol. 40, no. 11-12, pp. 582–594, 2001.
- [48] A. L. Ivanovskii, "Non-carbon nanotubes: synthesis and simulation," *Russian chemical reviews*, vol. 71, no. 3, pp. 175–194, 2002.
- [49] M. Endo, T. Hayashi, Y. A. Kim, and H. Muramatsu, "Development and application of carbon nanotubes," *Japanese Journal of Applied Physics*, vol. 45, no. 6R, p. 4883, 2006.
- [50] N. Govindaraju and R. Singh, "Chapter 8–synthesis and properties of boron nitride nanotubes. nanotube superfiber materials," 2014.
- [51] N. M. Bardhan, "30 years of advances in functionalization of carbon nanomaterials for biomedical applications: a practical review," *Journal of Materials Research*, vol. 32, no. 1, pp. 107–127, 2017.
- [52] Z. He, Y. Jiang, J. Zhu, Y. Li, L. Dai, W. Meng, L. Wang, and S. Liu, "Phosphorus doped multi-walled carbon nanotubes: An excellent electrocatalyst for the $\text{VO}_2^+/\text{VO}_2$ redox reaction," *ChemElectroChem*, vol. 5, no. 17, pp. 2464–2474, 2018.
- [53] E. Kianfar, "Recent advances in synthesis, properties, and applications of vanadium oxide nanotube," *Microchemical Journal*, vol. 145, pp. 966–978, 2019.
- [54] F. Dvorak, R. Zazpe, M. Krbal, H. Sopha, J. Prikryl, S. Ng, L. Hromadko, F. Bures, and J. M. Macak, "One-dimensional anodic TiO_2 nanotubes coated by atomic layer deposition: Towards advanced applications," *Applied Materials Today*, vol. 14, pp. 1–20, 2019.
- [55] E. S. Goda, M. Gab-Allah, B. S. Singu, and K. R. Yoon, "Halloysite nanotubes based electrochemical sensors: A review," *Microchemical Journal*, vol. 147, pp. 1083–1096, 2019.
- [56] G. Rahman, Z. Najaf, A. Mehmood, S. Bilal, S. A. Mian, G. Ali, et al., "An overview of the recent progress in the synthesis and applications of carbon nanotubes," *Carbon Journal of Carbon Research*, vol. 5, no. 1, p. 3, 2019.
- [57] S. Yu, H. Zhu, K. Eshun, A. Arab, A. Badwan, and Q. Li, "A computational study of the electronic properties of one-dimensional armchair phosphorene nanotubes," *Journal of Applied Physics*, vol. 118, no. 16, p. 164306, 2015.
- [58] Y. Aierken, O. Leenaerts, and F. M. Peeters, "Defect-induced faceted blue phosphorene nanotubes," *Physical Review B*, vol. 92, no. 10, p. 104104, 2015.

-
- [59] J. Xiao, M. Long, C.-S. Deng, J. He, L.-L. Cui, and H. Xu, "Electronic structures and carrier mobilities of blue phosphorus nanoribbons and nanotubes: a first-principles study," *The Journal of Physical Chemistry C*, vol. 120, no. 8, pp. 4638–4646, 2016.
- [60] L. Ju, Y. Dai, W. Wei, Y. Liang, and B. Huang, "Potential of one-dimensional blue phosphorene nanotubes as a water splitting photocatalyst," *Journal of Materials Chemistry A*, vol. 6, no. 42, pp. 21087–21097, 2018.
- [61] J. Hao, Z. Wang, and Q. Jin, "Dft study of structural, elastic, electronic and dielectric properties of blue phosphorus nanotubes," *Scientific reports*, vol. 9, no. 1, pp. 1–8, 2019.
- [62] E. Montes and U. Schwingenschl"ogl, "Superior selectivity and sensitivity of blue phosphorus nanotubes in gas sensing applications," *Journal of Materials Chemistry C*, vol. 5, no. 22, pp. 5365–5371, 2017.
- [63] M. Sun, J.-P. Chou, A. Hu, and U. Schwingenschl"ogl, "Point defects in blue phosphorene," *Chemistry of Materials*, vol. 31, no. 19, pp. 8129–8135, 2019.
- [64] Q.-X. Zhou, C.-Y. Wang, Z.-B. Fu, Y.-J. Tang, and H. Zhang, "Effects of various defects on the electronic properties of single-walled carbon nanotubes: A first principle study," *Frontiers of Physics*, vol. 9, no. 2, pp. 200–209, 2014.
- [65] V. Sorkin and Y. Zhang, "Effect of vacancies on the mechanical properties of phosphorene nanotubes," *Nanotechnology*, vol. 29, no. 23, p. 235707, 2018.
- [66] D. Ospina, C. Duque, M. Mora-Ramos, and J. Correa, "Effects of external electric field on the optical and electronic properties of blue phosphorene nanoribbons: A dft study," *Computational Materials Science*, vol. 135, pp. 43–53, 2017.
- [67] L.-G. Tien, C.-H. Tsai, F.-Y. Li, and M.-H. Lee, "Band-gap modification of defective carbon nanotubes under a transverse electric field," *Physical Review B*, vol. 72, no. 24, p. 245417, 2005.
- [68] F. Carta, A. Scozzafava, and C. T. Supuran, "Sulfonamides: a patent review (2008–2012)," *Expert opinion on therapeutic patents*, vol. 22, no. 7, pp. 747–758, 2012.
- [69] L. Ji, W. Chen, S. Zheng, Z. Xu, and D. Zhu, "Adsorption of sulfonamide antibiotics to multiwalled carbon nanotubes," *Langmuir*, vol. 25, no. 19, pp. 11608–11613, 2009.
- [70] H. Zhao, X. Liu, Z. Cao, Y. Zhan, X. Shi, Y. Yang, J. Zhou, and J. Xu, "Adsorption behavior and mechanism of chloramphenicols, sulfonamides, and non-antibiotic pharmaceuticals on multi-walled carbon nanotubes," *Journal of hazardous materials*, vol. 310, pp. 235–245, 2016.
-

- [71] Y. Liu, Y. Peng, B. An, L. Li, and Y. Liu, "Effect of molecular structure on the adsorption affinity of sulfonamides onto cnts: Batch experiments and dft calculations," *Chemosphere*, vol. 246, p. 125778, 2020.
- [72] R. Bhuvaneswari, V. Nagarajan, and R. Chandiramouli, "Molecular interaction of oxytetracycline and sulfapyridine on blue phosphorene nanotubes: A first-principles insight," *Physics Letters A*, vol. 394, p. 127198, 2021.
- [73] R. Srivastava, S. Nouseen, J. Chattopadhyay, P. M. Woi, D. N. Son, and B. P. Bastakoti, "Recent advances in electrochemical water splitting and reduction of co2 into green fuels on 2d phosphorene-based catalyst," *Energy Technology*, vol. 9, no. 1, p. 2000741, 2021.
- [74] P. Xiao, W. Chen, and X. Wang, "A review of phosphide-based materials for electrocatalytic hydrogen evolution," *Advanced Energy Materials*, vol. 5, no. 24, p. 1500985, 2015.
- [75] Y. Zheng, Y. Jiao, M. Jaroniec, and S. Z. Qiao, "Advancing the electrochemistry of the hydrogen-evolution reaction through combining experiment and theory," *Angewandte Chemie International Edition*, vol. 54, no. 1, pp. 52–65, 2015.
- [76] D. H. Youn, S. Han, J. Y. Kim, J. Y. Kim, H. Park, S. H. Choi, and J. S. Lee, "Highly active and stable hydrogen evolution electrocatalysts based on molybdenum compounds on carbon nanotube–graphene hybrid support," *ACS nano*, vol. 8, no. 5, pp. 5164–5173, 2014.
- [77] B. Conway and J. O. Bockris, "Electrolytic hydrogen evolution kinetics and its relation to the electronic and adsorptive properties of the metal," *The Journal of Chemical Physics*, vol. 26, no. 3, pp. 532–541, 1957.
- [78] I. T. McCrum and M. Koper, "The role of adsorbed hydroxide in hydrogen evolution reaction kinetics on modified platinum," *Nature Energy*, vol. 5, no. 11, pp. 891–899, 2020.
- [79] N. Cheng, S. Stambula, D. Wang, M. N. Banis, J. Liu, A. Riese, B. Xiao, R. Li, T.-K. Sham, L.-M. Liu, et al., "Platinum single-atom and cluster catalysis of the hydrogen evolution reaction," *Nature communications*, vol. 7, no. 1, pp. 1–9, 2016.
- [80] J. Bockris, I. Ammar, and A. Huq, "The mechanism of the hydrogen evolution reaction on platinum, silver and tungsten surfaces in acid solutions," *The Journal of Physical Chemistry*, vol. 61, no. 7, pp. 879–886, 1957.
- [81] G. R. Bhimanapati, Z. Lin, V. Meunier, Y. Jung, J. Cha, S. Das, D. Xiao, Y. Son, M. S. Strano, V. R. Cooper, et al., "Recent advances in two-dimensional materials beyond graphene," *ACS nano*, vol. 9, no. 12, pp. 11509–11539, 2015.

-
- [82] L. Wang, P. Hu, Y. Long, Z. Liu, and X. He, "Recent advances in ternary two-dimensional materials: synthesis, properties and applications," *Journal of Materials Chemistry A*, vol. 5, no. 44, pp. 22855–22876, 2017.
- [83] G. H. Jeong, S. P. Sasikala, T. Yun, G. Y. Lee, W. J. Lee, and S. O. Kim, "Nanoscale assembly of 2d materials for energy and environmental applications," *Advanced Materials*, vol. 32, no. 35, p. 1907006, 2020.
- [84] T. A. Shifa, F. Wang, Y. Liu, and J. He, "Heterostructures based on 2d materials: A versatile platform for efficient catalysis," *Advanced Materials*, vol. 31, no. 45, p. 1804828, 2019.
- [85] W.-l. Zhang, K. Zhang, and X.-j. Wu, "Enhanced catalytic hydrogen evolution reaction in phosphorene nanosheet via cobalt intercalation," *Chinese Journal of Chemical Physics*, vol. 32, no. 5, p. 572, 2019.
- [86] K. N. Dinh, Y. Zhang, J. Zhu, and W. Sun, "Phosphorene-based electrocatalysts," *Chemistry—A European Journal*, vol. 26, no. 29, pp. 6437–6446, 2020.
- [87] Y. Cai, J. Gao, S. Chen, Q. Ke, G. Zhang, and Y.-W. Zhang, "Design of phosphorene for hydrogen evolution performance comparable to platinum," *Chemistry of Materials*, vol. 31, no. 21, pp. 8948–8956, 2019.
- [88] L. Shao, H. Sun, L. Miao, X. Chen, M. Han, J. Sun, S. Liu, L. Li, F. Cheng, and J. Chen, "Facile preparation of nh 2-functionalized black phosphorene for the electrocatalytic hydrogen evolution reaction," *Journal of Materials Chemistry A*, vol. 6, no. 6, pp. 2494–2499, 2018.
- [89] Q. Wu, M. Liang, S. Zhang, X. Liu, and F. Wang, "Development of functional black phosphorus nanosheets with remarkable catalytic and antibacterial performance," *Nanoscale*, vol. 10, no. 22, pp. 10428–10435, 2018.
- [90] T. Wu, Y. Ma, Z. Qu, J. Fan, Q. Li, P. Shi, Q. Xu, and Y. Min, "Black phosphorus-graphene heterostructure-supported pd nanoparticles with superior activity and stability for ethanol electro-oxidation," *ACS applied materials & interfaces*, vol. 11, no. 5, pp. 5136–5145, 2019.
- [91] L. Bai, X. Wang, S. Tang, Y. Kang, J. Wang, Y. Yu, Z.-K. Zhou, C. Ma, X. Zhang, J. Jiang, et al., "Black phosphorus/platinum heterostructure: a highly efficient photocatalyst for solar-driven chemical reactions," *Advanced Materials*, vol. 30, no. 40, p. 1803641, 2018.
- [92] X. Wang, L. Bai, J. Lu, X. Zhang, D. Liu, H. Yang, J. Wang, P. K. Chu, S. Ramakrishna, and X.-F. Yu, "Rapid activation of platinum with black phosphorus for efficient hydrogen evolution," *Angewandte Chemie*, vol. 131, no. 52, pp. 19236–19242, 2019.
-

- [93] E. Kovalska, J. Luxa, M. Melle-Franco, B. Wu, I. Marek, P. K. Roy, P. Marvan, and Z. Sofer, "Single-step synthesis of platinoid-decorated phosphorene: perspectives for catalysis, gas sensing, and energy storage," *ACS applied materials & interfaces*, vol. 12, no. 45, pp. 50516–50526, 2020.
- [94] Y. Gan, X.-X. Xue, X.-X. Jiang, Z. Xu, K. Chen, J.-F. Yu, and Y. Feng, "Chemically modified phosphorene as efficient catalyst for hydrogen evolution reaction," *Journal of Physics: Condensed Matter*, vol. 32, no. 2, p. 025202, 2019.
- [95] J. Lu, X. Zhang, D. Liu, N. Yang, H. Huang, S. Jin, J. Wang, P. K. Chu, and X.-F. Yu, "Modulation of phosphorene for optimal hydrogen evolution reaction," *ACS applied materials & interfaces*, vol. 11, no. 41, pp. 37787–37795, 2019.
- [96] M. Wang, R. Song, X. Zhang, G. Liu, S. Xu, Z. Xu, J. Liu, and G. Qiao, "Defects engineering promotes the electrochemical hydrogen evolution reaction property of phosphorene surface," *international journal of hydrogen energy*, vol. 46, no. 2, pp. 1913–1922, 2021.
- [97] F. Liu, Z. Huang, H. Liu, Y. Liao, X. Qi, and J. Zhong, "Strain modulation of black phosphorene for the hydrogen evolution reaction activity," *physica status solidi (b)*, vol. 258, no. 11, p. 2100195, 2021.
- [98] P. Vishnoi, U. Gupta, R. Pandey, and C. N. Rao, "Stable functionalized phosphorenes with photocatalytic her activity," *Journal of Materials Chemistry A*, vol. 7, no. 12, pp. 6631–6637, 2019.
- [99] D. Liu, J. Wang, J. Lu, C. Ma, H. Huang, Z. Wang, L. Wu, Q. Liu, S. Jin, P. K. Chu, et al., "Direct synthesis of metal-doped phosphorene with enhanced electrocatalytic hydrogen evolution," *Small Methods*, vol. 3, no. 7, p. 1900083, 2019.
- [100] L. Ju, Y. Dai, W. Wei, Y. Liang, and B. Huang, "Potential of one-dimensional blue phosphorene nanotubes as a water splitting photocatalyst," *Journal of Materials Chemistry A*, vol. 6, no. 42, pp. 21087–21097, 2018.
- [101] Y. Cheng, Y. Song, and Y. Zhang, "The doping and oxidation of 2d black and blue phosphorene: a new photocatalyst for nitrogen reduction driven by visible light," *Physical Chemistry Chemical Physics*, vol. 21, no. 44, pp. 24449–24457, 2019.
- [102] A. Maibam, S. K. Das, P. P. Samal, and S. Krishnamurty, "Enhanced photocatalytic properties of a chemically modified blue phosphorene," *RSC Advances*, vol. 11, no. 22, pp. 13348–13358, 2021.
- [103] Y. Xiao, J. Wang, Y. Wang, and W. Zhang, "A new promising catalytic activity on blue phosphorene nitrogen-doped nanosheets for the orr as cathode in nonaqueous li-air batteries," *Applied Surface Science*, vol. 488, pp. 620–628, 2019.

-
- [104] C. Li, Y. Xu, W. Sheng, W.-J. Yin, G.-Z. Nie, and Z. Ao, "A promising blue phosphorene/c 2 n van der waals type-ii heterojunction as a solar photocatalyst: a first-principles study," *Physical Chemistry Chemical Physics*, vol. 22, no. 2, pp. 615–623, 2020.
- [105] B.-J. Wang, X.-H. Li, R. Zhao, X.-L. Cai, W.-Y. Yu, W.-B. Li, Z.-S. Liu, L.-W. Zhang, and S.-H. Ke, "Electronic structures and enhanced photocatalytic properties of blue phosphorene/bse van der waals heterostructures," *Journal of Materials Chemistry A*, vol. 6, no. 19, pp. 8923–8929, 2018.
- [106] A. Maibam, D. Chakraborty, K. Joshi, and S. Krishnamurty, "Exploring edge functionalised blue phosphorene nanoribbons as novel photocatalysts for water splitting," *New Journal of Chemistry*, vol. 45, no. 7, pp. 3570–3580, 2021.
- [107] L. Zhou and S.-Q. Shi, "Formation energy of stone-wales defects in carbon nanotubes," *Applied physics letters*, vol. 83, no. 6, pp. 1222–1224, 2003.
- [108] V. Choyal and S. Kundalwal, "Effect of stone-wales defects on the mechanical behavior of boron nitride nanotubes," *Acta Mechanica*, vol. 231, no. 10, pp. 4003–4018, 2020.
- [109] Y. V. Shtogun and L. M. Woods, "Electronic and magnetic properties of deformed and defective single wall carbon nanotubes," *Carbon*, vol. 47, no. 14, pp. 3252–3262, 2009.
- [110] S. L. Mielke, D. Troya, S. Zhang, J.-L. Li, S. Xiao, R. Car, R. S. Ruoff, G. C. Schatz, and T. Belytschko, "The role of vacancy defects and holes in the fracture of carbon nanotubes," *Chemical Physics Letters*, vol. 390, no. 4-6, pp. 413–420, 2004.
- [111] W. Orellana and P. Fuentealba, "Structural, electronic and magnetic properties of vacancies in single-walled carbon nanotubes," *Surface science*, vol. 600, no. 18, pp. 4305–4309, 2006.
- [112] A. Zobelli, C. Ewels, A. Gloter, G. Seifert, O. Stephan, S. Csillag, and C. Colliex, "Defective structure of bn nanotubes: from single vacancies to dislocation lines," *Nano letters*, vol. 6, no. 9, pp. 1955–1960, 2006.
- [113] H. Zhang, Z. Zhou, J. Qiu, P. Chen, and W. Sun, "Defect engineering of carbon nanotubes and its effect on mechanical properties of carbon nanotubes/polymer nanocomposites: A molecular dynamics study," *Composites Communications*, vol. 28, p. 100911, 2021.
- [114] M. Nasserian and J. Davoodi, "The effect of point defect on the thermal properties of silicon-germanium nanotubes,"
- [115] X. Zhou and P. Schmuki, "Noble-metal-free photocatalytic hydrogen evolution activity: Defect engineering in tio₂ nanotubes," in *ECS Meeting Abstracts*, no. 31, p. 1899, IOP Publishing, 2018.
-

- [116] M. Stiller, Defect Induced Magnetism in Titanium Dioxide. PhD thesis, Institute for Solid-state Physics, 2021.
- [117] R. Chegel and S. Behzad, "Effects of an electric field on the electronic and optical properties of zigzag boron nitride nanotubes," *Solid state communications*, vol. 151, no. 3, pp. 259–263, 2011.
- [118] J. O'keeffe, C. Wei, and K. Cho, "Bandstructure modulation for carbon nanotubes in a uniform electric field," *Applied physics letters*, vol. 80, no. 4, pp. 676–678, 2002.
- [119] C. Kim, B. Kim, S. M. Lee, C. Jo, and Y. H. Lee, "Effect of electric field on the electronic structures of carbon nanotubes," *Applied Physics Letters*, vol. 79, no. 8, pp. 1187–1189, 2001.
- [120] M. Kim, J. Lee, M. Je, B. Heo, H. Yoo, H. Choi, J. Choi, and K. Lee, "Electric field-driven one-step formation of vertical p–n junction tio 2 nanotubes exhibiting strong photocatalytic hydrogen production," *Journal of Materials Chemistry A*, vol. 9, no. 4, pp. 2239–2247, 2021.
- [121] W.-Q. Guo, H.-S. Zheng, S. Li, J.-S. Du, X.-C. Feng, R.-L. Yin, Q.-L. Wu, N.-Q. Ren, and J.-S. Chang, "Removal of cephalosporin antibiotics 7-aca from wastewater during the cultivation of lipid-accumulating microalgae," *Bioresource technology*, vol. 221, pp. 284–290, 2016.
- [122] N. Rego and D. Koes, "3dmol. js: molecular visualization with webgl," *Bioinformatics*, vol. 31, no. 8, pp. 1322–1324, 2015.
- [123] H. Nguyen, D. A. Case, and A. S. Rose, "Nglview–interactive molecular graphics for jupyter notebooks," *Bioinformatics*, vol. 34, no. 7, pp. 1241–1242, 2018.
- [124] N. M. O'Boyle, M. Banck, C. A. James, C. Morley, T. Vandermeersch, and G. R. Hutchison, "Open babel: An open chemical toolbox," *Journal of cheminformatics*, vol. 3, no. 1, pp. 1–14, 2011.
- [125] E. Bitzek, P. Koskinen, F. Gähler, M. Moseler, and P. Gumbsch, "Structural relaxation made simple," *Physical review letters*, vol. 97, no. 17, p. 170201, 2006.
- [126] E. A. Zuluaga-Hernández, E. Flórez, L. Dorkis, M. E. Mora-Ramos, and J. D. Correa, "Opto-electronic properties of blue phosphorene oxide with and without oxygen vacancies," *International Journal of Quantum Chemistry*, vol. 120, no. 2, p. e26075, 2020.
- [127] M. Dresselhaus, G. Dresselhaus, and R. Saito, "Physics of carbon nanotubes," *Carbon*, vol. 33, no. 7, pp. 883–891, 1995.
- [128] M. R. Mananghaya, "Hydrogen adsorption of nitrogen-doped carbon nanotubes functionalized with 3d-block transition metals," *Journal of Chemical Sciences*, vol. 127, no. 4, pp. 751–759, 2015.

-
- [129] D. Gehringer, T. Dengg, M. N. Popov, and D. Holec, "Interactions between a h₂ molecule and carbon nanostructures: A dft study," *C—Journal of Carbon Research*, vol. 6, no. 1, p. 16, 2020.
- [130] M. F. Fellah, "Pt doped (8, 0) single wall carbon nanotube as hydrogen sensor: A density functional theory study," *International Journal of Hydrogen Energy*, vol. 44, no. 49, pp. 27010–27021, 2019.
- [131] K. Tada, S. Furuya, and K. Watanabe, "Ab initio study of hydrogen adsorption to single-walled carbon nanotubes," *Physical Review B*, vol. 63, no. 15, p. 155405, 2001.
- [132] H. J. Kwon, Y. Kwon, T. Kim, Y. Jung, S. Lee, M. Cho, and S. Kwon, "Enhanced competitive adsorption of co₂ and h₂ on graphyne: A density functional theory study," *AIP Advances*, vol. 7, no. 12, p. 125013, 2017.
- [133] M. Dion, H. Rydberg, E. Schröder, D. C. Langreth, and B. I. Lundqvist, "Van der waals density functional for general geometries," *Physical review letters*, vol. 92, no. 24, p. 246401, 2004.
- [134] J. Klimeš, D. R. Bowler, and A. Michaelides, "Chemical accuracy for the van der waals density functional," *Journal of Physics: Condensed Matter*, vol. 22, no. 2, p. 022201, 2009.
- [135] D. Ma, W. Ju, T. Li, G. Yang, C. He, B. Ma, Y. Tang, Z. Lu, and Z. Yang, "Formaldehyde molecule adsorption on the doped monolayer mos₂: a first-principles study," *Applied Surface Science*, vol. 371, pp. 180–188, 2016.
- [136] D. Ma, Q. Wang, T. Li, C. He, B. Ma, Y. Tang, Z. Lu, and Z. Yang, "Repairing sulfur vacancies in the mos₂ monolayer by using co, no and no₂ molecules," *Journal of Materials Chemistry C*, vol. 4, no. 29, pp. 7093–7101, 2016.
- [137] A. Aasi, E. Aasi, S. Mehdi Aghaei, and B. Panchapakesan, "Green phosphorene as a promising biosensor for detection of furan and p-xylene as biomarkers of disease: A dft study," *Sensors*, vol. 22, no. 9, p. 3178, 2022.
- [138] J. Du and G. Jiang, "First-principle study on monolayer and bilayer snp₃ sheets as the potential sensors for no₂, no, and nh₃ detection," *Nanotechnology*, vol. 31, no. 32, p. 325504, 2020.
- [139] I. G. Pitt, R. G. Gilbert, and K. R. Ryan, "Application of transition-state theory to gas-surface reactions: Barrierless adsorption on clean surfaces," *The Journal of Physical Chemistry*, vol. 98, no. 49, pp. 13001–13010, 1994.
- [140] J. P. Perdew, K. Burke, and M. Ernzerhof, "Generalized gradient approximation made simple," *Physical review letters*, vol. 77, no. 18, p. 3865, 1996.

- [141] H. J. Monkhorst and J. D. Pack, "Special points for brillouin-zone integrations," *Physical review B*, vol. 13, no. 12, p. 5188, 1976.
- [142] S. Grimme, J. Antony, S. Ehrlich, and H. Krieg, "A consistent and accurate ab initio parametrization of density functional dispersion correction (dft-d) for the 94 elements h-pu," *The Journal of chemical physics*, vol. 132, no. 15, p. 154104, 2010.
- [143] J. K. Nørskov, T. Bligaard, A. Logadottir, J. R. Kitchin, J. G. Chen, S. Pandelov, and U. Stimming, "Trends in the exchange current for hydrogen evolution," *Journal of The Electrochemical Society*, vol. 152, no. 3, p. J23, 2005.
- [144] S. Trasatti, "Work function, electronegativity, and electrochemical behaviour of metals," *Journal of Electroanalytical Chemistry and Interfacial Electrochemistry*, vol. 39, no. 1, pp. 163–184, 1972.

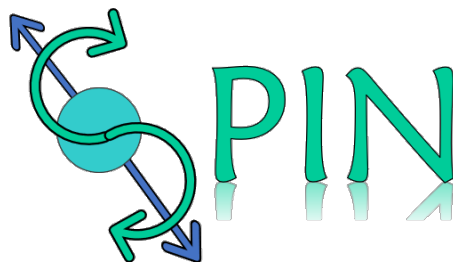


UNIVERSIDAD DE MEDELLIN

Facultad de ciencias básicas

Master thesis

Thesis to qualify for the title of Master in Modeling and Computational Science



Supplementary material:

**SPIN: [S]imple [P]ython [I]pywidgets [N]otebook
Interface to obtain the optoelectronic properties
of materials employing DFT**

José Manuel Vergara Álvarez

Advisor: Julian David Correa Abad, Ph.D.

Advisor: Elizabeth Florez Yepes, Ph.D.

Medellín, Colombia.
November 27th , 2022

Supplementary Material:
**Impact of different structural defects on fundamental properties
of blue phosphorene nanotubes**

J. M. Vergara, J. D. Correa, and E. Florez

Facultad de Ciencias Básicas, Universidad de Medellín, Medellín, Colombia

M. E. Mora-Ramos

Centro de Investigación en Ciencias-IICBA,

Universidad Autónoma del Estado de Morelos,

Av. Universidad 1001, CP 62209 Cuernavaca, Morelos, México

System	$E_f(\text{eV}/\text{\AA})$ SV-A	$E_f(\text{eV}/\text{\AA})$ SV-B	$E_f(\text{eV}/\text{\AA})$ DV	$E_f(\text{eV}/\text{\AA})$ SW
(7,7)	2,310	2,177	2,888	1,353
(8,8)	2,266	2,134	2,877	1,323
(9,9)	2,135	2,013	2,748	1,128
(10,10)	2,248	2,148	2,886	1,330
(11,11)	1,951	1,820	2,527	0,814
(12,12)	2,031	1,878	2,565	0,888
(13,13)	1,711	1,616	2,227	0,634
(14,14)	1,438	1,353	1,904	0,159
(7,0)	2,105	1,420	1,932	0,426
(8,0)	2,317	1,679	1,855	0,668
(9,0)	2,412	2,246	1,883	0,807
(10,0)	2,486	2,415	1,901	0,913
(11,0)	2,495	2,018	1,907	0,983
(12,0)	2,526	2,470	1,910	1,036
(13,0)	2,512	2,457	1,935	1,059
(14,0)	2,432	2,096	1,921	1,065
BlueP[1]	2.380	2.380	2.850	1.600

TABLE S1: The formation energy of all evaluated systems

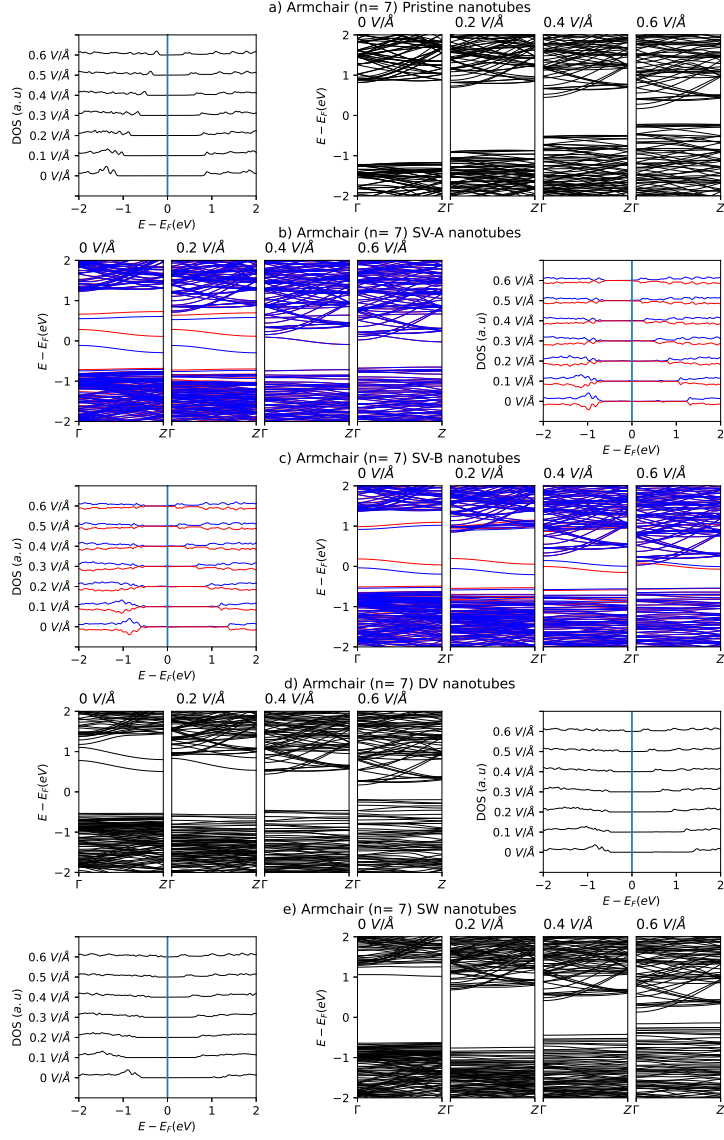


FIG. S1: Effect of electric field on energy band structure and density of states of pristine and different structural defect types on blue-phosphorene nanotubes for the smallest Armchair nanotube ($n = 14$) system. For band structure plots, values of $0, 0.2, 0.4$ and 0.6 V/\AA electric field intensity are considered.

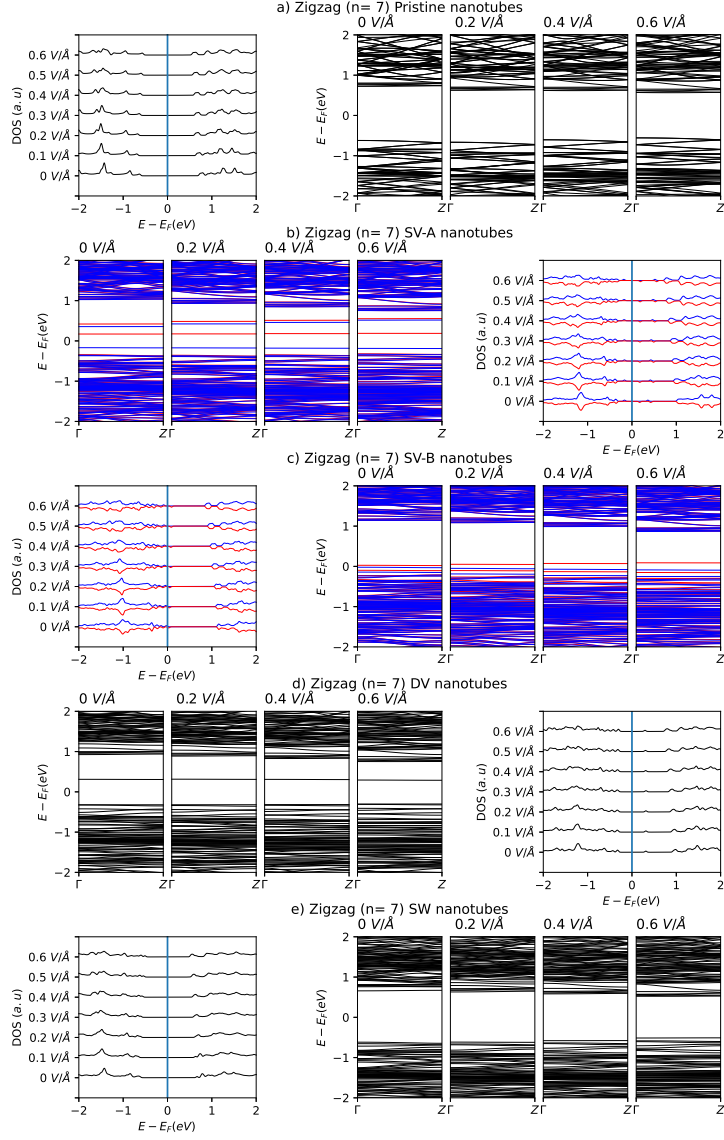


FIG. S2: Effect of electric field on energy band structure and density of states of pristine and different structural defect types on blue-phosphorene nanotubes for the smallest Zigzag nanotube ($n = 14$) system. For band structure plots, values of 0, 0.2, 0.4 and 0.6 $V/\text{\AA}$ electric field intensity are considered

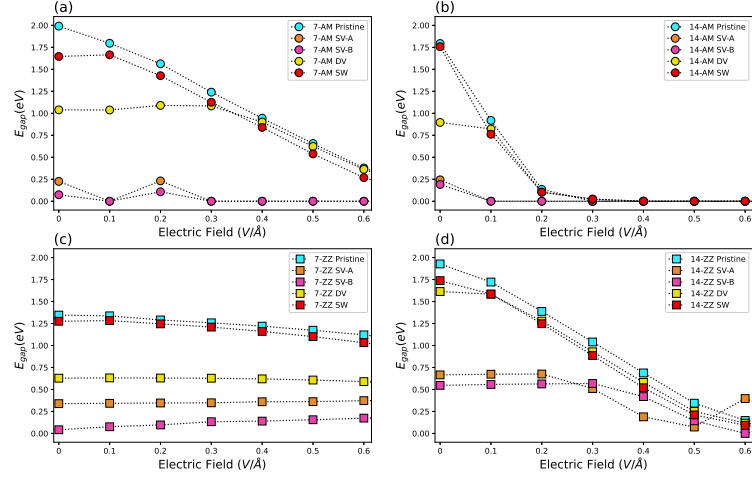


FIG. S3: The energy band gap as a function of the intensity of the externally applied electric field. Panels (a) and (b) are for the case of Armchair nanotubes with $n = 7$ and $n = 14$ respectively, and panels (c) and (d) are for Zigzag nanotubes with $n = 7$ and $n = 14$ respectively. In all cases we have considered different types of systems: Pristine, SV-A, SV-B (single vacancies), DV (double vacancy) and SW (Stone -Wales defect).

[1] M. Sun, J.-P. Chou, A. Hu, and U. Schwingenschogl, Chemistry of Materials **31**, 8129 (2019).

2*System		Refractive index $n(\omega)$																			
		Pristine E_{\perp}		Pristine E_{\parallel}		SV-A E_{\perp}		SV-A E_{\parallel}		SV-B E_{\perp}		SV-B E_{\parallel}		DV E_{\perp}		DV E_{\parallel}		SW E_{\perp}		SW E_{\parallel}	
		0	2.1	0	2.1	0	2.1	0	2.1	0	2.1	0	2.1	0	2.1	0	2.1	0	2.1	0	2.1
7*AM $n = 7$	0 V/Å	1,246	1,356	1,346	1,500	1,246	1,349	1,368	1,484	1,249	1,350	1,368	1,475	1,246	1,350	1,376	1,487	1,248	1,352	1,353	1,514
	0,1 V/Å	1,247	1,348	1,346	1,505	1,247	1,347	1,364	1,484	1,249	1,351	1,366	1,482	1,246	1,342	1,376	1,495	1,250	1,354	1,353	1,510
	0,2 V/Å	1,248	1,338	1,346	1,495	1,247	1,333	1,368	1,485	1,250	1,337	1,367	1,487	1,249	1,339	1,374	1,486	1,251	1,343	1,354	1,507
	0,3 V/Å	1,249	1,343	1,347	1,497	1,250	1,338	1,369	1,484	1,252	1,341	1,368	1,489	1,251	1,344	1,375	1,485	1,253	1,346	1,355	1,503
	0,4 V/Å	1,252	1,336	1,349	1,502	1,254	1,334	1,368	1,482	1,256	1,336	1,370	1,489	1,253	1,343	1,376	1,480	1,256	1,343	1,357	1,507
	0,5 V/Å	1,255	1,334	1,351	1,494	1,259	1,336	1,382	1,482	1,263	1,335	1,380	1,485	1,257	1,343	1,378	1,477	1,260	1,338	1,359	1,496
	0,6 V/Å	1,261	1,337	1,353	1,494	1,264	1,338	1,398	1,470	1,268	1,337	1,411	1,487	1,263	1,343	1,387	1,485	1,267	1,341	1,365	1,498
7*AM $n = 14$	0 V/Å	1,433	1,567	1,599	1,813	1,434	1,590	1,616	1,812	1,435	1,591	1,616	1,810	1,434	1,592	1,628	1,815	1,436	1,595	1,603	1,839
	0,1 V/Å	1,435	1,572	1,600	1,820	1,437	1,578	1,615	1,813	1,437	1,578	1,616	1,809	1,438	1,582	1,627	1,820	1,438	1,580	1,604	1,837
	0,2 V/Å	1,446	1,567	1,635	1,817	1,441	1,571	1,628	1,805	1,442	1,571	1,632	1,809	1,447	1,571	1,794	1,827	1,449	1,577	1,647	1,834
	0,3 V/Å	1,482	1,566	1,806	1,813	1,448	1,571	1,644	1,801	1,448	1,572	1,649	1,813	1,449	1,571	1,910	1,814	1,451	1,578	1,810	1,825
	0,4 V/Å	1,478	1,572	2,110	1,813	1,463	1,577	2,057	1,797	1,467	1,579	2,325	1,811	1,458	1,575	1,928	1,796	1,464	1,581	2,044	1,819
	0,5 V/Å	1,487	1,574	2,366	1,804	1,483	1,583	2,443	1,792	1,490	1,582	3,097	1,800	1,478	1,581	2,221	1,791	1,485	1,584	2,337	1,812
	0,6 V/Å	1,529	1,589	3,632	1,801	1,515	1,587	2,805	1,781	1,513	1,582	2,285	1,775	1,522	1,582	3,664	1,777	1,534	1,587	3,183	1,801
7*ZZ $n = 7$	0 V/Å	1,179	1,267	1,210	1,299	1,181	1,267	1,226	1,300	1,211	1,285	1,345	1,306	1,181	1,283	1,220	1,293	1,180	1,284	1,216	1,314
	0,1 V/Å	1,179	1,267	1,210	1,299	1,181	1,297	1,225	1,300	1,201	1,286	1,323	1,305	1,181	1,286	1,220	1,296	1,180	1,286	1,216	1,315
	0,2 V/Å	1,180	1,293	1,211	1,302	1,181	1,296	1,225	1,302	1,196	1,289	1,312	1,306	1,181	1,286	1,221	1,300	1,182	1,306	1,217	1,318
	0,3 V/Å	1,181	1,295	1,211	1,304	1,182	1,296	1,225	1,304	1,190	1,291	1,288	1,306	1,182	1,287	1,221	1,303	1,183	1,308	1,217	1,320
	0,4 V/Å	1,181	1,281	1,211	1,304	1,182	1,301	1,225	1,306	1,189	1,288	1,287	1,308	1,183	1,286	1,222	1,305	1,183	1,313	1,218	1,321
	0,5 V/Å	1,182	1,301	1,212	1,308	1,183	1,303	1,225	1,309	1,189	1,291	1,280	1,310	1,184	1,284	1,223	1,307	1,184	1,320	1,218	1,322
	0,6 V/Å	1,183	1,292	1,212	1,310	1,184	1,304	1,225	1,310	1,189	1,295	1,272	1,314	1,185	1,285	1,224	1,309	1,186	1,323	1,219	1,324
7*ZZ $n = 14$	0 V/Å	1,284	1,412	1,376	1,537	1,284	1,414	1,380	1,529	1,284	1,414	1,382	1,535	1,283	1,414	1,375	1,533	1,285	1,415	1,380	1,545
	0,1 V/Å	1,285	1,389	1,376	1,528	1,284	1,389	1,380	1,522	1,285	1,391	1,382	1,530	1,284	1,396	1,376	1,531	1,287	1,396	1,381	1,538
	0,2 V/Å	1,286	1,392	1,376	1,518	1,286	1,392	1,381	1,515	1,286	1,395	1,382	1,521	1,285	1,395	1,376	1,525	1,288	1,396	1,381	1,534
	0,3 V/Å	1,289	1,390	1,378	1,523	1,289	1,390	1,382	1,516	1,289	1,391	1,383	1,524	1,288	1,388	1,378	1,525	1,291	1,393	1,383	1,532
	0,4 V/Å	1,293	1,371	1,379	1,523	1,293	1,373	1,392	1,517	1,294	1,371	1,385	1,521	1,292	1,373	1,379	1,527	1,296	1,378	1,385	1,530
	0,5 V/Å	1,300	1,376	1,385	1,524	1,300	1,374	1,447	1,512	1,303	1,377	1,458	1,524	1,300	1,378	1,391	1,528	1,304	1,380	1,414	1,535
	0,6 V/Å	1,312	1,380	1,439	1,525	1,321	1,377	1,597	1,506	1,326	1,379	1,626	1,520	1,313	1,382	1,618	1,528	1,316	1,385	1,548	1,535

TABLE S2: Static refractive index, refractive index at $\hbar\omega = 2.1$ eV of all evaluated systems for different values of the external electric field. The calculation includes two distinct polarizations of the incident photons: E_{\parallel} corresponds to light polarized along the direction parallel to, and E_{\perp} to light polarized perpendicular to the BPNT growth direction.

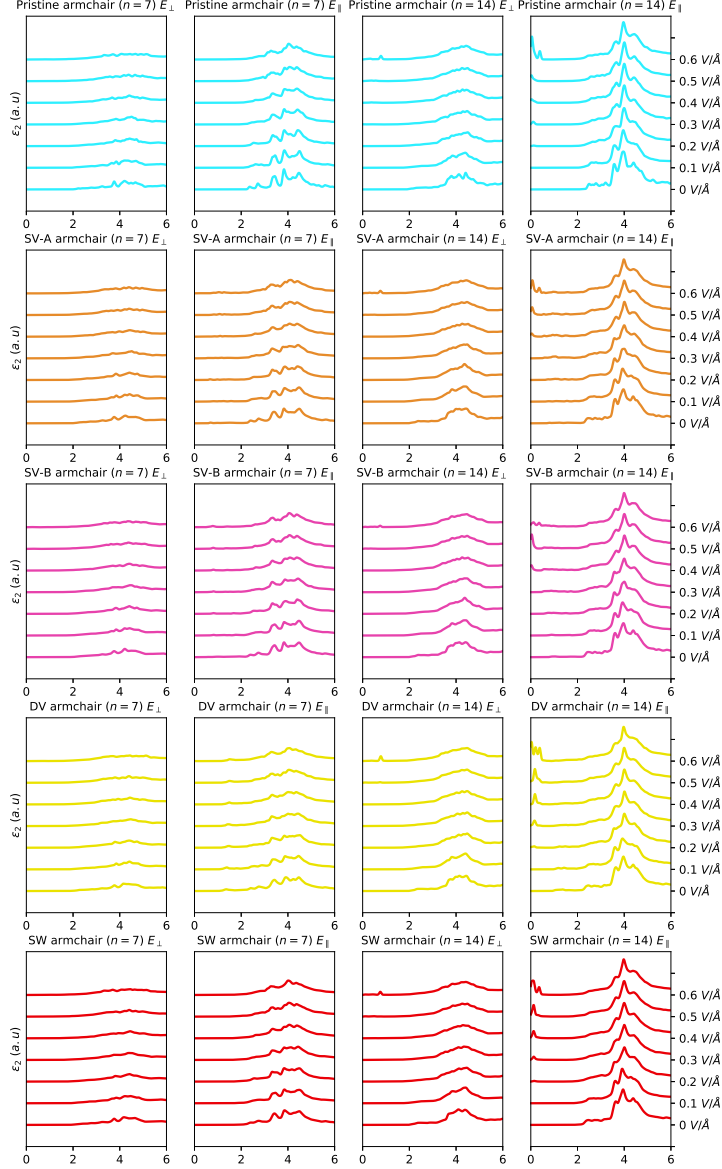


FIG. S4: The imaginary part of the dielectric function as a function of the intensity of the externally applied electric field for the case of Armchair nanotubes with $n = 7$ and $n = 14$ respectively. In all cases we have considered different types of systems: Pristine, SV-A, SV-B (single vacancies), DV (double vacancy) and SW (Stone -Wales defect). The calculation includes two distinct polarizations of the incident photons: E_{\parallel} corresponds to light polarized along the direction parallel to, and E_{\perp} to light polarized perpendicular to the BPNT growth direction.

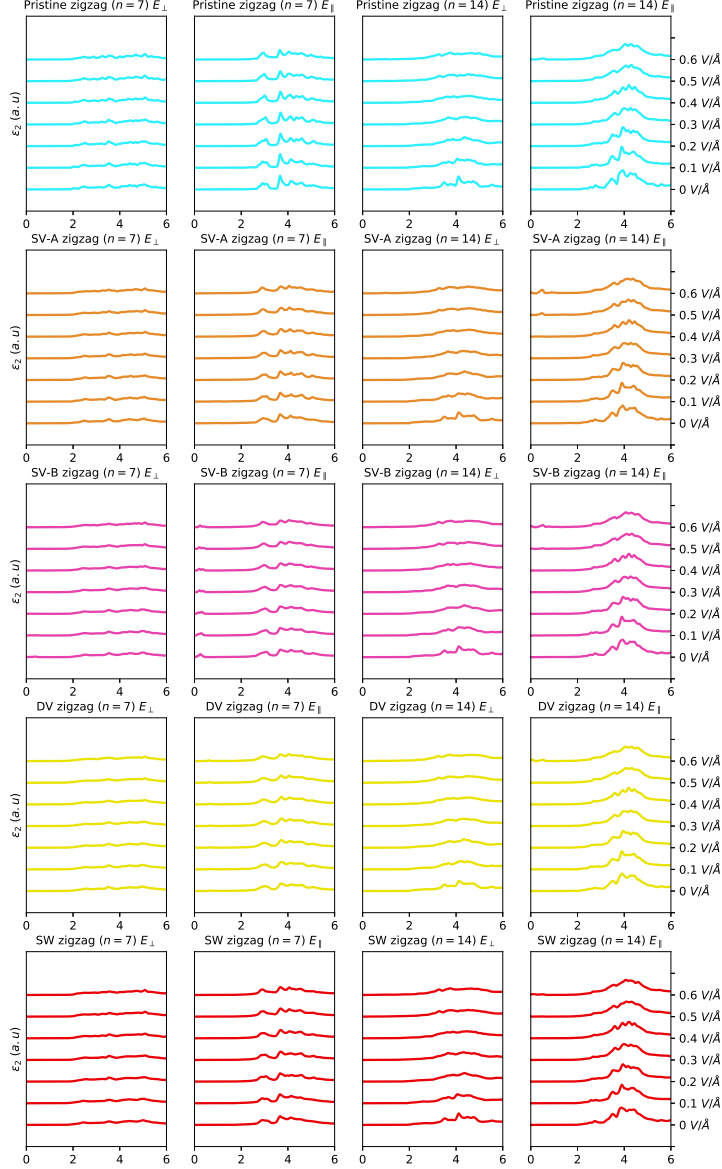


FIG. S5: The imaginary part of the dielectric function as a function of the intensity of the externally applied electric field for the case of Zigzag nanotubes with $n = 7$ and $n = 14$ respectively. In all cases we have considered different types of systems: Pristine, SV-A, SV-B (single vacancies), DV (double vacancy) and SW (Stone -Wales defect). The calculation includes two distinct polarizations of the incident photons: E_{\parallel} corresponds to light polarized along the direction parallel to, and E_{\perp} to light polarized perpendicular to the BPNT growth direction.

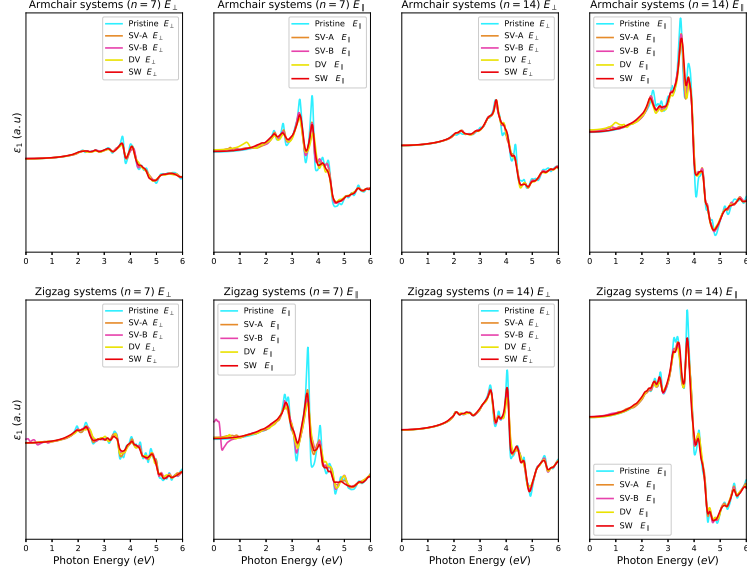


FIG. S6: The real part of the dielectric function of smallest and biggest ($n = 7$ and $n = 14$ respectively) pristine and defective blue phosphorene nanotubes systems as a function of the incident photon energy. The calculation includes two distinct polarizations of the incident photons: E_{\parallel} corresponds to light polarized along the direction parallel to, and E_{\perp} to light polarized perpendicular to the BPNT growth direction. Curves for the different defective systems are identified.

Supplementary Material:
Adsorption affinity of Sulfonamides onto
Blue-phosphorene nanotubes

J. M. Vergara¹, J. D. Correa¹, E. Flórez¹

^a*Facultad de Ciencias Básicas, Universidad de Medellín, Medellín, Colombia*

System	SAM position	E_{ads} (without VdW)	E_{ads} (with VdW)
	Benzene	0,174	-0,279
Pristine ZZ	<i>NH₂</i>	-0,030	-0,191
	<i>SO₂NH₂</i>	-0,008	-0,130
	<i>2H</i>	0,197	-0,094
	Benzene	0,199	-0,312
Pristine AM	<i>2H</i>	0,131	-0,205
	<i>NH₂</i>	0,156	-0,053
	<i>SO₂NH₂</i>	0,136	-0,028
	Benzene	0,168	-0,517
SV ZZ	<i>2H</i>	0,035	-0,497
	<i>NH₂</i>	-0,033	-0,380
	<i>SO₂NH₂</i>	0,048	-0,272
	Benzene	0,226	-0,373
SV AM	<i>2H</i>	0,249	-0,221
	<i>NH₂</i>	0,094	-0,161
	<i>SO₂NH₂</i>	0,173	-0,122

Table S1: Results interaction of pristine and single-vacancy (SV) with SAM molecules with and without taking into account Van der Wals interactions; Adsorption energy (E_{ads}) is presented in eV.

Molecule	Position	System	E_{ads} without VdW corrections
SDZ	Benzene	Pristine ZZ	0,087
		Pristine AM	0,120
SMD	Benzene	Pristine ZZ	0,050
		Pristine AM	0,173
SMR	Benzene	Pristine ZZ	0,239
		Pristine AM	0,241
SMT	Benzene	Pristine ZZ	0,135
		Pristine AM	0,222
SMX	Benzene	Pristine ZZ	0,258
		Pristine AM	0,094

Table S2: Results interaction of pristine with different Sulfonamides molecules without taking into account Van der Wals interactions; Adsorption energy (E_{ads}) is presented in eV.

			$\theta_0 = 10^{12}$ (Visible light)			
System	Molecule	Position	τ 300K	τ 310K	τ 320K	τ 330K
Pristine ZZ	SAM	Benzene	$4,9 \times 10^{-08}$	$3,4 \times 10^{-08}$	$2,5 \times 10^{-08}$	$1,8 \times 10^{-08}$
		<i>NH₂</i>	$1,6 \times 10^{-09}$	$1,3 \times 10^{-09}$	$1,0 \times 10^{-09}$	$8,3 \times 10^{-10}$
		<i>SO₂NH₂</i>	$1,5 \times 10^{-10}$	$1,3 \times 10^{-10}$	$1,1 \times 10^{-10}$	$9,7 \times 10^{-11}$
		<i>2H</i>	$3,8 \times 10^{-11}$	$3,4 \times 10^{-11}$	$3,0 \times 10^{-11}$	$2,7 \times 10^{-11}$
Pristine AM	SAM	Benzene	$1,8 \times 10^{-07}$	$1,2 \times 10^{-07}$	$8,3 \times 10^{-08}$	$5,9 \times 10^{-08}$
		<i>2H</i>	$2,8 \times 10^{-09}$	$2,2 \times 10^{-09}$	$1,7 \times 10^{-09}$	$1,4 \times 10^{-09}$
		<i>NH₂</i>	$7,9 \times 10^{-12}$	$7,4 \times 10^{-12}$	$6,9 \times 10^{-12}$	$6,5 \times 10^{-12}$
		<i>SO₂NH₂</i>	$2,9 \times 10^{-12}$	$2,8 \times 10^{-12}$	$2,7 \times 10^{-12}$	$2,6 \times 10^{-12}$
SV ZZ	SAM	Benzene	$4,8 \times 10^{-04}$	$2,5 \times 10^{-04}$	$1,4 \times 10^{-04}$	$7,8 \times 10^{-05}$
		<i>2H</i>	$2,2 \times 10^{-04}$	$1,2 \times 10^{-04}$	$6,7 \times 10^{-05}$	$3,9 \times 10^{-05}$
		<i>NH₂</i>	$2,4 \times 10^{-06}$	$1,5 \times 10^{-06}$	$9,7 \times 10^{-07}$	$6,4 \times 10^{-07}$
		<i>SO₂NH₂</i>	$3,7 \times 10^{-08}$	$2,6 \times 10^{-08}$	$1,9 \times 10^{-08}$	$1,4 \times 10^{-08}$
SV AM	SAM	Benzene	$1,9 \times 10^{-06}$	$1,2 \times 10^{-06}$	$7,6 \times 10^{-07}$	$5,0 \times 10^{-07}$
		<i>2H</i>	$5,1 \times 10^{-09}$	$3,9 \times 10^{-09}$	$3,0 \times 10^{-09}$	$2,4 \times 10^{-09}$
		<i>NH₂</i>	$5,0 \times 10^{-10}$	$4,1 \times 10^{-10}$	$3,4 \times 10^{-10}$	$2,8 \times 10^{-10}$
		<i>SO₂NH₂</i>	$1,1 \times 10^{-10}$	$9,7 \times 10^{-11}$	$8,4 \times 10^{-11}$	$7,4 \times 10^{-11}$
			$\theta_0 = 10^{16}$ (UV light)			
System	Molecule	Position	τ 300K	τ 310K	τ 320K	τ 330K
Pristine ZZ	SAM	Benzene	$4,9 \times 10^{-12}$	$3,4 \times 10^{-12}$	$2,5 \times 10^{-12}$	$1,8 \times 10^{-12}$
		<i>NH₂</i>	$1,6 \times 10^{-13}$	$1,3 \times 10^{-13}$	$1,0 \times 10^{-13}$	$8,3 \times 10^{-14}$
		<i>SO₂NH₂</i>	$1,5 \times 10^{-14}$	$1,3 \times 10^{-14}$	$1,1 \times 10^{-14}$	$9,7 \times 10^{-15}$
		<i>2H</i>	$3,8 \times 10^{-15}$	$3,4 \times 10^{-15}$	$3,0 \times 10^{-15}$	$2,7 \times 10^{-15}$
Pristine AM	SAM	Benzene	$1,8 \times 10^{-11}$	$1,2 \times 10^{-11}$	$8,3 \times 10^{-12}$	$5,9 \times 10^{-12}$
		<i>2H</i>	$2,8 \times 10^{-13}$	$2,2 \times 10^{-13}$	$1,7 \times 10^{-13}$	$1,4 \times 10^{-13}$
		<i>NH₂</i>	$7,9 \times 10^{-16}$	$7,4 \times 10^{-16}$	$6,9 \times 10^{-16}$	$6,5 \times 10^{-16}$
		<i>SO₂NH₂</i>	$2,9 \times 10^{-16}$	$2,8 \times 10^{-16}$	$2,7 \times 10^{-16}$	$2,6 \times 10^{-16}$
SV ZZ	SAM	Benzene	$4,8 \times 10^{-08}$	$2,5 \times 10^{-08}$	$1,4 \times 10^{-08}$	$7,8 \times 10^{-09}$
		<i>2H</i>	$2,2 \times 10^{-08}$	$1,2 \times 10^{-08}$	$6,7 \times 10^{-09}$	$3,9 \times 10^{-09}$
		<i>NH₂</i>	$2,4 \times 10^{-10}$	$1,5 \times 10^{-10}$	$9,7 \times 10^{-11}$	$6,4 \times 10^{-11}$
		<i>SO₂NH₂</i>	$3,7 \times 10^{-12}$	$2,6 \times 10^{-12}$	$1,9 \times 10^{-12}$	$1,4 \times 10^{-12}$
SV AM	SAM	Benzene	$1,9 \times 10^{-10}$	$1,2 \times 10^{-10}$	$7,6 \times 10^{-11}$	$5,0 \times 10^{-11}$
		<i>2H</i>	$5,1 \times 10^{-13}$	$3,9 \times 10^{-13}$	$3,0 \times 10^{-13}$	$2,4 \times 10^{-13}$
		<i>NH₂</i>	$5,0 \times 10^{-14}$	$4,1 \times 10^{-14}$	$3,4 \times 10^{-14}$	$2,8 \times 10^{-14}$
		<i>SO₂NH₂</i>	$1,1 \times 10^{-14}$	$9,7 \times 10^{-15}$	$8,4 \times 10^{-15}$	$7,4 \times 10^{-15}$

Table S3: Results interaction of pristine and single-vacancy (SV) with SAM molecule; recovery time (τ) is presented in *s*.

Supplementary Information:
Impact of single Pt atom adsorption on fundamental
properties of blue phosphorene and its activity toward
hydrogen evolution reaction

J. M. Vergara^a, J. D. Correa^a, AA Koverga^b, E. Flórez^a

^a*Facultad de Ciencias Básicas, Universidad de Medellín, Medellín, Colombia*

^b*Department of Chemistry, Division of Fundamental Sciences (IEFQ), Technological
Institute of Aeronautics (ITA), São Jose dos Campos, São Paulo CEP:12228-900,
Brazil*

System	Initial Site	Final Site	$E_{ads}(eV)$	Work function (eV)	Normal $d(P - H)$ (Å)
BP-Pt	fcc	fcc	-4,200	5,404	1,365
	bridge	fcc	-4,196	5,395	1,309
	hcp	hcp	-4,068	5,634	1,147
	top	top	-3,622	5,724	1,852

Table S1: Adsorption energy values and optimized geometries for BP-Pt

System	Initial Site	Final Site	$E_{ads}(eV)$	Work function (eV)	Normal $d(P - H)$ (Å)
BP-H	top	top	-1,843	4,421	0,757
	top-VdW	top	-1,894	4,422	0,757
	fcc	bridge	-1,757	4,951	1,049
	hcp	bridge	-1,754	4,928	1,022
	bridge	fcc	-1,549	5,133	0,732

Table S2: Adsorption energy values and optimized geometries for BP-H

System	Initial Site	Final Site	$E_{ads}(eV)$	Work function (eV)	Normal $d(P - H)$ (Å)
BP-Pt-H	$hcp_{(1)}$	$bridge_{(away-Pt)}$	-2,866	5,031	0,190
	$fcc_{(2)}$	$bridge_{(away-Pt)}$	-2,859	5,041	0,153
	$bridge_{(2)}$	$top_{(near-Pt)}$	-2,423	4,888	1,602
	$top_{(1)}$	$bridge_{(near-Pt)}$	-2,300	4,900	0,929
	$hcp_{(2)}$	$bridge_{(near-Pt)}$	-2,299	4,905	0,901
	$top_{(3)}$	$top_{(away-Pt)}$	-2,089	4,636	0,605
	$top_{(2)}$	$top_{(away-Pt)}$	-2,016	4,622	0,505
	$bridge_{(1)}$	$top_{(away-Pt)}$	-1,863	4,533	0,524
	$top_{(4)}$	$top_{(near-Pt)}$	-1,542	5,058	1,630
	$fcc_{(1)}$	fcc	-1,297	5,088	0,569

Table S3: Adsorption energy values and optimized geometries for BP-Pt-H

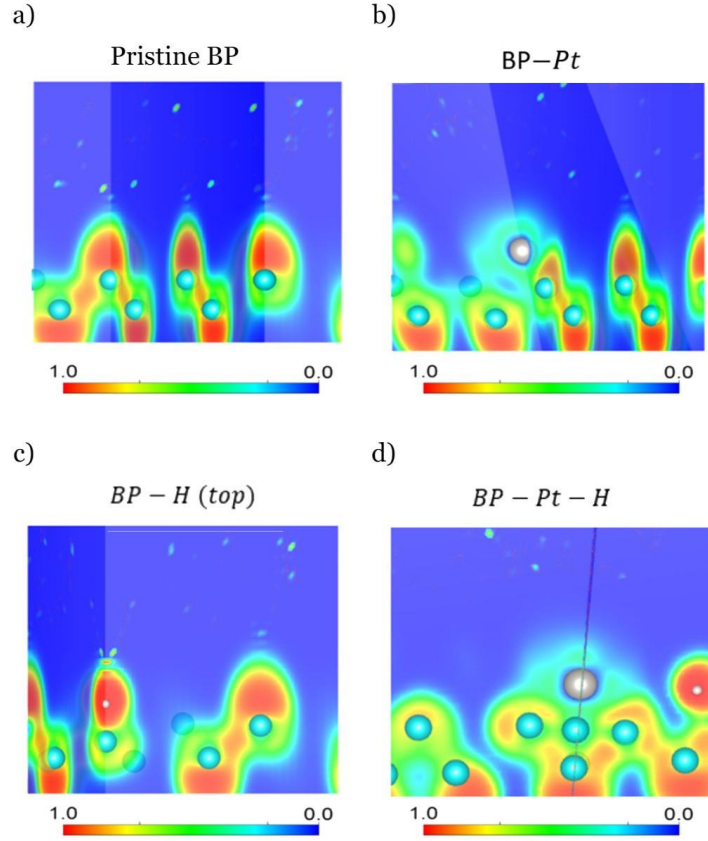


Figure S1: Electronic localization function for different evaluated systems.

System	ΔG_{H^*} (eV)	Ref
Pt-SnO	0.09	Ref. [1]
Pt- $W_2B_2O_2$ nanosheets	0.17	Ref. [2]
Pt-TiSe ₂	0.006	Ref. [3]
Pt-CoS ₂	0.03	Ref. [4]
Pt-Mo-MoC	-0.05(-0.91)	Ref. [5]
Pt-C-MoC	-0.38 (-0.62)	Ref. [5]
Pt-W-WC	-0.36 (-1.05)	Ref. [5]
Pt-C-WC	-0.40 (-1.43)	Ref. [5]
Pt-BP	-0.14 (0.65)	This-work

Table S4: Comparison of our results with other materials as reported in previous literatures. Where possible ΔG_{H^*} values on

S1. Stability of Pt on Blue phosphorene monolayer

The cohesive energy is given by:

$$E_{\text{coh}} = \frac{E_{\text{Pt}_n} - nE_{\text{Pt}}}{n}$$

Here E_{Pt_n} is the total energy of relaxed bulk system, E_{Pt} and E_{P} is the energy of the isolated Pt atom in vacuum and N is total number of atoms. Replacing corresponding values:

$$E_{\text{coh}} = \frac{-24.386 - 4 \times (-0.518)}{4} = -5.578 \text{ eV}$$

For $BP - Pt$ the obtained value of $E_{\text{ads}} = -4,2 \text{ eV}$.

The electromotive force (EMF) of such cell can be written as

$$EMF = \frac{E_{\text{ads}} - E_{\text{coh}}}{zF}$$

Where F is Faraday constant and z - number of transferred electrons.

Introducing Standard Hydrogen Electrode in place of Pt electrode would result in EMF of this cell being equal to the Pt Standard redox potential $E_{\text{Pt}^{z+}/\text{Pt}}^0$. A potential at which the dissolution of monolayer would occur (E_{diss}), therefore, can be obtained by combining EMFs for these two cells:

$$E_{\text{diss}} = E_{\text{Pt}^{z+}/\text{Pt}}^0 - \frac{E_{\text{ads}} - E_{\text{coh}}}{zF}$$
$$E_{\text{diss}} = 1.188 - \frac{-4.2 + 5.58}{2 \cdot 96500}$$
$$E_{\text{diss}} < 1.188 \text{ V}$$

Therefore, BP-Pt system is going to be somewhat unstable in these conditions. Potentially it can be further stabilized by increasing Pt surface coverage, but this requires further study.

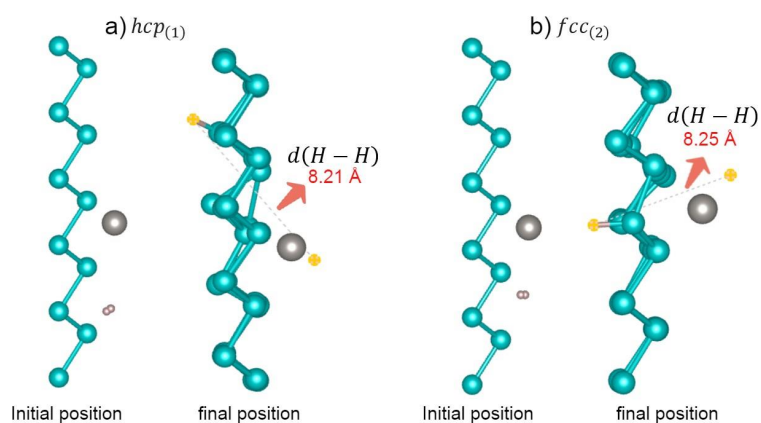


Figure S2: Schematic view of initial and final site for hcp(1) and fcc(2) positions on Tilted

References

- [1] Sun Z, Gao Z, Zhang C, Guan L, Tao J. Atomically dispersed low-cost transition metals catalyze efficient hydrogen evolution on two-dimensional SnO nanosheets. *International Journal of Hydrogen Energy*. 2021;46(56):28602- 12.
- [2] Li B, Wu Y, Li N, Chen X, Zeng X, Arramel; Zhao, X.; Jiang, J. Single Metal Atoms Supported on MBenes for Robust Electrochemical Hydrogen Evolution *ACS Appl Mater Interfaces*. 2020;12(8):9261-7.
- [3] Song Z, Yi J, Qi J, Zheng Q, Zhu Z, Tao L, et al. Line defects in monolayer $TiSe_2$ with adsorption of Pt atoms potentially enable excellent catalytic activity. *Nano Research*. 2022;15(5):4687-92.
- [4] Shi J, Chen T, Sun X. The effect of heteroatom doping on the active metal site of CoS_2 for hydrogen evolution reaction. *RSC Advances*. 2022;12(27):17257-63.

- [5] Koverga AA, Flórez E, Jimenez-Orozco C, Rodriguez JA. Not all platinum surfaces are the same: Effect of the support on fundamental properties of platinum adlayer and its implications for the activity toward hydrogen evolution reaction. *Electrochimica Acta*. 2021;368:137598.